Mathematisches Forschungsinstitut Oberwolfach

Report No. 15/2025

DOI: 10.4171/OWR/2025/15

Mathematical Methods in Quantum Chemistry

Organized by
Geneviève Dusson, Besançon
Michael Herbst, Lausanne
Benjamin Stamm, Stuttgart

9 March – 14 March 2025

Abstract. Quantum chemistry focuses on modelling and simulating the behaviour of molecular systems using the fundamental principles of quantum mechanics. However, the underlying equations, such as the Schrödinger equation for computing the ground state of N electrons, which is a partial differential equation defined on $\mathbb{R}^{3N}$, suffer from the curse of dimensionality. As a result, simulating even moderately sized molecules demands advanced techniques in analysis, approximation and reduced-order modelling for overcoming the naive computational complexity. In this workshop, the rapidly growing mathematical community working in the field together with several quantum chemists and physicists were gathered to discuss recent advances in areas such as (1) the mathematical and numerical analysis of standard models used in the field, including Density Functional Theory, Coupled Cluster, and the Density Matrix Renormalization Group (2) the development of efficient numerical methods, relying e.g. on the development of error bounds and (3) the opportunities of recent data-driven methods towards the approximation of wavefunctions or density matrices.

Mathematics Subject Classification (2020): 81Q05, 81V55, 65Y20.

Introduction by the Organizers

Quantum chemistry is concerned with the understanding and accurate prediction of physical properties of atomistic systems at a scale where quantum effects cannot be neglected. This leads to high-dimensional partial differential equations (PDEs), starting with the Schrödinger equation, an eigenvalue PDE posed on $\mathbb{R}^{3N}$ for a system with N electrons. The simulation of such systems is very expensive and

requires many approximations to be feasible at all. This includes (1) the setup of the equations modelling the physical system, (2) the discretization of the unknown continuous solution as well as (3) the numerical algorithms employed to solve the linear algebra part.

Solving key challenges of the 21st century, such as drug design, renewable energy or quantum computing, is fundamentally linked to understanding such quantum properties of matter. As a result a noteworthy fraction of the world's supercomputing time ($> 50\%$ of compute share on some machines) is currently spent on solving these mathematically very challenging problems. Advances on the understanding of the involved models and numerical methods are thus highly desired and provide a unique opportunity for significant impact of the mathematical community.

Despite the need for an interdisciplinary viewpoint to tackle mathematical challenges collaborations between mathematicians and application researchers in chemistry, physics or materials science are relatively recent. We have been thus delighted to bring together 48 researchers, experts in multiple mathematical disciplines (analysis, numerical analysis, statistics), but also experts from the application domain — making this workshop from our point of view a full success to seed further collaborations across traditional field boundaries.

The topics of our meeting covered the broad scope of mathematical research in electronic structure theory. Considering density-functional theory (DFT) — a mean-field-type model with considerable practical importance — Andre Laestadius, Robert van Leeuwen, Mathieu Lewin and Markus Penz presented new results on the analytical study of the DFT model, targeting fundamental questions on the differentiability and invertability of this model, on the structure of Hohnberg-Kohn theorems on lattices or the potential non-convexity of the energy.

On a related note Kieron Burke and Julien Toulouse presented on new routes for constructing DFT models for practical calculations, either explicitly violating electron count to improve approximations or incorporating effects from quantum electrodynamics in relativistic formulations of DFT — for which obtaining a consistent mathematical model is challenging.

A second workhorse of quantum chemistry is coupled cluster (CC) theory, known for its accurate predictions. In this domain Fabian Faulstich, Laura Grazioli and Simen Kvaal discussed new insights, such as a connection to algebraic geometry, the challenges of treating magnetic fields within CC theory as well as a new mathematical formulation of CC based on the bivariational principle, which enables a new route to formulate *a posteriori* error estimates applicable to this challenging model.

Beyond Kvaal's contribution the development of *a posteriori* error bounds has been a particular focus of this meeting with further presentations by Mi-Song Dupuy, Muhammad Hassan and Gaspard Kemlin on the estimation of discretisation errors in various settings as well as the contribution of Lin Lin on the estimation of the finite-size error — that is the error resulting from modelling an infinite periodic crystal using only a finite system size. While study of error

estimation techniques for electronic structure methods has thus advanced considerably compared to the last MFO workshop, it still remains far from the level of maturity of other branches of applied mathematics.

Another aspect, which was considered with a number of contributions was the combination of statistical and analytical techniques in electronic structure theory. This included the use of statistical learning as a technique to correct for deficiencies in electronic structure models, e.g. in the talk of Katharine Fisher, or as a technique to directly learn Kohn-Sham density matrices as in the presentation of Liwei Zhang. An approach to employ neural networks for the generation of optimised subspaces for eigenvalue computations has been presented by Xiaoying Dai. James Kermode provided us with an overview of applications of atomistic machine learning in materials modelling as well as recent methods to quantify errors in machine learning models for practical settings. Other uses of stochastic methods discussed during the meeting included Quantum Monte Carlo approaches in the contribution by Dexuan Zhou and stochastic variants of DFT for large-scale computations by Michael Lindsey.

Örs Legeza presented large-scale HPC-implementations of highly accurate tensor network state methods via DMRG-calculations. Additional theoretical insights on this ansatz were complemented by Gero Friesecke. Continuing the exploration of applications Frank Neese provided an overview of a state-of-the-art toolbox in computational chemistry and the associated challenges in scaling this code to high-performance computers.

The analytical study and simulation of 2D-incommensurate systems is of recent interest due to particular properties. Huajie Chen presented recent advances on the planewave approximation of such systems and Daniel Massat presented a momentum space algorithm for computing observables of trilayer graphene.

The final set of contributions provides various insights into the richness and diversity of topics in this field. Eric Cancès presented on the mathematical structure of impurity models and embedding theories. Thomas Bondo Pedersen provided insights on quantum dynamics beyond the usually applied Born-Oppenheimer approximation with Caroline Lasser providing complementary insights into the theoretical study of methods in quantum dynamics. Virginie Ehrlacher presented on observability results in the setting of periodic crystals. Insights into the coupling of perturbation theory and reduced basis methods for eigenvalue problems was provided by Louis Garrigue.

This workshop has shown how the exchange of ideas, concepts, models and methods can lead to very fruitful discussions of interdisciplinary nature, but where mathematics plays the central role. The mathematical concepts that were addressed were very diverse with sometimes astonishing connections such as the consideration of the CC-theory under the aspect of algebraic geometry or the frequent use of concepts from (computational) Riemannian geometry to account for constraints in the quantum mechanical models. Overall it has been a very stimulating week and the participants left with a plethora of ideas and inspirations.

Acknowledgement: The MFO and the workshop organizers would like to thank the National Science Foundation for supporting the participation of junior researchers in the workshop by the grant DMS-2230648, "US Junior Oberwolfach Fellows".

Workshop: Mathematical Methods in Quantum Chemistry

Table of Contents

Abstracts

The ground state energy is not (always) convex in the number of electrons

Mathieu Lewin
(joint work with Simone Di Marino and Luca Nenna)

We present here recent results from [1, 2].

Let us start by introducing the ground state energy of N electrons in a general external potential $V : \mathbb{R}^3 \to \mathbb{R}$:

$$E[N,V] := \min \sigma\big(H_N^V\big), \qquad H_N^V = \sum_{j=1}^N \left(-\frac{\Delta_{x_j}}{2} + V(x_j)\right) + \sum_{1\le j<k\le N} \frac{1}{|x_j - x_k|}.$$

The Hamiltonian H_N^V acts on the fermionic space $\bigwedge_1^N L^2(\mathbb{R}^3 \times \{\uparrow,\downarrow\},\mathbb{C})$. For a molecule containing M nuclei of charges $z_1, ..., z_M$ placed at $R_1, ..., R_M$ the external potential equals

$$V(x) = -\sum_{m=1}^M \frac{z_m}{|x - R_m|}.$$

Experimental data show that, at least for atoms, the ground state energy is convex in the number of electrons N. The interpretation is that the binding energy decreases whenever N increases, which expresses the fact that the core electrons are more tightly bound to the nuclei than the core electrons. It seems natural to ask whether this experimental observation holds for the Born-Oppenheimer Hamiltonian H_N^V, i.e. whether $N \mapsto E[N,V]$ is convex. The importance of the convexity in N was first mentioned in the context of density functional theory (DFT) by Perdew, Parr, Levy and Balduz [6] in 1982. It was later conjectured for different classes of V's in [3, 7, 5].

Although the convexity is still completely open for real atoms and molecules that have integer charges $z_m \in \mathbb{N}$, we provided in [1] the first counter-example, for nuclei with small fractional charges.

Theorem 1 (Non-convexity for 6 nuclei of small nuclear charges [1])**.** *There exist $R_1, ..., R_6 \in \mathbb{R}^3$, $z_1, ..., z_6 > 0$ and $e_4 < e_2 < e_1 < 0$ such that, for*

$$V_\ell(x) = -\sum_{m=1}^6 \frac{z_m/\sqrt{\ell}}{|x - \ell\, R_m|},$$

we have for all $N \ge 5$

$$E[1,V_\ell] = \frac{e_1}{\ell} + o\left(\frac{1}{\ell}\right), \qquad E[2,V_\ell] = E[3,V_\ell] = \frac{e_2}{\ell} + o\left(\frac{1}{\ell}\right)$$

$$E[N,V_\ell] = E[4,V_\ell] = \frac{e_4}{\ell} + o\left(\frac{1}{\ell}\right)$$

and hence convexity fails at $N = 3$ in the limit $\ell \to \infty$. The corresponding Hamiltonian $H^N_{V_\ell}$ admits a ground state for $N = 1$, $N = 2$ or $N = 4$ electrons, but not for $N = 3$ or $N \geq 5$ electrons.

The statement is that for $N = 3$ one electron must escape to infinity, whereas for $N = 2$ and $N = 4$ all the electrons can be bound by the 6 nuclei. In other words, the third electron can only be bound to the system if there is a fourth electron. This certainly goes against our intuition.

Since the nuclei have the tiny charge $z_m/\sqrt{\ell}$, they can bind at most one electron each [4], resulting in the hydrogenic energy $-z_m^2/(2\ell)$. This is of the same order as the interaction between the electrons, explaining our choice of scaling. To leading order the energy behaves like a classical optimization problem where we place N electrons at 6 sites $R_1, ..., R_6$ where they have the energy $-z_m^2/2$. Theorem 1 thus follows from a classical counter-example, whose exact statement is as follows.

Theorem 2 (Non-convexity for classical electrons hoping on 6 sites [1])**.** *There exist $R_1, ..., R_6 \in \mathbb{R}^3$, $z_1, ..., z_6 > 0$ such that the corresponding energy*

$$e_N := \min_{\substack{n_j \in \{0,1\} \\ \sum_{j=1}^6 n_j = N}} \left\{ -\sum_{j=1}^6 \frac{z_j^2}{2} n_j + \sum_{1 \leq j < k \leq 6} \frac{n_j\, n_k}{|R_j - R_k|} \right\}$$

satisfies $e_4 < e_2 < e_3 < e_5 < e_1 < e_6 < 0$.

Here the variable $n_j \in \{0, 1\}$ describes whether we put an electron at R_j or not. It is the fact that the classical energy strictly increases at $N = 3, 5, 6$ that implies the non-existence of ground states in the quantum case. In the quantum problem, the electrons can choose to escape to infinity instead of staying close to the nuclei.

The classical counter-example of Theorem 2 was found numerically, based on a previous counter-example that we had constructed in [2] in a seemingly completely different setting. In [2] we studied a generalization of multi-marginal optimal transport (MMOT) to the grand-canonical setting and found an example showing that it can be strictly below the MMOT energy. This turned out to be dual to the problem presented here, in the sense of Legendre transforms. This is how we found the above counter-example.

References

[1] S. Di Marino, M. Lewin, and L. Nenna, *Ground state energy is not always convex in the number of electrons*, J. Phys. Chem. A, **128** (2024), pp. 10697–10706.

[2] ———, *Grand-Canonical Optimal Transport*, Arch. Rat. Mech. Anal., **249** (2025), p. art. 12.

[3] E. H. Lieb, *Density functionals for Coulomb systems*, Int. J. Quantum Chem., **24** (1983), pp. 243–277.

[4] ———, *Bound on the maximum negative ionization of atoms and molecules*, Phys. Rev. A, **29** (1984), pp. 3018–3028.

[5] P. T. Nam, *The ionization problem in quantum mechanics*, in The Physics and Mathematics of Elliott Lieb. The 90th Anniversary Volume II, R. L. Frank, A. Laptev, M. Lewin, and R. Seiringer, eds., EMS Press, 2022, ch. 34, pp. 93–120.

[6] J. P. Perdew, R. G. Parr, M. Levy, and J. L. Balduz, *Density-functional theory for fractional particle number: Derivative discontinuities of the energy*, Phys. Rev. Lett., **49** (1982), pp. 1691–1694.
[7] B. Simon, *Fifteen problems in mathematical physics*, in Perspectives in Mathematics: Anniversary of Oberwolfach 1984, W. Jäger, J. Moser, and R. Remmert, eds., Birkhäuser, 1984, pp. 423–454.

Some insights on quantum embedding methods

Eric Cancès

Quantum embedding methods offer scalable frameworks for studying large interacting quantum systems, including lattice models, quantum chemistry problems, and correlated materials. They decompose the original complex system into smaller, or simpler, more manageable "local" many-body problems coupled via a "low-level" descriptor, which is refined through self-consistent iterations. The resulting subproblems are then solved using accurate, computationally intensive techniques ("high-level" methods).

Different quantum embedding techniques impose specific self-consistency conditions to bridge the low-level and high-level descriptions. For example, dynamical mean-field theory (DMFT) [4] aligns the diagonal blocks of the time-dependent one-particle Green's functions (or self-energies) between the two levels, while density-matrix embedding theory (DMET) [3] ensures consistency in the diagonal blocks of the one-particle reduced density matrices (1-RDM).

In the first part of my talk, I presented a unified framework encompassing DMFT and DMET.

The second part of my talk was focused on DMET. I presented a recent mathematical result [1] showing that in the weakly interacting limit, conventional DMET is exact up to second-order corrections in the coupling parameter. However, conventional DMET is constrained by the requirement that the global 1-RDM (low-level descriptor) be an orthogonal projector, limiting flexibility in bath construction and potentially impeding accuracy in strongly correlated regimes. In the generalized DMET framework we introduced [5], the low-level descriptor can be an arbitrary 1-RDM and the bath construction is based on optimizing a quantitative criterion related to the maximal disentanglement between different fragments. This yields an alternative yet controllable bath space construction for generic 1-RDMs, lifting a key limitation of conventional DMET. We expect that this more flexible framework, which leads to several new variants of DMET, can improve the robustness and accuracy of DMET.

Lastly, I presented a mathematical analysis of DMFT in a specific framework [2]. After recalling the definition and properties of one-body time-ordered Green's functions and self-energies, and the mathematical structure of the Anderson impurity model, I described a specific impurity solver, namely the Iterative Perturbation Theory (IPT) solver, which can be conveniently formulated using Matsubara's

Green's functions. Within this framework, it can be proved under certain assumptions that the DMFT equations for the spin-unpolarized translation-invariant Hubbard model admit a solution for any set of physical parameters.

These are joint works with a number of people credited in references [1, 2, 5] below.

References

[1] E. Cancès, F.M. Faulstich, A. Kirsch, E. Letournel, and A. Levitt, *Some mathematical insights on Density Matrix Embedding Theory*, CPAM (2025).

[2] E. Cancès, A. Kirsch and S. Perrin–Roussel, *A mathematical analysis of IPT-DMFT*, arXiv:2406.03384 (2024).

[3] G. Knizia and G.K.L. Chan, *Density Matrix Embedding: A simple alternative to Dynamical Mean-Field Theory*, Physical Review Letters **109**, 186404 (2012).

[4] A. Georges, G. Kotliar, W. Krauth, and M.J. Rozenberg, *Dynamical mean-field theory of strongly correlated fermion systems and the limit of infinite dimensions*, Reviews of Modern Physics **68**, 13–125 (1996).

[5] A. Negre, F. Faulstich, R. Kim, T. Ayral, L. Lin, and E. Cancès, *New perspectives on Density-Matrix Embedding Theory*, arXiv:2503.09881 (2025).

Mathematical structure of observable-functional theories

Markus Penz

(joint work with Robert van Leeuwen)

Setting and general assumptions: To keep things (mostly) simple, we consider a finite-dimensional complex Hilbert space $\mathcal{H}$ of dimension $L = \dim \mathcal{H}$. We take the self-adjoint $\hat{A}$ as the *universal* part of a quantum system's Hamiltonian and $\hat{B}_i$, $i = 1, \dots, m$, as the *observables* coupling to a potential $\boldsymbol{\beta} \in \mathbb{R}^m$.

$$\hat{H}(\boldsymbol{\beta}) := \hat{A} + \sum_{i=1}^{m} \beta_i \hat{B}_i \tag{1}$$

We assume that the set $\{\hat{B}_0 = \hat{I}, \hat{B}_1, \dots, \hat{B}_m\}$ (including the identity operator $\hat{I}$) is linearly independent and all $\hat{B}_i$ mutually commute. For dealing with normalized states, we define the compact state manifold $\mathcal{M} := \{\Psi \in \mathcal{H} \mid \|\Psi\| = 1\}$. The ground-state problem has then the variational formulation

$$E(\boldsymbol{\beta}) := \min_{\Psi \in \mathcal{M}} \langle \hat{H}(\boldsymbol{\beta}) \rangle_\Psi . \tag{2}$$

The aim of the functional theory is to decrease the complexity of this optimization problem by reducing the search space. To achieve this, we define the vector-valued map from states in $\mathcal{M}$ to the expectation values of the general observables

$$\boldsymbol{g}(\Psi) := (\langle \hat{B}_1 \rangle_\Psi, \dots, \langle \hat{B}_m \rangle_\Psi) \in \mathbb{R}^m . \tag{3}$$

This allows to rewrite the expectation value of $\hat{H}(\boldsymbol{\beta})$ as $\langle \hat{H}(\boldsymbol{\beta}) \rangle_\Psi = \langle \hat{A} \rangle_\Psi + \boldsymbol{\beta} \cdot \boldsymbol{g}(\Psi)$. The universal part can then be treated in a separate variational problem. We

define the constraint set $\mathcal{M}_{\boldsymbol{b}} := \{\Psi \in \mathcal{M} \mid \boldsymbol{g}(\Psi) = \boldsymbol{b}\} = \boldsymbol{g}^{-1}(\boldsymbol{b})$ and the pure-state constrained-search functional

$$\tilde{F}(\boldsymbol{b}) := \begin{cases} \min\limits_{\Psi \in \mathcal{M}_{\boldsymbol{b}}} \langle \hat{A} \rangle_\Psi & \text{if } \boldsymbol{b} \in \mathcal{B} \\ \infty & \text{else.} \end{cases} \tag{4}$$

Here, the effective domain $\mathcal{B} \subseteq \mathbb{R}^m$ of $\tilde{F}$ (later shown to be compact) amounts to the image of $\mathcal{M}$ under $\boldsymbol{g}$. The ground-state problem Eq. (2) can now be reformulated with the universal functional and a substantially reduced search space, $E(\boldsymbol{\beta}) = \min_{\boldsymbol{b} \in \mathcal{B}} \{\tilde{F}(\boldsymbol{b}) + \boldsymbol{\beta} \cdot \boldsymbol{b}\}$. Since the energy functional $E(\boldsymbol{\beta})$ is concave by its definition in Eq. (2), the functional theory can be transformed into a fully convex form. This is achieved via the Legendre–Fenchel transform of $E(\boldsymbol{\beta})$ that defines the *convex* universal functional [1]

$$F(\boldsymbol{b}) := \sup_{\boldsymbol{\beta} \in \mathbb{R}^m} \{E(\boldsymbol{\beta}) - \boldsymbol{\beta} \cdot \boldsymbol{b}\}. \tag{5}$$

It can be shown that $F(\boldsymbol{b})$ is the same as Eq. (4) if the constrained search is extended to ensemble states [1] and as such it is the convex hull of $\tilde{F}(\boldsymbol{b})$ [2, Prop. 18]. Thus, $F(\boldsymbol{b})$ has the same proper domain $\mathcal{B}$ and $F(\boldsymbol{b}) \leq \tilde{F}(\boldsymbol{b})$. The supremum above is not necessarily a maximum since now the search space is not compact. We will later give conditions when it is indeed a maximum and an optimizer $\boldsymbol{\beta} \in \mathbb{R}^m$ always exists.

Representability by pure states: The set $\mathcal{B} = \boldsymbol{g}(\mathcal{M})$ can be constructed as follows. Since the $\hat{B}_i$ (including $i = 0$) all commute, there is an orthonormal basis $\{\Phi_k\}$ of $\mathcal{H}$ that simultaneously diagonalizes all the $\hat{B}_i$,

$$\hat{B}_i \Phi_k = \Lambda_{ki} \Phi_k, \quad \boldsymbol{g}(\Phi_k) = (\Lambda_{k1}, \ldots, \Lambda_{km}), \tag{6}$$

and $\Lambda_{k0} = 1$. This defines a real $L \times (m+1)$ matrix Λ_{ki} of eigenvalues. Every $\Psi \in \mathcal{M}$ can now be written $\Psi = \sum_{k=1}^{L} c_k \Phi_k$, $c_k \in \mathbb{C}$, $\sum_{k=1}^{L} |c_k|^2 = 1$. Substituting $\lambda_k = |c_k|^2$ we then get

$$\boldsymbol{g}(\Psi) = \sum_{k=1}^{L} \lambda_k \boldsymbol{g}(\Phi_k), \quad \lambda_k \geq 0, \quad \sum_{k=1}^{L} \lambda_k = 1. \tag{7}$$

Thus, $\mathcal{B}$ is the convex hull of $\{\boldsymbol{g}(\Phi_k)\}$ and the $\boldsymbol{g}(\Phi_k)$ form the vertices of the polyhedron $\mathcal{B}$. This also shows that $\mathcal{B}$ is closed and consequently it is compact as a subset of $\mathbb{R}^m$. Given any $\boldsymbol{b} \in \mathcal{B}$, we can find a $\Psi \in \mathcal{M}_{\boldsymbol{b}}$ by determining a (in general non-unique) set $\{\lambda_k\}$ that solves Eq. (7) and then taking $c_k = \sqrt{\lambda_k}$ (or with any other phase choice).

Representability by ensemble ground states: From Eq. (4) it follows that $F(\boldsymbol{b}) \leq \tilde{F}(\boldsymbol{b}) \leq \|\hat{A}\| < \infty$ on $\mathcal{B}$ and thus by some standard results from convex analysis (see for example [3, Th. 2.14, Prop. 2.36, and Prop. 2.33]) it holds that for every $\boldsymbol{b}$ from the *interior* of $\mathcal{B}$ there is a $\boldsymbol{\beta} \in \mathbb{R}^m$ such that $E(\boldsymbol{\beta}) = F(\boldsymbol{b}) + \boldsymbol{\beta} \cdot \boldsymbol{b}$. In other words, for all $\boldsymbol{b} \in \operatorname{int} \mathcal{B}$ the supremum in Eq. (5) is a maximum where an optimizer $\boldsymbol{\beta} \in \mathbb{R}^m$ can be found. But since the functional involved is given by constrained search over *ensemble* states, the corresponding ground state of $\hat{H}(\boldsymbol{\beta})$

that maps to $\boldsymbol{b}$ might be an ensemble state itself. In exceptional situations linked to degeneracies [4], the representability by ground states also holds for $\boldsymbol{b}$ on the boundary of $\mathcal{B}$. That one actually needs to rely on ensemble states is shown with examples where a $\boldsymbol{b} \in \mathsf{int}\,\mathcal{B}$ is not representable by pure ground states [2].

Unique representability (regular and critical values, Hohenberg–Kohn (HK) theorem): Finally, we ask if, or when, the above form of ground-state representability with a $\boldsymbol{\beta} \in \mathbb{R}^m$ is unique. In DFT this is the content of the HK theorem. A $\Psi \in \mathcal{H}$ is called *regular point* if all the $\hat{B}_i\Psi$, $i = 0, \ldots, m$, are linearly independent, else it is called a *critical point*. The set of all critical points is denoted $\mathcal{C} \subseteq \mathcal{H}$. The image of $\mathcal{C} \cap \mathcal{M}$ under $\boldsymbol{g}$ gives the *critical values* $\mathcal{B}_\mathrm{c} \subseteq \mathcal{B}$. A $\boldsymbol{b} \in \mathcal{B} \setminus \mathcal{B}_\mathrm{c}$ is then called a *regular value*. In other words, a $\boldsymbol{b} \in \mathcal{B}$ is called regular if for all $\Psi \in \mathcal{M}_{\boldsymbol{b}}$ all the $\hat{B}_i\Psi$, $i = 0, \ldots, m$, are linearly independent, else they are called critical. This explains why the $\hat{B}_i$ have been chosen linearly independent in the first place, because else no $\boldsymbol{b}$ can ever be regular. An alternative characterization of the critical points can be given with the help of the Gram matrix $\mathcal{G}(\Psi)$ defined by $\mathcal{G}_{ij}(\Psi) := \langle \hat{B}_i\Psi, \hat{B}_j\Psi\rangle$, $i, j = 0, \ldots, m$. Then the HK theorem in the current setting is the following: If the pure ground states (degeneracy is possible) of $\hat{H}(\boldsymbol{\beta})$ and $\hat{H}(\boldsymbol{\beta}')$ yield the same *regular* $\boldsymbol{b}$ then $\boldsymbol{\beta} = \boldsymbol{\beta}'$. **Proof:** For fixed $\boldsymbol{b}$ and $\boldsymbol{\beta}, \boldsymbol{\beta}'$ the ground-state energies are $E(\boldsymbol{\beta}^{(\prime)}) = \min_{\Psi \in \mathcal{M}_{\boldsymbol{b}}} \langle \hat{A}\rangle_\Psi + \boldsymbol{\beta}^{(\prime)} \cdot \boldsymbol{b}$. Since the minimum is independent of $\boldsymbol{\beta}^{(\prime)}$, we can take the same Ψ for both Hamiltonians. Subtracting the two Schrödinger equations $\hat{H}(\boldsymbol{\beta}^{(\prime)})\Psi = E(\boldsymbol{\beta}^{(\prime)})\Psi$ gives

$$\sum_{i=1}^{m} (\beta_i - \beta_i')\hat{B}_i\Psi = (\overbrace{E(\boldsymbol{\beta})}^{-\beta_0} - \overbrace{E(\boldsymbol{\beta}')}^{-\beta_0'})\Psi \Longrightarrow \sum_{i=0}^{M} (\beta_i - \beta_i')\hat{B}_i\Psi = 0. \tag{8}$$

Since all $\hat{B}_i\Psi$ are linearly independent, it readily follows $\beta_i = \beta_i'$ for all $i = 0, 1, \ldots, m$. This concludes the proof. The classical Sard's theorem [5] applied to $\boldsymbol{g} : \mathcal{M} \to \mathcal{B}$ then tells us that the set of critical values $\mathcal{B}_\mathrm{c}$ has measure zero in $\mathbb{R}^m$, so almost all $\boldsymbol{b} \in \mathcal{B}$ are regular and qualify for the HK property. It follows that only for critical $\boldsymbol{b}$ counterexamples to the HK theorem can be found [2] and it is known that those $\boldsymbol{b} \in \mathcal{B}_\mathrm{c}$ that produce counterexamples always correspond to the intersection of so-called degeneracy regions in $\mathcal{B}$ [4].

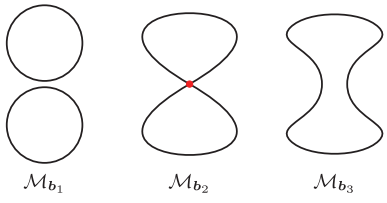

For a regular value $\boldsymbol{b} \in \mathcal{B} \setminus \mathcal{B}_\mathrm{c}$ we also know that the constraint set $\mathcal{M}_{\boldsymbol{b}}$ is a closed submanifold (constraint manifold) of $\mathcal{M}$ by the submersion theorem [5]. Different possible situations are depicted in the figure (multiple connected components; with a critical point; connected). A tangent vector Φ to $\mathcal{M}_{\boldsymbol{b}}$ at any $\Psi \in \mathcal{M}_{\boldsymbol{b}}$ is defined by the condition

$$\lim_{\epsilon \to 0} \frac{1}{\epsilon} \left(\langle \hat{B}_i\rangle_{\Psi + \epsilon\Phi} - \langle \hat{B}_i\rangle_\Psi \right) = 2\,\mathsf{Re}\langle \Phi, \hat{B}_i\Psi\rangle = 0. \tag{9}$$

The $\hat{B}_i\Psi$ are thus not normal vectors to $\mathcal{M}_{\boldsymbol{b}}$ at $\Psi \in \mathcal{M}_{\boldsymbol{b}}$ in the usual Hilbert-space sense, but they are orthogonal with respect to the Kähler metric that is defined by $g(\Phi, \Psi) = \mathsf{Re}\langle\Phi, \Psi\rangle$ [6]. A noteworthy recent paper discusses the geometry of expectation values by [7] and employs very similar concepts and even features an algebraic formulation of DFT. An obvious open research question is the generalization to infinite-dimensional $\mathcal{H}$, but maybe keeping the number of observables $\hat{B}_i$ finite.

References

[1] E. H. Lieb, *Density functionals for Coulomb-systems*, Int. J. Quantum Chem. **24** (1983), 243–277.

[2] M. Penz and R. van Leeuwen, *Density-functional theory on graphs*, J. Chem. Phys. **155** (2021), 244111.

[3] V. Barbu and T. Precupanu, *Convexity and Optimization in Banach Spaces*, 4th ed. (Springer, 2012).

[4] M. Penz and R. van Leeuwen, *Geometry of degeneracy in potential and density space*, Quantum **7** (2023), 918.

[5] R. Abraham, J. E. Marsden, and T. Ratiu, *Manifolds, Tensor Analysis, and Applications* (Springer, 1988).

[6] A. Ashtekar and T. A. Schilling, *Geometrical formulation of quantum mechanics*, in *On Einstein's Path: Essays in Honor of Engelbert Schucking* (Springer, 1999) pp. 23–65.

[7] C. Song, *Quantum geometry of expectation values*, Phys. Rev. A **107** (2023), 062207.

Finite-size error in quantum chemistry methods for periodic systems

Lin Lin

In recent years, there has been a growing interest in employing quantum chemistry methods to compute ground-state and excited-state properties for periodic systems [10, 8, 5, 7, 13, 3, 16, 11, 6, 21, 4, 17, 22, 15, 2, 1, 14]. Unlike molecular systems, periodic systems, including solids and surfaces, require calculating properties in the thermodynamic limit (TDL), a theoretical state in which the system size approaches infinity. However, directly tackling finite-size effects by enlarging the supercell size is very demanding, even for relatively inexpensive DFT calculations with modern-day supercomputers. For more accurate theories, this task is often computationally intractable. Understanding the finite-size scaling, i.e., the scaling of the finite-size error with respect to the system size, and employing finite-size error correction schemes are, therefore, crucial for obtaining accurate results using moderate-sized calculations.

There are two primary strategies to approximate the TDL. The first involves expanding the computational supercells within real space. The second strategy involves performing calculations using a fixed unit cell and refining discretization of the Brillouin zone within reciprocal space using a $\mathbf{k}$-point mesh, such as the Monkhorst-Pack mesh [12]. We focus on the latter approach, where the number of $\mathbf{k}$ points is denoted by $N_{\mathbf{k}}$. If the Monkhorst-Pack mesh includes the Gamma point of the Brillouin zone, this approach is equivalent to using a supercell comprised of

$N_{\mathbf{k}}$ unit cells. The convergence toward the TDL can be studied by increasing this single parameter $N_{\mathbf{k}}$ toward infinity.

An innovative theoretical observation provided in Ref. [18] is that the finite-size error can be largely comprehended if assuming HF single-particle orbitals can be acquired exactly at any given $\mathbf{k}$ point in the Monkhorst-Pack mesh. This perspective helps to disentangle the contribution due to the relatively manageable single-particle effects from the collective and more complex electron correlation effects. Based on this assumption, the finite-size error can be rigorously examined from a numerical quadrature perspective. Specifically, the value of a physical observable at the TDL can often be written as a multidimensional integral over the Brillouin zone. As the Monkhorst-Pack mesh forms a uniform grid discretizing the Brillouin zone, the analysis simplifies to investigating the quadrature error of certain trapezoidal rule in a periodic region, a topic widely discussed in numerical analysis literature. The novelty here lies in the recognition that the associated integrands possess a unique singularity structure that is asymptotically of a specific fractional form. Reference [18], therefore, develops a new Euler-MacLaurin type of analysis that facilitates the study of the finite-size error associated with HF and MP2 methods, taking into account this fractional form singularity.

For a periodic system, let the unit cell and Bravais lattice be denoted by Ω and $\mathbb{L}$, and let the reciprocal lattice and reciprocal unit cell be denoted by $\mathbb{L}^*$ and Ω^*, respectively. Let $\mathcal{K}$ be a Monkhorst-Pack mesh of size $N_{\mathbf{k}}^{\frac{1}{3}} \times N_{\mathbf{k}}^{\frac{1}{3}} \times N_{\mathbf{k}}^{\frac{1}{3}}$ in Ω^*. Let the eigenvectors (orbitals) and eigenvalues (orbital energies) of Hartree-Fock Hamiltonian on $\mathcal{K}$ be denoted by

$$\left\{ \psi_{n\mathbf{k}}(\mathbf{r}) = \frac{1}{\sqrt{N_{\mathbf{k}}}} e^{i\mathbf{k}\cdot\mathbf{r}} u_{n\mathbf{k}}(\mathbf{r}), \varepsilon_{n\mathbf{k}} \right\} \quad \text{for } \mathbf{k} \in \mathcal{K}$$

where $u_{n\mathbf{k}}(\mathbf{r})$ is the periodic component $u_{n\mathbf{k}}(\mathbf{r}+\mathbf{R}) = u_{n\mathbf{k}}(\mathbf{r}), \quad \mathbf{R} \in \mathbb{L}$. Then we may define the pair product of orbitals and its Fourier transform

$$\varrho_{n'\mathbf{k}',n\mathbf{k}}(\mathbf{r}) = \overline{u}_{n'\mathbf{k}'}(\mathbf{r}) u_{n\mathbf{k}}(\mathbf{r}) = \frac{1}{|\Omega|} \sum_{\mathbf{G}\in\mathbb{L}^*} \hat{\varrho}_{n'\mathbf{k}',n\mathbf{k}}(\mathbf{G}) e^{\mathrm{i}\mathbf{G}\cdot\mathbf{r}}.$$

The two-electron repulsion integral (ERI), which plays a central role in the analysis, takes the form

$$\frac{1}{|\Omega|\, N_{\mathbf{k}}} {\sum_{\mathbf{G}\in\mathbb{L}^*}}' \frac{4\pi}{|\mathbf{q}+\mathbf{G}|^2} \hat{\varrho}_{n_1\mathbf{k}_1,n_3\mathbf{k}_3}(\mathbf{G}) \hat{\varrho}_{n_2\mathbf{k}_2,n_4\mathbf{k}_4}(\mathbf{G}^{\mathbf{k}_3,\mathbf{k}_4}_{\mathbf{k}_1,\mathbf{k}_2} - \mathbf{G}).$$

The primed summation over $\mathbf{G}$ means that the possible term with $\mathbf{q}+\mathbf{G}=\mathbf{0}$ is excluded in the numerical calculation. The Fock Exchange energy takes the form

$$E_{\mathrm{X}}(N_{\mathbf{k}}) = -\frac{1}{N_{\mathbf{k}}} \sum_{ij} \sum_{\mathbf{k}_i\mathbf{k}_j\in\mathcal{K}} \langle i\mathbf{k}_i, j\mathbf{k}_j | j\mathbf{k}_j, i\mathbf{k}_i \rangle$$

To the best of our knowledge, the first rigorous analysis of finite-size error in Hartree-Fock (HF) theory (using a quadrature analysis) and second-order Møller-Plesset perturbation theory (MP2) for insulating systems has been conducted only recently [18].

Theorem 1 (Informal statement of [18, Theorem 3.1, 5.1])**.** *For certain insulators, in the absence of finite-size corrections,*

$$\left|E_{\mathbf{X}}^{\mathrm{TDL}} - E_{\mathbf{X}}\left(N_{\mathbf{k}}\right)\right| = \widetilde{\mathcal{O}}\left(N_{\mathbf{k}}^{-\frac{1}{3}}\right).$$

Madelung constant correction evaluates a_0 up to h.o.t. then

$$\left|E_{\mathbf{X}}^{\mathrm{TDL}} - E_{\mathbf{X}}^{\mathrm{corr}}\left(N_{\mathbf{k}}\right)\right| = \widetilde{\mathcal{O}}\left(N_{\mathbf{k}}^{-1}\right).$$

Beyond the Hartree-Fock level, the Nesbet's theorem for correlation energy states

(1)

$$E_{\#}^{N_{\mathbf{k}}} = \frac{1}{N_{\mathbf{k}}^3} \sum_{\mathbf{k}_i \mathbf{k}_j \mathbf{k}_a \in \mathcal{K}} \sum_{ijab} \left(2\left\langle i\mathbf{k}_i, j\mathbf{k}_j | a\mathbf{k}_a, b\mathbf{k}_b\right\rangle - \left\langle i\mathbf{k}_i, j\mathbf{k}_j | b\mathbf{k}_b, a\mathbf{k}_a\right\rangle\right) T_{ijab}^{\#,N_{\mathbf{k}}}(\mathbf{k}_i, \mathbf{k}_j, \mathbf{k}_a),$$

where T_{ijab} is called the T_2 amplitude, and # indicates the level of theory.

Interestingly, for the coupled cluster doubles (CCD) theory, which is mathematically the simplest and representative form of CC theory, earlier numerical calculations did not provide conclusive evidence regarding its finite-size scaling, with different studies suggesting either an inverse volume scaling [9, 3] or inverse length scaling [11]. More recent calculations demonstrate that the electron correlation energy in periodic coupled cluster calculations should follow an inverse volume scaling, even in the absence of finite-size correction schemes. This observation points to a significant gap in the theoretical understanding of the finite-size error: How can we reconcile the following seemingly paradoxical facts?

(1) Without finite-size corrections, the finite-size error in CCD exhibits inverse volume scaling.
(2) Without finite-size corrections, the finite-size error in MP3 exhibits inverse length scaling. This rate is sharp and cannot be improved.
(3) All MP3 diagrams are encompassed within the CCD formulation.

We elucidate the origin of the inverse volume scaling behavior [20]. Our analysis consists of two steps. First, we show that the Madelung constant correction, commonly used to reduce finite-size errors in Fock exchange energy and orbital energies, can also be applied to reduce the finite-size error in ERI contractions within the CCD amplitude equation. We prove that with the Madelung constant correction, the finite-size errors in CCD(n) and converged CCD calculations satisfy the desired inverse volume scaling. In the second step of our analysis, we observe that upon convergence of the CCD amplitude equations, the Madelung constant corrections to both orbital energies and ERI contractions perfectly cancel each other out for any finite-sized system. Combining this result with the first step, we conclude that the finite-size error of the correlation energy in converged CCD calculations satisfies the desired inverse volume scaling without the need for any additional correction schemes. However, prior to the convergence of the amplitude equations, this perfect cancellation does not occur, and the finite-size error of CCD(n) calculations remains $\mathcal{O}(N_{\mathbf{k}}^{-\frac{1}{3}})$. A similar lack of cancellation occurs when the orbital energies take their exact value at the TDL but the ERI contractions are

not corrected, resulting in an $\mathcal{O}(N_{\mathbf{k}}^{-\frac{1}{3}})$ finite-size error for both converged CCD and CCD(n) calculations studied in Ref. [19]. The results are summarized in the Table below.

Theory	Correction to orbital energies ε	Correction to ERI	Finite-size scaling	Reference
HF	N/A	✗	$N_{\mathbf{k}}^{-\frac{1}{3}}$	[18, Thm 3.1]
HF	N/A	✓	$N_{\mathbf{k}}^{-1}$	[18, Thm 5.1]
MP2	✓	N/A	$N_{\mathbf{k}}^{-1}$	[18, Thm 4.1]
MP3	✓	✗	$N_{\mathbf{k}}^{-\frac{1}{3}}$	[19, Cor 2]
MP3	✓	✓	$N_{\mathbf{k}}^{-1}$	[20, Thm 1]
CCD(n)/CCD	✓	✗	$N_{\mathbf{k}}^{-\frac{1}{3}}$ / $N_{\mathbf{k}}^{-\frac{1}{3}}$	[19, 2, Thm 1 / Cor 3]
CCD(n)/CCD	✓	✓	$N_{\mathbf{k}}^{-1}$ / $N_{\mathbf{k}}^{-1}$	[20, Thm 1 / Thm 2]
CCD(n)/CCD	✗	✓	$N_{\mathbf{k}}^{-\frac{1}{3}}$ / $N_{\mathbf{k}}^{-\frac{1}{3}}$	[20, Thm 1 / Thm 2]
CCD(n)/CCD	✗	✗	$N_{\mathbf{k}}^{-\frac{1}{3}}$ / $N_{\mathbf{k}}^{-1}$	[20, Thm 3 / Cor 1]

References

[1] S. Banerjee and A. Y. Sokolov. Non-Dyson algebraic diagrammatic construction theory for charged excitations in solids. *J. Chem. Theory Comput.*, 18(9):5337–5348, 2022.

[2] S. J. Bintrim, T. C. Berkelbach, and H.-Z. Ye. Integral-direct Hartree–Fock and Møller–Plesset perturbation theory for periodic systems with density fitting: Application to the benzene crystal. *J. Chem. Theory Comput.*, 18(9):5374–5381, 2022.

[3] G. H. Booth, A. Grüneis, G. Kresse, and A. Alavi. Towards an exact description of electronic wavefunctions in real solids. *Nature*, 493(7432):365–370, 2013.

[4] Y. Gao, Q. Sun, M. Y. Jason, M. Motta, J. McClain, A. F. White, A. J. Minnich, and G. K.-L. Chan. Electronic structure of bulk manganese oxide and nickel oxide from coupled cluster theory. *Phy. Rev. B*, 101(16):165138, 2020.

[5] T. Gruber and A. Grüneis. Ab initio calculations of carbon and boron nitride allotropes and their structural phase transitions using periodic coupled cluster theory. *Phy. Rev. B*, 98(13):134108, 2018.

[6] T. Gruber, K. Liao, T. Tsatsoulis, F. Hummel, and A. Grüneis. Applying the coupled-cluster ansatz to solids and surfaces in the thermodynamic limit. *Phys. Rev. X*, 8(2):021043, 2018.

[7] A. Grüneis. A coupled cluster and Møller-Plesset perturbation theory study of the pressure induced phase transition in the LiH crystal. *J. Chem. Phys.*, 143(10):102817, 2015.

[8] A. Grüneis, M. Marsman, and G. Kresse. Second-order Møller–Plesset perturbation theory applied to extended systems. II. Structural and energetic properties. *J. Chem. Phys.*, 133(7):074107, 2010.

[9] K. Liao and A. Grüneis. Communication: Finite size correction in periodic coupled cluster theory calculations of solids. *J. Chem. Phys.*, 145(14):141102, 2016.

[10] M. Marsman, A. Grüneis, J. Paier, and G. Kresse. Second-order Møller–Plesset perturbation theory applied to extended systems. I. Within the projector-augmented-wave formalism using a plane wave basis set. *J. Chem. Phys.*, 130(18):184103, 2009.

[11] J. McClain, Q. Sun, G. K. L. Chan, and T. C. Berkelbach. Gaussian-based coupled-cluster theory for the ground-state and band structure of solids. *J. Chem. Theory Comput.*, 13(3):1209–1218, 2017.

[12] H. J. Monkhorst and J. D. Pack. Special points for Brillouin-zone integrations. *Phys. Rev. B*, 13(12):5188, 1976.
[13] C. Müller and B. Paulus. Wavefunction-based electron correlation methods for solids. *Phys. Chem. Chem. Phys.*, 14(21):7605–7614, 2012.
[14] V. A. Neufeld and T. C. Berkelbach. Highly accurate electronic structure of metallic solids from coupled-cluster theory with nonperturbative triple excitations. *arXiv preprint arXiv:2303.11270*, 2023.
[15] V. A. Neufeld, H.-Z. Ye, and T. C. Berkelbach. Ground-state properties of metallic solids from ab initio coupled-cluster theory. *J. Phys. Chem. Lett.*, 13(32):7497–7503, 2022.
[16] T. Schäfer, B. Ramberger, and G. Kresse. Quartic scaling MP2 for solids: A highly parallelized algorithm in the plane wave basis. *J. Chem. Phys.*, 146(10):104101, 2017.
[17] X. Wang and T. C. Berkelbach. Excitons in solids from periodic equation-of-motion coupled-cluster theory. *J. Chem. Theory Comput.*, 16(5):3095–3103, 2020.
[18] X. Xing, X. Li, and L. Lin. Unified analysis of finite-size error for periodic Hartree-Fock and second order Møller-Plesset perturbation theory. *Math. Comp.*, 93:679, 2024.
[19] X. Xing and L. Lin. Finite-size effects in periodic coupled cluster calculations. *J. Comput. Phys.*, 500:112755, 2024.
[20] X. Xing and L. Lin. Origin of inverse volume scaling in periodic coupled cluster calculations towards thermodynamic limit. *Phys. Rev. X*, 14:011059, 2024.
[21] I. Y. Zhang and A. Grüneis. Coupled cluster theory in materials science. *Front. Mater.*, 6:123, 2019.
[22] T. Zhu and G. K.-L. Chan. All-electron Gaussian-based G_0W_0 for valence and core excitation energies of periodic systems. *J. Chem. Theory Comput.*, 17(2):727–741, 2021.

On the relation between Galerkin approximations and canonical best-approximations of solutions to some non-linear Schrödinger equations

Muhammad Hassan
(joint work with Yvon Maday and Yipeng Wang)

This talk was concerned with solutions to the following Gross-Pitaevskii type energy minimisation problems:

$$E^*_{\mathrm{src}} := \min_{u\in X}\Big\{\frac{1}{2}\int_\Omega |\nabla u(\mathbf{x})|^2\,d\mathbf{x} + \frac{1}{2}\int_\Omega V(\mathbf{x})|u(\mathbf{x})|^2\,d\mathbf{x} + \frac{1}{4}\int_\Omega |u(\mathbf{x})|^4\,d\mathbf{x}, -\big\langle f,u\big\rangle_{X^*\times X}\Big\} \tag{1}$$

$$E^*_{\mathrm{eig}} := \min_{\substack{u\in X\\ \|u\|_{L^2(\Omega)}=1}} \Big\{\frac{1}{2}\int_\Omega |\nabla u(\mathbf{x})|^2\,d\mathbf{x} + \frac{1}{2}\int_\Omega V(\mathbf{x})|u(\mathbf{x})|^2\,d\mathbf{x} + \frac{1}{4}\int_\Omega |u(\mathbf{x})|^4\,d\mathbf{x}\Big\}, \tag{2}$$

under one of the following two settings:

Setting One: $\Omega = (-1,1)^d$, $d \in \{1,2,3\}$ and $X = H^1_0(\Omega)$. Moreover, the source function $f \in H^s(\Omega)$ for $s \geq 0$ while the effective potential V is positive and $V \in H^{r_v}(\Omega)$ for $r_v > d/2$;

Setting Two: Ω is a d-dimensional torus with $d \in \{1, 2, 3\}$ and $X = H^1(\Omega)$. Moreover, the source function $f \in H^s(\Omega)$ for $s \geq 0$ while the effective potential V is bounded below by $V_{\min} > 0$ and $V \in H^{r_v}(\Omega)$ for $r_v > d/2$.

Under these hypotheses, it is well-known that there exists a unique minimiser u^*_{src} to the unconstrained minimisation problem (1) and there exists a unique positive minimiser u^*_{eig} to the constrained minimisation problem (2). Additionally, elliptic regularity theory together with a bootstrapping argument implies that

$$u^*_{\mathrm{src}} \in H^{t_{\mathrm{src}}+2}(\Omega) \qquad \text{and} \qquad u^*_{\mathrm{eig}} \in H^{t_{\mathrm{eig}}+2}(\Omega), \tag{3}$$

with $t_{\mathrm{src}} = \min\{s, r_v, 3-\epsilon\}$ and $t_{\mathrm{eig}} = \min\{r_v, 3-\epsilon\}$ for any $\epsilon > 0$ in the case of **Setting One** and $t_{\mathrm{src}} = \min\{s, r_v\}$ and $t_{\mathrm{eig}} = r_v$ in the case of **Setting Two**.

In order to approximate these minimisers numerically, one typically introduces a sequence of finite-dimensional approximation spaces $\{X_\delta\}_{\delta>0}$, $X_\delta \subset X$, such that the standard approximation property is satisfied:

$$\forall u \in X: \qquad \lim_{\delta \to 0^+} \inf_{v_\delta \in X_\delta} \|u - v_\delta\|_X = 0. \tag{4}$$

We then seek, for a given approximation space X_δ, the solutions to the following discrete energy minimisation problems:

$$\begin{aligned} E^\delta_{\mathrm{src}} := \min_{u_\delta \in X_\delta} \Big\{ &\frac{1}{2}\int_\Omega |\nabla u_\delta(\mathbf{x})|^2 \, d\mathbf{x} + \frac{1}{2}\int_\Omega V(\mathbf{x})|u_\delta(\mathbf{x})|^2 \, d\mathbf{x} \\ &+ \frac{1}{4}\int_\Omega |u_\delta(\mathbf{x})|^4 \, d\mathbf{x} - \big\langle f, u_\delta \big\rangle_{X^* \times X} \Big\} \end{aligned} \tag{5}$$

$$\begin{aligned} E^\delta_{\mathrm{eig}} := \min_{\substack{u_\delta \in X_\delta \\ \|u_\delta\|_{L^2(\Omega)}=1}} \Big\{ &\frac{1}{2}\int_\Omega |\nabla u_\delta(\mathbf{x})|^2 \, d\mathbf{x} + \frac{1}{2}\int_\Omega V(\mathbf{x})|u_\delta(\mathbf{x})|^2 \, d\mathbf{x} \\ &+ \frac{1}{4}\int_\Omega |u_\delta(\mathbf{x})|^4 \, d\mathbf{x} \Big\}. \end{aligned} \tag{6}$$

The exact choice of the approximation spaces $\{X_\delta\}_{\delta>0}$ depends on the problem setting. Finite element or spectral polynomial discretisations may be chosen for **Setting One** in which case δ represents the maximal finite element diameter or the reciprocal of the maximal polynomial degree. In the case of **Setting Two**, a natural choice is a spectral Fourier discretisation in which case δ represents the reciprocal of the maximal wave-number (classically denoted by N). In either case, it is well known that for any given $\delta > 0$, there exists a unique solution $u^*_{\delta,\mathrm{src}} \in X_\delta$ to the unconstrained discrete minimisation problem (5), and for all δ small enough, we have the error estimate

$$\|u^*_{\mathrm{src}} - u^*_{\delta,\mathrm{src}}\|_{L^2(\Omega)} \lesssim \delta \|u^*_{\mathrm{src}} - u^*_{\delta,\mathrm{src}}\|_X \lesssim \delta \inf_{v_\delta \in X_\delta} \|u^*_{\mathrm{src}} - v_\delta\|_X \lesssim \delta^2 \|u^*_{\mathrm{src}}\|_{H^2(\Omega)}. \tag{7}$$

This estimate can be improved if the exact minimiser u^*_{src} possesses additional Sobolev regularity (in the sense of Estimate (3)) and if the approximation spaces $\{X_\delta\}_{\delta>0}$ satisfy certain properties.

Under **Settings One** and **Two** and with the same choice of discretisation spaces, it has been proven[1] in [2] that there exists at least one solution $u^*_{\delta,\mathrm{eig}} \in X_\delta$ to the constrained discrete minimisation problem (6). Additionally, for all δ small enough and any discrete minimiser $u^*_{\delta,\mathrm{eig}}$ that satisfies $\left(u^*_{\delta,\mathrm{eig}}, u^*_{\mathrm{eig}}\right)_{L^2(\Omega)} \geq 0$, we again have the error estimate

(8)
$$\|u^*_{\mathrm{eig}} - u^*_{\delta,\mathrm{eig}}\|_{L^2(\Omega)} + \delta\|u^*_{\mathrm{eig}} - u^*_{\delta,\mathrm{eig}}\|_X \lesssim \delta \inf_{v_\delta \in X_\delta} \|u^*_{\mathrm{eig}} - v_\delta\|_X \lesssim \delta^2 \|u^*_{\mathrm{eig}}\|_{H^2(\Omega)}.$$

As before, this estimate can be improved if the exact constrained minimiser u^*_{eig} possesses additional Sobolev regularity (in the sense of Estimate (3)) and if the approximation spaces $\{X_\delta\}_{\delta>0}$ satisfy certain properties.

The aim of this talk was to present results from a recent preprint [4] showing that in contrast to the standard error estimates (7) and (8), improved convergence rates can be obtained for the error between the discrete minimisers $u^*_{\delta,\mathrm{src}}$ and $u^*_{\delta,\mathrm{eig}}$ and the $(\cdot,\cdot)_X$-best approximation in X_δ of the exact minimisers u^*_{src} and u^*_{eig}. Roughly speaking, denoting by Π^X_δ, the $(\cdot,\cdot)_X$-orthogonal projection operator onto X_δ, we will show that, under appropriate hypothesis, for each $m \in \{0,1\}$, each $\mathrm{pb} \in \{\mathrm{src},\mathrm{eig}\}$, and all δ small enough it holds that

$$\|u^*_{\delta,\mathrm{pb}} - \Pi^X_\delta u^*_{\mathrm{pb}}\|_{H^m(\Omega)} \leq \delta^{q(m)} \|u^*_{\mathrm{pb}} - \Pi^X_\delta u^*_{\mathrm{pb}}\|_X, \tag{9}$$

where the exact rate $q(m)$ depends on the choice of discretisation (finite element or spectral) but is always larger than or equal to one and can even reach $q(1) = 2$.

While these results appear to be interesting, per se, independently of applications (for instance, as remarked in [1], the results for the eigenvalue problem belong to the 'Galerkin folklore'), they are motivated in the present case by our proposal, based on *a posteriori estimators*, of near-optimal strategies for calculating the numerical solution of a PDE to a precision fixed in advance. Non-linear periodic eigenvalues problems such as Equation (2) with the plane-wave discretisation are frequently encountered in quantum chemistry and electronic structure calculations, and iterative algorithms to solve these problems – known as Self-Consistant Field methods – are therefore particularly relevant. In this context, following and in continuation of what is proposed in [3], we propose in [5] new error-balance strategies in order to achieve a given solution accuracy whilst minimising the computational cost. Our strategy in [5] involves first performing a large number of iterations in small-dimensional plane-wave bases (dealing with modes up to n with $n \ll N$). Subsequently, the dimension of the plane-wave approximation spaces is increased in a controlled way to compute the higher modes of the eigenvector solution. The fact that the numerical solution displays superconvergence to the projection of the exact solution justifies this strategy. Indeed, performing a large number of iterations on small discrete problems (thus with small cost) provides a numerical solution whose low modes are very accurate. The additional iterations, in higher-dimensional spaces, are then concentrated purely on the high modes (i.e. on the

[1]The spectral polynomial discretisation is not analysed in the cited reference but the arguments are similar.

orthogonal space to the first n modes). This results in a much smaller *effective* spectral radius of the underlying iteration matrix which leads to very few iterations being needed to attain the required accuracy. In [5], strategies are proposed where only one iteration is required in the highest-dimensional space.

References

[1] C. Beattie. Galerkin eigenvector approximations. *Mathematics of computation*, 69(232):1409–1434, 2000.

[2] E. Cancès, R. Chakir, and Y. Maday. Numerical analysis of nonlinear eigenvalue problems. *Journal of Scientific Computing*, 45(1):90–117, 2010.

[3] G. Dusson and Y. Maday. A posteriori analysis of a nonlinear gross–pitaevskii-type eigenvalue problem. *IMA Journal of Numerical Analysis*, 37(1):94–137, 2017.

[4] M. Hassan, Y. Maday, and Y. Wang. On the relation between Galerkin approximations and canonical best-approximations of solutions to some non-linear Schrödinger equations. *arXiv preprint*, arXiv:2502.07638, 2025.

[5] M. Hassan, Y. Maday, and Y. Wang. A posteriori error estimates and their use for a least-cost strategy to achieve target accuracy. *in preparation*.

[6] Y. Wang. *A posteriori error estimation for electronic structure calculations using ab initio methods and its application to reduce calculation costs*. PhD thesis, Sorbonne Université, 2023.

Subspace Method based on Neural Networks for Eigenvalue Problems

Xiaoying Dai

(joint work with Yunying Fan, Zhiqiang Sheng)

Motivated by the work introduced in [1], we propose a subspace method based on neural networks for eigenvalue problems with high accuracy and low cost. We first construct a neural networks based orthogonal basis by some deep learning method and dimensionality reduction technique, and then we use some classical method, e.g., the Galerkin method, to discretize the eigenvalue problem in the subspace spanned by the orthogonal basis, and then obtain the approximate solution.

We consider the following typical eigenvalue problem:

$$\begin{cases} Lu = \lambda u & \text{in } \Omega, \\ u = 0 & \text{on } \partial\Omega, \end{cases}$$

where the differential operator $L := -\nabla \cdot (\alpha \nabla) + \beta$ and $\alpha = (\alpha_{ij})_{ij}$ is symmetric positive definite with $\alpha_{ij} \in W^{1,\infty}(\Omega)(i, j = 1, \cdots, d)$, and $0 \leq \beta \in L^{\infty}(\Omega)$.

The associate weak form of the eigenvalue problem above is as follows: Find $(\lambda, u) \in \mathbb{R} \times H_0^1(\Omega)$ such that $b(u, u) = 1$ and

$$a(u, v) = \lambda b(u, v), \quad \forall v \in H_0^1(\Omega), \tag{1}$$

where $a(u, v) = (\alpha \nabla u, \nabla v) + (\beta u, v)$ and $b(u, v) = (u, v)$.

Let V_h be a finite dimensional subspace of V. The finite dimensional discretization of (1) is as follows: Find $(\lambda, u_h) \in \mathbb{R} \times V_h$ such that $b(u_h, u_h) = 1$ and

$$a(u_h, v_h) = \lambda b(u_h, v_h), \quad \forall v_h \in V_h. \tag{2}$$

We now set V_h to be the subspace spanned by some neural network based functions $\varphi(\mathbf{x}, \theta)$:

$$\varphi(\mathbf{x}, \theta) = \mathcal{T}_{L+1} \circ \sigma \circ \mathcal{T}_L \circ \cdots \circ \sigma \circ \mathcal{T}_1(\mathbf{x})$$

with

$$\mathcal{T}_l(\mathbf{x}) := \mathcal{L}_{W_l, b_l}(\mathbf{x}) = W_l \cdot \mathbf{x} + b_l, l = 1, \cdots, L+1,$$

$\mathbf{x} \in \mathbb{R}^d, \theta := \{W_1, \cdots, W_{L+1}, b_1, \cdots, b_{L+1}\}$, $W_l \in \mathbb{R}^{n_l \times n_{l-1}}$ and $b_l \in \mathbb{R}^{n_l}$ are the weights and bias of the l-th layer, n_l is the number of neurons of the l-th layer ($n_0 = d, n_{L+1} = M$) and $\sigma(\cdot)$ is the activation function.

We set $u_{NN}(\mathbf{x}; \theta, \mathbf{w}) = \sum\limits_{j=1}^{M} w^{(j)} \varphi_j(\mathbf{x}; \theta)$, $\mathbf{w} = (w^{(1)}, w^{(2)}, \cdots, w^{(M)})^T$. Substituting $u_{NN}(\mathbf{x}; \theta, \mathbf{w})$ into (2) and choosing $v_h(\mathbf{x}) = \varphi_i(\mathbf{x}; \theta)$, we get

$$\sum_{j=1}^{M} w^{(j)} a(\varphi_j, \varphi_i) = \lambda \sum_{j=1}^{M} w^{(j)} b(\varphi_j, \varphi_i), i = 1, \cdots, M.$$

We then obtain the following algebraic eigenvalue problem

$$A(\theta)\mathbf{w} = \lambda B(\theta)\mathbf{w},$$

where

$$A(\theta) = (a(\varphi_i(\mathbf{x}; \theta), \varphi_j(\mathbf{x}; \theta)))_{ij}, B(\theta) = ((\varphi_i(\mathbf{x}; \theta), \varphi_j(\mathbf{x}; \theta)))_{ij} \in \mathbb{R}^{M \times M}, \mathbf{w} \in \mathbb{R}^M.$$

The problem is how to find the optimal θ. Following [1], we use some deep learning method to find the optimal θ.

For this, we first define the loss function for computing the first k eigenpairs as follows:

$$\mathcal{L}(\theta, w) = \text{Trace}\Big(\mathcal{B}^{-1}(u_{NN,1}(\mathbf{x}; \theta, w_1), \cdots, u_{NN,k}(\mathbf{x}; \theta, w_k)) \\ \mathcal{A}(u_{NN,1}(\mathbf{x}; \theta, w_1), \cdots, u_{NN,k}(\mathbf{x}; \theta, w_k))\Big),$$

where $u_{NN,i}(\mathbf{x}; \theta, \mathbf{w}_i) = \sum\limits_{j=1}^{M} w_i^{(j)} \varphi_j(\mathbf{x}, \theta)$ is an approximation of the k-th eigenvector, and

$$\mathcal{A}(u_{NN,1}, \ldots, u_{NN,k}) = (a(u_{NN,i}, u_{NN,j}))_{ij} \in \mathbb{R}^{k \times k},$$

$$\mathcal{B}(u_{NN,1}, \ldots, u_{NN,k}) = (b(u_{NN,i}, u_{NN,j}))_{ij} \in \mathbb{R}^{k \times k}.$$

By fixing $\mathbf{w} = (\mathbf{w}_1, \cdots, \mathbf{w}_k)$ to be $\bar{\mathbf{w}}$, we can then obtain the optimal θ^* by solving the following minimization problem

$$\theta^* = \arg\min_{\theta \in \Theta} \mathcal{L}(\theta, \bar{\mathbf{w}}).$$

We now obtain the framework of our subspace method based on neural networks for eigenvalue problems.

- Initialize the neural network architecture, give and fix coefficients $\bar{\mathbf{w}}$.
- Obtain the parameters θ by minimizing the loss function

$$\theta^* = \arg\min_{\theta\in\Theta} \mathcal{L}(\theta, \bar{\mathbf{w}}).$$

- Construct an orthogonal basis from the trained neural networks based functions by some dimensionality reduction technique.
- Find the Galerkin projection of the orginal eigenvalue problems in the subspace spanned by the orthogonal basis, and obtain the following algebraic eigenvalue problem

$$A\mathbf{w} = \lambda B\mathbf{w}$$

with A and B the stiffmatrix and mass matrix, respectivley.

We have applied our method to solution of some typical eigenvalue problems in 2D, including the Laplace eigenvalue problem, the Harmonic oscillator problems, and the Schrodinger equation for Hydrogen atom. For those examples, our method can obtain approximate eigenpairs with the error of eigenvalues being below 10^{-11} and the L^2 norm and H^1 norm error of eigenfunctions being nearly below 10^{-7}, but with the required number of epochs ranging from 20 to 400.

Our method can in fact be viewed as a method combining the machine learning with the classical methods. That is, first use the machine learning method and model order reduction method to get some neural networks based orthogonal basis, then calculate the Galerkin projection of the eigenvalue problem onto the subspace spanned by the orthogonal basis and obtain an approximate solution, just like what the classical methods do.

This talk is based on the work with Yunying Fan and Zhiqiang Sheng[2].

References

[1] Z. Xu and Z. Sheng, *Subspace method based on neural networks for solving the partial differential equation*, arXiv:2404.08223 (2024).

[2] X. Dai, Y. Fan and Z. Sheng, *Subspace Method based on Neural Networks for Eigenvalue Problems*, arXiv:2410.13358 (2024).

Error analysis for time-dependent variational approximation

Caroline Lasser

(joint work with Rémi Carles, Clotilde Fermanian-Kammerer, Marlis Hochbruck, Christian Lubich)

We have considered the time-dependent Schrödinger equation

$$i\partial_t\psi(t) = H(t)\psi(t), \quad \psi(0) = \psi_0$$

for a time-dependent, self-adjoint Hamiltonian operator $H(t)$ and square integrable initial data ψ_0. We have explored the systematic construction of approximate solutions in the context of the time-dependent variational principle. Choosing an approximation manifold $\mathcal{M}$, an approximate solution $u(t) \approx \psi(t)$, $u(t) \in \mathcal{M}$, is

sought by solving a linear least squares problem for the unknown time-derivative $\partial_t u(t) \in \mathcal{T}_{u(t)}\mathcal{M}$,

$$\|i\partial_t u(t) - Hu(t)\| = \min_{\partial_t u(t)} !$$

The talk has focused on the following two guiding examples.

First example: Magnetic Schrödinger equation. The Hamiltonian operator is of the form

$$H(t) = \frac{1}{\varepsilon}\left((-i\varepsilon\nabla_x - A(t,x))^2 + V(t,x)\right)$$

with $\varepsilon > 0$ a small semiclassical parameter. $A(t,x)$ and $V(t,x)$ are smooth potentials, which are of sublinear and subquadratic growth in x, respectively. The global prefactor $\frac{1}{\varepsilon}$ in front of the whole Schrödinger operator accounts for the adequate long semiclassical time scale. The initial data $\psi_0 \in L^2(\mathbb{R}^d)$ are a semiclassically scaled complex Gaussian wave packet. The variational approximation $u(t,x)$ is a Gaussian wave packet of general covariance whose nonlinear parametrisation is determined by the variational principle.

Second example: System-bath Hamiltonian. The Hamiltonian

$$H = H_x + H_y + W(x,y)$$

acts on $L^2(\mathbb{R}^{d_x} \times \mathbb{R}^{d_y})$ with a smooth and subquadratic coupling potential $W(x,y)$. The variational approximation $u(t,x,y) = u^{(x)}(t,x)u^{(y)}(t,y)$ is the time-dependent Hartree approximation.

A posteriori norm analysis. Formulating the variational equation of motion in terms of the orthogonal projector $P_{u(t)}$ onto the tangent space $\mathcal{T}_{u(t)}\mathcal{M}$ as

$$i\partial_t u(t) = P_{u(t)}H(t)u(t),$$

a standard variation of constants argument provides the estimate

$$\|u(t) - \psi(t)\| \leq \int_0^t \|P_{u(t)}^{\perp} H(s)u(s)\| \,\mathrm{d}s.$$

For a Gaussian wave packet with covariance of $\mathcal{O}(\sqrt{\varepsilon})$, this estimate is $\mathcal{O}(\sqrt{\varepsilon})$. For the time-dependent Hartree approximation [2], it provides error bounds with respect to first order derivatives of the coupling potential W.

A posteriori observable analysis. For expectation values with respect to an observable $\mathbf{B}$, one has the error representation formula [3]

$$\langle \mathbf{B} \rangle_{u(t)} - \langle \mathbf{B} \rangle_{\psi(t)} = \int_0^t \left\langle \left[U(s,t)\mathbf{B}U(t,s), P_{u(s)}^{\perp} H(s) P_{u(s)} \right] \right\rangle_{u(s)} \mathrm{d}s,$$

where $U(t,s)$ denotes the unitary propagator for the Hamiltonian. The presence of (a) averages and (b) commutators explains, that observable accuracy is typically better than norm accuracy. For semiclassical Gaussian wave packets, observable accuracy is spectacularly high [1], namely $\mathcal{O}(\varepsilon^2)$, which underpins the successes of the approximation in real life molecular quantum dynamics simulations. For the time-dependent Hartree approximation, the corresponding observable error

estimate requires less Sobolev regularity of the approximate wave function than the norm estimate.

Outlook. We have concluded the talk with the potential applicability of the presented error analysis to linear combinations of Gaussians, shallow neural networks and general tensors.

Acknowledgment. This research has partially been funded by the Deutsche Forschungsgemeinschaft (DFG, German Research Foundation), TRR 352, Project-ID 470903074.

References

[1] S. Burkhard, B. Dörich, M. Hochbruck, C. Lasser, *Variational Gaussian approximation for the magnetic Schrödinger equation*, J. Phys. A **57** 295202 (2024).
[2] I. Burghardt, R. Carles, C. Fermanian-Kammerer, B. Lasorne, C. Lasser, *Dynamical approximations for composite quantum systems: Assessment of error estimates for a separable ansatz*, J. Phys. A: Math Theor. **55** 224010 (2022).
[3] C. Lasser, C. Lubich, *Computing quantum dynamics in the semiclassical regime*, Acta Numerica **29** 229–401 (2020).

Quantum dynamics without the Born-Oppenheimer approximation

Thomas Bondo Pedersen
(joint work with Ludwik Adamowicz, Hâkon E. Kristiansen, Simen Kvaal, Caroline Lasser, Simon E. Schrader, Aleksander P. Woźniak)

The development over the past 2–3 decades of experimental techniques to generate laser pulses with duration down to a few tens of attoseconds has opened exciting new opportunities in materials science and atomic and molecular physics and chemistry. The enormous potential for groundbreaking discoveries is reflected in the 2023 Nobel Prize in Physics awarded to Agostini, Krausz, and L'Hullier for their pioneering efforts in the experimental and theoretical developments underpinning modern ultrafast science. Attosecond laser pulses not only allow us to "see" the dynamics of electrons in real time, they may eventually allow us to steer molecular dynamics and chemical transformations by controlling the force field that drives nuclear motion. Achieving this goal, however, requires substantial efforts aimed at reliable simulations of molecular quantum dynamics.

Computing the molecular quantum dynamics during and after interaction with an attosecond laser pulse poses a range of challenges that go well beyond the current state of the art in quantum chemistry, including breakdown of the adiabatic Born-Oppenheimer approximation and the virtually unavoidable presence of ionization and chemical bond-breaking fragmentation processes. This talk describes our ongoing efforts to address these challenges [1, 2, 3, 4, 5, 6, 7].

Essentially all approaches to nonadiabatic molecular dynamics start from the clamped-nuclei Born-Oppenheimer approximation and the associated potential-energy surfaces. Such an approach is, however, not generally well-defined for

charged particles interacting with a time-dependent external field and, consequently, we decided to treat electronic and nuclear degrees of freedom on an equal footing without invoking the Born-Oppenheimer approximation at any stage.

We thus consider the time-dependent Schrödinger equation for a molecular system interacting with an electromagnetic field. To simplify the problem somewhat, we invoke the electric-dipole appoximation to describe the interaction of the electrons and nuclei with the field, which allows us to separate the center-of-mass motion from the internal dynamics for an electrically neutral system (beyond the electric-dipole approximation, the center-of-mass motion is coupled to the field, complicating the treatment significantly). Choosing the internal coordinate system to be parallel to the laboratory frame with origin at a reference particle labelled 0, the nonrelativistic internal Hamiltonian becomes (using atomic units throughout)

$$H = \sum_{i=1}^{n} \left(\frac{p_i^2}{2m_i} + \frac{q_0 q_i}{r_i} \right) + \sum_{i<j} \left(\frac{q_i q_j}{r_{ij}} + \frac{p_i p_j}{M_0} \right) + E(t) \sum_{i=1}^{n} q_i r_i, \tag{1}$$

where $E(t)$ is the laser field in the electric-dipole approximation.

Inspired by decades of work on solving the time-independent molecular Schrödinger equation with high accuracy without invoking the Born–Oppenheimer approxiation [8], we expand the n-body wavefunction in a basis of explicitly correlated Gaussian wave packets,

$$\phi(r; \alpha(t)) = \exp\left(-(r-q)^T C (r-q) + \mathrm{i} p^T (r-q) \right), \tag{2}$$

where the complex symmetric width matrix $C = A + \mathrm{i}B$, $A > 0$, and the center q and momentum p are considered time-dependent parameters collected in the varable $\alpha(t)$. These functions form a complete basis of $L^2(\mathbb{R}^{3n})$ such that the molecular wavefunction can be expressed as

$$\Psi(r,t) = \mathcal{P} \sum_{i=1}^{M(t)} \phi(r; \alpha_i(t)) c_i(t), \tag{3}$$

where $\mathcal{P}$ implements the required permutational symmetries to obtain a definite pre-defined spin state while obeying the Pauli principle. We have shown numerically that remarkably few Gaussians are required to accurately represent complicated dynamics induced by violent laser pulses, at least for low-dimensional (1d and 2d) systems [2, 4].

The parameters $M(t)$, $\alpha_i(t)$, and $c(t)$ can in principle be determined from the Dirac-Frenkel variation princple. This approach, however, is notorious for its numerical instability (the Gramian of the tangent manifold quickly becomes ill-conditioned, even for rather simple model simulations). To circumvent this issue, we instead use Rothe's method [9]. We first invoke the Crank-Nicolson discretization in time only, which provides us with an equation for the wavefunction at time t_{i+1} in terms of a known wavefunction at time t_i:

$$A_i \Psi_{i+1} = A_i^\dagger \Psi_i, \qquad A_i = 1 + \mathrm{i} \frac{\Delta t}{2} H(t_i + \Delta t/2). \tag{4}$$

We then use the expansion 3 for Ψ_{i+1} and determine the parameters by variational minimization.

The talk contains numerical examples taken from [5, 6, 7], highlighting both pros and cons of the approach, including an unforeseen difficulty arising from potential-energy operator singularities and the associated cusp conditions on the wavefunction [5], which we bypass by regularization. Finally, the problem of determining molecular structure from non-Born-Oppenheimer calculations is discussed on the basis of [3].

References

[1] L. Adamowicz, S. Kvaal, C. Lasser, T. B. Pedersen, *Laser-induced dynamic alignment of the HD molecule without the Born–Oppenheimer approximation*, J. Chem. Phys. **157**, 144302 (2022).

[2] S. Kvaal, C. Lasser, T. B. Pedersen, L. Adamowicz, *No need for a grid: Adaptive fully-flexible Gaussians for the time-dependent Schrödinger equation*, arXiv:2207.00271 (2022).

[3] L. Lang, H. M. Cezar, L. Adamowicz, T. B. Pedersen, *Quantum definition of molecular structure*, J. Am. Chem. Soc. **146**, 1760–1764 (2024).

[4] A. P. Woźniak, L. Adamowicz, T. B. Pedersen, S. Kvaal, *Gaussians for electronic and rovibrational quantum dynamics*, J. Phys. Chem. A **128**, 3659–3671 (2024).

[5] S. E. Schrader, H. E. Kristiansen, T. B. Pedersen, S. Kvaal, *Time evolution as an optimization problem: The hydrogen atom in strong laser fields in a basis of time-dependent Gaussian wave packets*, J. Chem. Phys. **161**, 044105 (2024).

[6] S. E. Schrader, T. B. Pedersen, S. Kvaal, *Multidimensional quantum dynamics with explicitly correlated Gaussian wave packets using Rothe's method*, J. Chem. Phys. **162**, 024109 (2025).

[7] A. P. Woźniak, L. Adamowicz, T. B. Pedersen, S. Kvaal, *Rothe time propagation for coupled electronic and rovibrational quantum dynamics*, arXiv:2503.09813 (2025).

[8] S. Bubin, M. Pavanello, W.-C. Tung, K. L. Sharkey, L. Adamowicz, *Born–Oppenheimer and non-Born–Oppenheimer, atomic and molecular calculations with explicitly correlated Gaussians*, Chem. Rev. **113**, 36–79 (2013).

[9] E. Rothe, *Zweidimensionale parabolische Randwertaufgaben als Grenzfall eindimensionaler Randwertaufgaben*, Math. Ann. **102**, 650–670 (1930).

Planewave approximations for quantum incommensurate systems

Huajie Chen

(joint work with Daniel Massatt, Ting Wang, Aihui Zhou, Yuzhi Zhou)

Low dimensional materials have attracted extraordinary level of interest in the materials science and physics communities due to the unique electronic, optical, and mechanical properties. In particular, when two layers of 2D materials are stacked on top of each other with a small misalignment (such as a twist), they produce incommensurate moiré patterns. It is of great importance to study these structures from a theoretical and computational point of view. The conventional method for simulating the incommensurate systems is to construct a supercell approximation with artificial strain, which then allows for the use of Bloch theory and conventional band-structure methods. However, these approaches are usually computationally expensive, as one may need extremely large supercells to achieve the required accuracy.

This work [3] studies the density of states (DoS) and local density of states (LDoS) of a linear Schrödinger operator for incommensurate systems from the mathematical perspective. We focus on the following Schrödinger operator for a bi-layer incommensurate system

$$H := -\frac{1}{2}\Delta + v_1 + v_2,$$

where $v_j : \mathbb{R}^d \to \mathbb{R}$ $(j = 1, 2)$ are smooth and periodic functions with respect to two incommensurate lattices.

The first issue is that a quantitative characterization of the DoS of the Schrödinger operator for incommensurate systems is missing. In [1], the property of the integrated DoS was studied for one-dimensional almost-periodic systems. In [2], the DoS was introduced in the weak sense within the tight-binding models. These works on DoS can not be directly generalized to continuous models with arbitrary dimensions. The DoS and spatial LDoS of the Schrödinger operator H are written as

$$D(E) = \underline{\mathrm{Tr}}\big(\delta(E - H)\big) \qquad \text{and} \qquad D(E; x) = \big\langle x\big|\delta(E - H)\big|x\big\rangle$$

for $E \in \mathbb{R}$ and $x \in \mathbb{R}^d$ respectively. To make the objects numerically tractable, we consider the problem in the weak sense [3], and provide rigorous justifications of these objects. Although the linear Schrödinger operator has a simple form, the lack of compactness, broken translation symmetry, and continuous nature of the operator make it difficult to address the above objects of an incommensurate system. To handle these problems, we use the spectral theory to study $g(H)$: While $g(H)$ is not a trace class operator, it can be decomposed into a discrete collection of trace class operators.

The second problem is how to efficiently evaluate the (well-defined) DoS and LDoS of an incommensurate system. In [4], the Hamiltonian was discretized by a planewave basis set with a brute cutoff, and the DoS was approximated by the resulting eigenvalues. This type of approach essentially transfers the low dimensional incommensurate problem into a high dimensional periodic problem, which is expensive most of the time and converges slowly with respect to the planewave cutoff. In this work, we propose an efficient numerical scheme [3] based on our formulation of DoS in reciprocal space. In particular, we approximate the reciprocal LDoS within a planewave framework and then evaluate the DoS via a trapezoidal rule. We further improve the heuristic planewave method in [4] by introducing a novel cutoff scheme. In particular, we split the cutoff of wave vectors in the high dimensional reciprocal space into two directions: one increases the planewave frequency while the other one traverses the reciprocal space. A key observation is that the errors of the planewave approximations decay at completely different speeds as the cutoff increases along the two directions. Therefore, we truncate the wave vectors in the two different directions with different cutoffs, such that the cutoff for high frequency direction can be much smaller. We provide a rigorous numerical analysis [3], as well as numerical simulations of some typical incommensurate systems, to show the efficiency of our algorithms.

References

[1] J. Avron and B. Simon, *Almost periodic Schrödinger operators I: Limit periodic potentials*, Comm. Math. Phys., **82** (1982), 101–120.

[2] D. Massatt, M. Luskin, and C. Ortner, *Electronic density of states for incommensurate layers*, Multiscale Modeling Simul., **15** (2017), 476–499.

[3] T. Wang, H. Chen, A. Zhou, Y. Zhou, and D. Massatt, *Convergence of the planewave approximations for quantum incommensurate systems*, Multiscale Modeling Simul., **23** (2025), 545–576.

[4] Y. Zhou, H. Chen, and A. Zhou, *Plane wave methods for quantum eigenvalue problems of incommensurate systems*, J. Comput. Phys., **384** (2019), 99–113.

Momentum Space Algorithm for Electronic Structure of Double-Incommensurate Trilayer Graphene

Daniel Massatt

(joint work with Kenneth Beard)

Moiré 2D materials are highly tunable through variables including twist angle, species of layers, and number of layers. Various configurations lead to useful physical phenomena and possible applications, including many-body physics such as correlated insulators and superconductivity. To understand many-body models, a careful single-particle model must first be constructed. For example in twisted bilayer graphene, the Bistritzer-MacDonald model [1, 2, 3] is frequently used as a starting point for modeling magic-angle physics, where exotic correlated physics is observed such as correlated insulators, superconductivity, and the fractional quantum hall effect. More complex geometries including double-incommensurate trilayers, however, become difficult to accurately quantify even in the single-particle regime. Correlated physics including superconductivity is observed in double-twisted trilayer graphene, making an efficient algorithm for computing electronic behavior in the single-particle regime critical for understanding correlated physics of trilayers.

In this work, which is in preparation, we present a momentum space algorithm for computing observables for double-incommensurate trilayer graphene with rigorous error analysis compared to the real space tight-binding model including the density of states and the momentum local density of states (LDoS). The momentum LDoS of a Hamiltonian H with momentum basis $|k\rangle$ is given by

$$D_\varepsilon(k, E) = \langle k|\delta_\varepsilon(E - H)|k\rangle. \tag{1}$$

Here $\delta_\varepsilon(\cdot)$ is a normalized Gaussian with standard deviation ε. ε can be considered a spectral resolution parameter. The smaller ε is chosen, the higher the resolution of the spectral information. Our proposed algorithm involves transforming into momentum space as done in [4], where the Hamiltonian becomes a lattice model describing cattering channels, we denote $\widehat{H}(k)$. However, $\widehat{H}(k)$ has a 4-dimensional degree of freedom space, and when truncated by a parameter L, the computational cost for computing momentum LDoS scales as $O(L^4)$ using sparsity of $\widehat{H}(k)$ and the Kernel Polynomial Method for computing (1). It is observed that convergence

is poor. Our analysis indeed indicates it scales as $p(\varepsilon^{-1})e^{-\varepsilon\gamma L}$ for some $\gamma > 0$ and a polynomial $p(\cdot)$. We introduce a two-truncation scheme where one truncation focuses on k remaining close to the K-point of graphene, i.e. where graphene Dirac cones are featured, and the second parameter controlling the number of scatterings admitted. If the approximate momentum LDoS is called $D_\varepsilon^{rL}(k, E)$, then we have the following convergence for twisted trilayer graphene:

$$|D_\varepsilon(k, E) - D_\varepsilon^{rL}(k, E| \leq p(\varepsilon^{-1})(e^{-\gamma\varepsilon L} + e^{-\gamma' r}). \tag{2}$$

We require the following assumptions for this result: interlayer coupling is sufficiently weak, (k, E) are near the Dirac point of graphene, and the twist angles are small. Further, if θ is the largest twist angle, $\gamma' = O(\theta^{-1})$, resulting in rapid convergence in r. This allows computation costs to scale as $O((L \log L)^2)$ instead of $O(L^4)$ for the same accuracy results of the previous algorithm.

This algorithmic technique can be generalized to other observables including density of states and conductivity for trilayers. A natural follow-on question is whether an efficient single-particle basis can be constructed to develop many-body models, as many-body models are significantly more expensive to use in computations than single-particle models. Here the single-particle model still is already computationally intensive unlike the twisted bilayer graphene momentum space models.

References

[1] R. Bistritzer, & A.H. MacDonald, *Moiré bands in twisted double-layer graphene.* Proc. Natl. Acad. Sci. U.S.A. **108** (30) 12233–12237 (2011).

[2] Cao, Y., Fatemi, V., Fang, S. et al. *Unconventional superconductivity in magic-angle graphene superlattices.* Nature **556**, 43–50 (2018).

[3] Z. Song, B. Bernevig. *Magic-Angle Bilayer Graphene as a Topological Heavy Fermion Problem.* Phys. Rev. Lett. **129**, 047601 (2022).

[4] Z. Zhu, S. Carr, D. Massatt, M. Luskin, E. Kaxiars. *Twisted Trilayer Graphene: A Precisely tunable Platform for Correlated Electrons.* Phys. Rev. Lett. **125**, 116404 (2020).

Using Moreau–Yosida Regularization in Density-Functional theory

Andre Laestadius

(joint work with Markus Penz, Mihaly A. Csirik, Michael F. Herbst, Vebjørn H. Bakkestuen)

Moreau-Yosida (MY) regularization was introduced to density-functional theory (DFT) by Kvaal et al. in 2014 [1]. Let $f : X \to \mathbb{R} \cup \{+\infty\}$ be convex and lower semicontinuous, then the MY regularization of f with parameter $\varepsilon > 0$ is given by

$$f_\varepsilon(\rho) = \inf_{\sigma \in X} \left(f(\sigma) + \frac{1}{2\varepsilon} \|\sigma - \rho\|_X^2 \right). \tag{1}$$

Here X is (at least) a reflexive, strictly convex Banach space. We let X^* be the potential space, dual to the density space X. We denote by $J : X \to X^*$ the

(normalized) duality mapping given by

$$J(\rho) = \{v \in X^* \mid \|\rho\|_X^2 = \|v\|_{X^*}^2 = \langle v, \rho\rangle\}.$$

The unique minimizer of Eq. (1), denoted ρ_ε and called the proximal point of ρ, satisfies the stationarity condition

$$\underline{\partial} f(\rho_\varepsilon) + \frac{1}{\varepsilon} J(\rho_\varepsilon - \rho) \ni 0. \tag{2}$$

In Eq. (2) we have used the fact that $\underline{\partial}(\|\rho\|_X^2/2) = J(\rho)$ with $\underline{\partial}$ denoting the subdifferential, i.e., $\underline{\partial} f(\rho)$ is the subdifferential of f at ρ given by

$$\underline{\partial} f(\rho) = \{v \in X^* \mid f(\sigma) \geq f(\rho) + \langle v, \sigma - \rho\rangle\}.$$

In Kohn–Sham (KS) DFT we use the particle density ρ to describe a system of N electrons modeled by the Hamiltonian

$$\begin{aligned}\hat{\mathcal{H}}^\lambda(v) &= \hat{T} + \lambda \hat{W} + \hat{V}(v)\\ &=: \hat{\mathcal{H}}_0^\lambda + \hat{V}(v),\end{aligned}$$

where λ is a nonnegative coupling constant, $\hat{T} = -\frac{1}{2}\sum_{j=1}^N \Delta_{x_j}$ the kinetic energy operator, $\hat{W} = \frac{1}{2}\sum_{j\neq k} |x_j - x_k|^{-1}$ the electron–electron interaction term, and $\hat{V}(v) = \sum_{j=1}^N v(x_j)$ the external potential operator specified by $v : \mathbb{R}^3 \to \mathbb{R}$. We let the interacting ground-state energy of a system described by the external potential v_{ext} computed from $\hat{H}^\lambda(v)$ with $\lambda = 1$ and $v = v_{\text{ext}}$ be denoted by $E(v)$. Similarly, we denote by $E_{\text{KS}}(v_{\text{KS}})$ the non-interacting ground-state energy computed from $\hat{H}^\lambda(v)$ with $\lambda = 0$ and $v = v_{\text{KS}}$. From this set-up we define two convex and lower semicontinuous density functionals and their corresponding energy minimization

$$\begin{cases} F(\rho) = \sup_{v\in X^*} \left(E(v) - \langle v, \rho\rangle\right) \\ E(v) = \inf_{\rho\in X} \left(F(\rho) + \langle v, \rho\rangle\right) \end{cases}$$

$$\begin{cases} F_{\text{KS}}(\rho) = \sup_{v\in X^*} \left(E_{\text{KS}}(v) - \langle v, \rho\rangle\right) \\ E_{\text{KS}}(v) = \inf_{\rho\in X} \left(F_{\text{KS}}(\rho) + \langle v, \rho\rangle\right) \end{cases}$$

The idea of KS DFT is then to find an effective potential v_{KS} such that $E(v_{\text{ext}})$ and $E_{\text{KS}}(v_{\text{KS}})$ share a minimizing density ρ_{gs}, i.e., that ρ_{gs} is both a ground-state (gs) particle density of the physical system ($\lambda = 1$) and the non-interacting KS system ($\lambda = 0$). In a typical *forward* KS calculation, both ρ_{gs} and v_{KS} are unknown and an iterative scheme is employed that relies on approximating the exchange-correlation energy $E_{\text{xc}}(\rho) = F(\rho) - F_{\text{KS}}(\rho) - E_{\text{H}}(\rho)$, where $E_{\text{H}}(\rho)$ is the direct Coulomb energy (Hartree energy).

A potential useful practical application of MY regularization is that it provides a framework for performing density-potential inversion within an exact mathematical structure. Obtaining the effective potential v_{KS} from the interacting ground-state density ρ_{gs} is in the literature referred to as an *inverse* KS procedure. Now, assume that we are given a ρ_{gs} of an interacting system described by v_{ext}, which

means that $-v_{\mathrm{ext}} \in \underline{\partial} F(\rho_{\mathrm{gs}})$. The main assumption in the KS approach is that there exists an effective potential v_{KS} such that

$$-v_{\mathrm{KS}} \in \underline{\partial} F_{\mathrm{KS}}(\rho_{\mathrm{gs}}) \neq \emptyset.$$

Combining this assumption with that stationary condition of the proximal point of ρ_{gs}, Eq. (2), we obtain [2]

$$v_{\mathrm{KS}} = \lim_{\varepsilon \to 0} \frac{1}{\varepsilon} J((\rho_{\mathrm{gs}})_\varepsilon - \rho_{\mathrm{gs}}). \tag{3}$$

Equation (3) thus allows us to compute the effective KS potential using the simpler functional F_{KS} (that neglects the difficult interaction part coming from $\hat{W}$) given that

(i) we have knowledge of ρ_{gs},
(ii) ρ_{gs} is indeed non-interacting v-representable, i.e., $\underline{\partial} F_{\mathrm{KS}}(\rho_{\mathrm{gs}}) \neq \emptyset$, and
(iii) we have an efficient way of computing the proximal point $(\rho_{\mathrm{gs}})_\varepsilon$ and the limit in Eq. (3) numerically.

Regarding the last point, (iii), we are currently working on an implementation in a periodic setting ($X = H^{-1}_{\mathrm{per}}$) such that we can evaluate v_{KS} numerically employing a plane wave basis [3]. In this particular setting $J(\rho) = G^\mu * \rho$, where $G^\mu(x) = (4\pi|x|)^{-1} e^{-\mu|x|}$ is the Yukawa potential (with parameter $\mu > 0$). It is an open question how well the above described MY inverse KS approach can be used to determine v_{KS} for physical systems.

This work has received funding from the ERC-STG-2021 under grant agreement No. 101041487 REGAL.

References

[1] S. Kvaal, U. Ekström, A.M. Teale and T. Helgaker, *Differentiable but exact formulation of density-functional theory*, Journal of Chemical Physics **140** (2014), 18A518.
[2] M. Penz, M.A. Csirik and A. Laestadius, *Density-potential inversion from Moreau–Yosida regularization*, Electronic Structure **5** (2023), 014009.
[3] M.F. Herbst, V.H. Bakkestuen and A. Laestadius, *Kohn–Sham inversion with mathematical guarantees*, preprint (2025), arXiv:2409.04372.

A geometrical formulation of the Hohenberg-Kohn theorem on lattices

Robert van Leeuwen
(joint work with Markus Penz)

We give a geometrical perspective on spin-lattice density-functional theory (DFT) based on references [1, 2, 3] in which we closely follow the notation of [3]. Our main result will be an entirely geometrical formulation of the Hohenberg-Kohn (HK) theorem on lattices.

We consider putting N spin-$\frac{1}{2}$ particles on $M > N/2$ sites. The corresponding one-particle Hilbert space is thus $\mathbb{C}^{2M}$ which gets promoted into the N-particle Hilbert space $\mathcal{H} = (\mathbb{C}^{2M})^{\wedge N}$ by an N-fold antisymmetric tensor product. We denote a lattice index by $i \in \{1, \ldots, M\}$ and a spin index by $\alpha \in \{\uparrow, \downarrow\}$ and employ

shorthand notation for index tuples, $i\alpha \equiv (i, \alpha)$. We use the usual fermionic creation and annihilation operators $\hat{a}^\dagger_{i\alpha}, \hat{a}_{i\alpha}$ of the spin-lattice basis and write $\hat{\rho}_{i\alpha} = \hat{a}^\dagger_{i\alpha}\hat{a}_{i\alpha}$ for the number (density) operator and denote $\hat{\rho}_i = \hat{\rho}_{i\uparrow} + \hat{\rho}_{i\downarrow}$. We then consider the general class of Hamiltonians

$$\hat{H}_v = \hat{H}_0 + \sum_i v_i \hat{\rho}_i. \tag{1}$$

where $\hat{H}_0$ is a fixed Hamiltonian and $v = (v_1, \ldots, v_M)$ represents an external potential. We will take $\hat{H}_0$ to be of the general form

$$\hat{H}_0 = \sum_{ij,\alpha\beta} h_{i\alpha,j\beta}\, \hat{a}^\dagger_{i\alpha}\hat{a}_{j\beta} + \hat{W}, \tag{2}$$

where $\hat{W}$ is a general two-body interaction [1, 3] and h a Hermitian matrix. To $\hat{H}_0$ we can associate a graph in which we we say that $i\alpha$ and $j\beta$ are connected (or *adjacent*), written $i\alpha \sim j\beta$, whenever $h_{i\alpha,j\beta} \neq 0$.

The usual density, $\rho_i = \langle \hat{\rho}_i \rangle$, as site occupancy naturally allows $\rho_i \in [0, 2]$, due to the antisymmetry of the wave function and the possibility of filling two different spin channels. Additionally, we have the normalization to the number of particles N,

$$\sum_i \rho_i = N. \tag{3}$$

We thus define the density set

$$\mathcal{D} = \left\{ \rho \in \mathbb{R}^M \mid 0 \leq \rho_i \leq 2, \sum\nolimits_i \rho_i = N \right\} \tag{4}$$

for standard lattice DFT with spin-$\frac{1}{2}$ particles. This results in a doubly scaled $(M, N/2)$-hypersimplex for ρ_i if N even. If N odd the density space for ρ_i is slightly more complex, but it is always described by a $(M-1)$-dimensional convex polytope. If the particles are assumed spinless instead, the restricting inequality is $0 \leq \rho_i \leq 1$ and the resulting shape is a (M, N)-hypersimplex [1]. For each $v \in \mathcal{V}$ we now define the ground-state energy functional

$$E(v) = \inf_\Psi \langle \hat{H}_v \rangle_\Psi, \tag{5}$$

where the variation extends over all $\Psi \in \mathcal{H}$ normalized to 1. This functional is concave in v because of linearity in v and the properties of the infimum. Another immediate result is that this infimum is realized by some (or rather many) $\Psi \in \mathcal{H}$ since the variation domain is compact in the case of a finite lattice. One could thus equally write 'min' instead of 'inf'. The respective optimizer is then a ground-state wave function for $\hat{H}_v$.

If for a given $\rho \in \mathcal{D}$ there is further a potential $v \in \mathcal{V}$ such that the density is achieved by the corresponding (possibly ensemble) ground state of $\hat{H}_v$ then one calls this density *v-representable*. This is a subtle notion, but it can be proven that all densities from the interior of $\mathcal{D}$ are v-representable, while only a certain few densities on the boundary of $\mathcal{D}$ have this property [4, 1, 2]. Importantly, this

notion depends on the choice of $\hat{H}_0$ that then also determines which boundary densities can be reached.

The theoretical basis for DFT is the convex *universal density functional* that can be defined on $\mathcal{D}$ as the density-matrix constrained-search functional [1]

$$F(\rho) = \inf_{\Gamma \mapsto \rho} \mathrm{Tr}\hat{H}_0\Gamma. \tag{6}$$

Here, variation is over all density matrices that yield the given density ρ. The ground-state energy for a given $v \in \mathcal{V}$ is then

$$E(v) = \inf_{\Gamma} \mathrm{Tr}\hat{H}_v\Gamma = \inf_{\rho\in\mathcal{D}} \left\{F(\rho) + \langle v, \rho\rangle\right\}. \tag{7}$$

In other words, $E(v)$ is the Legendre–Fenchel transform (with non-standard sign convention) of $F(\rho)$ and concave as such. The back-transformation then gives $F(\rho)$ again,

$$F(\rho) = \sup_{v\in\mathcal{V}} \left\{E(v) - \langle v, \rho\rangle\right\}. \tag{8}$$

The optimum in Eqs. (7) and (8) is attained where the (concave or convex) functionals allow a zero tangent functional. Here, a tangent functional to a convex functional f at $\rho \in \mathcal{D}$ is any $v \in \mathcal{V}$ such that $f(\rho') \geq f(\rho) + \langle v, \rho' - \rho\rangle$ for all $\rho' \in \mathcal{D}$. For concave functionals the inequality is reversed. Further note that if f is non-differentiable at ρ, i.e., it has a kink, the tangent functional is non-unique. The set of all tangent functionals to a convex functional f is called the subdifferential, written $\underline{\partial} f(\rho)$. With $f(\rho) = F(\rho) + \langle v, \rho\rangle$ we have

$$0 \in \underline{\partial} f(\rho) = \underline{\partial} F(\rho) + v \quad \Leftrightarrow \quad -v \in \underline{\partial} F(\rho) \tag{9}$$

as a condition for $v \in \mathcal{V}$ being a maximizer in Eq. (8) and thus fulfilling $F(\rho) = E(v) - \langle v, \rho\rangle$. But this conversely implies $E(v) = F(\rho) + \langle v, \rho\rangle$ and so this $\rho \in \mathcal{D}$ is the minimizer in Eq. (7) and equivalently an element in the superdifferential of the concave $E(v)$,

$$\rho \in \overline{\partial} E(v). \tag{10}$$

So the above relation tells us that ρ is a ground-state density for v. The ground-state density can be non-unique if degeneracy occurs for the chosen v and this phenomenon will lead us to the next, important definition.

We define a *degeneracy region* $D(v) \subseteq \mathcal{D}$ as the set of densities coming from all (ensemble) ground states of the Hamiltonian $\hat{H}_v$ with a $v \in \mathcal{V}$ that facilitates ground-state degeneracy. By what has been said above, it is equal to the superdifferential of the concave ground-state energy functional $E(v)$,

$$\begin{aligned} D(v) &= \{\rho \in \mathcal{D} \mid \Gamma \mapsto \rho, \mathrm{Tr}\hat{H}_v\Gamma = E(v)\} \\ &= \overline{\partial} E(v) = \{\rho \in \mathcal{D} \mid \forall v' \in \mathcal{V} :\ E(v') \leq E(v) + \langle v' - v, \rho\rangle\}. \end{aligned} \tag{11}$$

A density region consists of v-representable densities (by definition) and it is always convex and closed. When the density variable does not contain any spin

information, degeneracy can be such that it only affects the internal spin degree-of-freedom and is thus not expressed in the density alone. Then $D(v)$ remains a single point and we call the degeneracy 'internal'.

Finally, we need to highlight that even though we presented these notions within a specific spin-lattice DFT setting, they hold quite generally, even for the infinite-dimensional continuum setting. Details about the proof and the intricate shape of density regions can be found in our study on the geometry of degeneracy [2]. We here summarize the results of [2]:

(1) If two density regions $D(v)$ and $D(v')$ intersect then $D(v) \cap D(v')$ is either a single ground-state density point or a density region itself. In both cases it results from all potentials that are a convex combination of v and v'.
(2) If a density region $D(v)$ touches the boundary of $\mathcal{D}$ then this density point results from all potentials that lie on a ray that extends from v to infinity.
(3) All densities that are not on the boundary of $\mathcal{D}$ are v-representable. Densities on the boundary of $\mathcal{D}$ need to be part of a degeneracy region in order to be v-representable. All v-representable densities that are not described by (a) or (b) are even *uniquely* v-representable.

We are thus in the position to formulate a purely geometrical HK theorem: *All ground-state densities that are not on the boundary of the density domain and that are not at the intersection of degeneracy regions are uniquely given by a potential.*

Examples for all mentioned situations (a)-(c) can be found in our previous works on the topic [1, 2, 3] and seemed to have been overlooked previously as counterexamples to the HK theorem.

References

[1] M.Penz and R. van Leeuwen, *Density-functional theory on graphs*, J.Chem. Phys. **155**, 244111 (2021)
[2] M.Penz and R. van Leeuwen, *Geometry of degeneracy in potential and density space*, Quantum **7**, 918 (2023)
[3] M.Penz and R. van Leeuwen, *Geometrical perspective on spin-lattice density-functional theory*, J.Chem. Phys. **161**, 150901 (2024)
[4] J.T. Chayes, I. Chayes and M.R.Ruskai, *Density functional approach to quantum lattice systems*, J. Stat. Phys. **38**, 497 (1985)

Approximate normalizations for approximate density functionals

Kieron Burke
(joint work with Kimberly Daas)

It is a truth universally acknowledged that any density functional calculation should yield a density that integrates to the number of electrons in the system. No matter how little is known about the functionals involved, this truth is so well fixed in the minds of practitioners that the normalization step passes almost unnoticed [2]. In the sixty years since the foundational papers, it has never been questioned that, even when minimizing an approximate energy functional, the best

normalization constraint is to require that the density integrates to the number of electrons in the system.

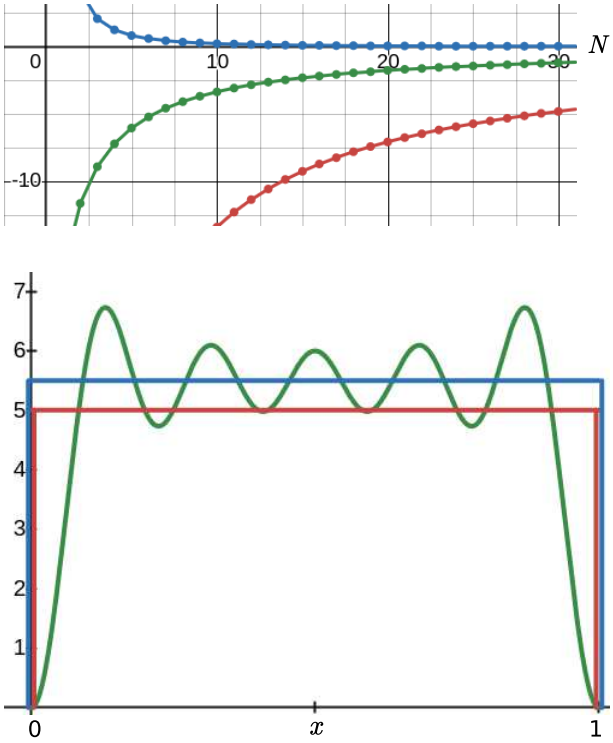

FIGURE 1. *Bottom*: Red is the TF density, green the exact density, and blue the normalization-corrected density for $N = 5$. *Top*: Percent errors for the corresponding energies, obtained by evaluating the TF functional on the densities.

In our work, we question this assumption by showing that approximate normalizations, defined as,

$$\int d\mathbf{r}\, n(\mathbf{r}) = \widetilde{N} = N + \Delta N \tag{1}$$

derived from asymptotic considerations, yields better energies for approximate functionals. Let us start with a simple example: N non-interacting, spinless electrons in one dimensional box with hard walls, i.e. the infamous particle(s)-in-a-box with $v = 0$ and $L = 1$. Fig. 1 compares three approximations for the energy $E(N)$. The first is the standard Density Functional Theory (DFT) treatment, where $n(x)$ is found by self-consistently finding the minimum of an approximate density functional, i.e. $n(x) = N$. In this case, we use the Thomas-Fermi energy [3, 4], which only contains the leading-order term in the large N expansion. This energy is

given by $\widetilde{E}(N)$, and visualized in red in the top panel, with its density in the bottom panel. The TF functional evaluated on the exact density is shown in green and is defined as $\widetilde{E}_{\mathrm{d}}(N)$. The blue curves come from our normalization-corrected functional,

$$\widetilde{E}_{\mathrm{nc}}(N) = \widetilde{E}(\widetilde{N}), \quad \widetilde{N} = N + \Delta N. \tag{2}$$

where $\Delta N = 1/2$, outperforms the other two approximations for all N. Thus, for this 1D case, ignoring the density oscillations yields a better energy than accounting for them and has the advantage of staying within the family of densities belonging to the TF functional, called the *foliation* of its graph space [5]. For a box or cavity, the TF densities are constants, and our correction yields the constant that best approximates the bulk, at the expense of the edge.

For one-dimensional systems, this normalization correction can be derived from WKB theorem by carefully keeping track of the Maslov index. In higher dimensions, we can use Weyl asymptotics [6, 7] to obtain exact information about the energy levels for many Hamiltonians, e.g. cavities [8]. Weyl asymptotics state that

$$E(N) = C_1 N^{1+2/d} + C_2 N^{1+1/d} + \cdots, \tag{3}$$

where C_1 and C_2 depend explicitly on the geometry of the cavity. In all of the studied cavity problems, in both 2 and 3 dimensions, the normalization correction improves massively on the TF energy and the density-corrected analogue. The results for $N = 100$ and $N = 1000$ for the 2D and 3D cavity problems can be found in Table 1.

	N	$E(N)$	$\widetilde{E}(N)$	$\widetilde{E}_{\mathrm{nc}}(N) = \widetilde{E}(\widetilde{N})$
2D	100	11,408	10,000 (-12%)	11,378 (-0.3%)
	1000	1,042,850	1,000,000 (-4%)	1,042,608 (-0.02%)
3D	100	5141	3633 (−29%)	5039 (−2%)
	1000	198838	168647 (−15%)	197873 (−0.5%)

TABLE 1. Exact and approximate energy values for the 2D circular cavity of radius one and 3D box with incommensurate edges $1 \times \sqrt{2} \times \pi$.

There exists no general recipe to find the normalization correction for general 3D cases, but for a few select systems the asymptotics are known. Indeed, for these cases our normalization correction is given by

$$\widetilde{E}(N) = AN^p, \ \Delta N = BN^q. \tag{4}$$

A key feature is that q is just a simple function of the dimensions (d), $q = \frac{1-d}{d}$, unlike p, A, or B. Moreover, the sign of B is related to the sign of the divergences in the potential, intuitively correcting the error of the TF density in the bulk.

For the noble gas dimers, a correction of $\Delta N = -3(14c_0)^{-1}N^{2/3}$ with $c_0 = 0.769745\ldots$ gives a percentage error of 1.5%, which is 10 times better than the

TF functional. The same high accuracy is found for the Bohr atom [9, 10, 11], which consists of non-interacting fermions (singly) occupying hydrogenic orbitals. Two different normalization corrections were used, one mimicking the interacting example ($Z = N \gg 1$ with $\Delta N = -\frac{3^{\frac{2}{3}}}{14} N^{\frac{2}{3}}$) and one mimicking the non-interacting examples ($Z = 1$ and $N \gg 1$ with $\Delta N = -\frac{3^{\frac{2}{3}}}{2} N^{\frac{2}{3}}$). The former is found to be more accurate, even outperforming the Scott correction [12] by almost a factor of 10 for $N = 55$.

Lastly, we look at the LDA exchange energy, which can be understood as an infinite box, analogously to the TF calculation of Fig. 1. We take an optimistic leap and assume that similar forms as Eq. 4 apply, so that we can multiply the density by $1 + \Delta N/N$, with $\Delta N = BN^{2/3}$. This yields

$$E_{\mathrm{x}}^{\mathrm{LDA}}(\mathrm{NC}) = (1 + B/N^{1/3})^{4/3} E_{\mathrm{x}}^{\mathrm{LDA}}. \tag{5}$$

We have chosen $B = 0.125$ by eye, which gives PBE-like [13] accuracy for large atoms, mirroring the improvements for the total energy of the previous examples.

In the future, there are many variations of our correction that could be applied to approximate Exchange Correlation functionals, not just the LDA one we derived here. The normalization-correction is also easy to implement for all the cases we have discussed. In the future, we will derive the exact normalization correction to any Exchange Correlation functionals and derive an exact machinery for general 3D Coulombic systems. Lastly, energy differences and density-dependent quantities should be studied as well, such as the ionization energies, electron affinities, or dipole moments. These investigations will shed some light on whether these corrections work only for the total energy or whether these are general corrections for any important quantity.

References

[1] Clay, A., Datchev, K., Miao, W., Wasserman, A., Daas, K.J., Burke, K. *Approximate normalizations for approximate density functionals* arXiv:2504.03845 (2025).

[2] Jane Austen, *Pride and Prejudice* (1813).

[3] Thomas, L. *The Calculation of Atomic Fields.* Mathematical Proceedings of the Cambridge Philosophical Society, **23**, 542–548 (1927).

[4] Fermi, Enrico *Un Metodo Statistico per la Determinazione di alcune Prioprietà dell'Atomo.* Rend. Accad. Naz. Lincei. **6**, 602–607 (1927).

[5] Alberto Candel and Lawrence Conlon, *Foliations I* Graduate Studies in Mathematics **23** (2000).

[6] Weyl, H. *Nachrichten von der Gesellschaft der Wissenschaften zu Göttingen, Mathematisch-Physikalische Klasse*, pages 110–117 (1911).

[7] H. Weyl, *Über die Randwertaufgabe der Strahlungstheorie und asymptotische Spektralgesetze.* J. reine angew. Math., **143**, pages 177–202 (1913).

[8] Victor Ivrii, *100 years of Weyl's law*, Bull. Math. Sci., **6**, pages 379–452 (2016).

[9] Heilmann, Ole J. and Lieb, Elliott H. *Electron density near the nucleus of a large atom*, Phys. Rev. A., **52** (5), pages 3628–3643 (1995).

[10] Berthold-Georg Englert, *Semiclassical Theory of Atoms* in *Lecture Notes in Physics*, Springer Berlin Heidelburg (1988).

[11] Pavel Okun and Kieron Burke, *Semiclassics: The hidden theory behind the success of DFT.* Chapter 7 in *Density Functionals for Many-Particle Systems*, World Scientific (2023).
[12] Scott, J. M. C., *The Binding Energy of the TF Atom*, Ser. 7 **43**, No. 343.
[13] Perdew, J. P. and Burke, K. and Ernzerhof, M., *Generalized Gradient Approximation Made Simple* Phys. Rev. Lett. **77** (1996).

A New Algorithm for Large-Scale Self-Consistent Field Calculations

Frank Neese

The vast majority of computer time that is spent world-wide on quantum chemical investigations undoubtedly goes into the solution of the self-consistent field (SCF) equations. In form of the Hartree-Fock (HF) method, the SCF solution forms the basis for subsequent electron correlation calculations. However, a far more prominent use of the SCF method is the solution of the Kohn-Sham (KS) equations in the framework of density functional theory (DFT). From a mathematical point of view, the KS and HF equations are closely related. They both have the identical one-electron part and Coulomb interaction. In the HF method, there furthermore is the exact exchange term that in KS is either absent or added in fractional form in hybrid functionals. Instead of the exchange term, KS features an exchange correlation (XC) potential the precise form of which varies with the specific approximation used. Since the precised form of the XC potential contains complicated fractional powers of the electron density, it is usually handled by numerical integration techniques.

In terms of scaling with systems size, the one-electron term scales cubically ($O(N^3)$) due to the presence of the electron nuclear attraction term which is a long-range Coulomb interaction. With proper thresholding techniques, the computational effort can be brought down to $O(N^2)$. The pre-factor for this term is very small and in addition, these integrals only need to be calculated once in each SCF while all other terms need to be recomputed in each SCF iteration given the nature of the SCF equations. The exchange correlation potential is readily reduced to $O(N)$ scaling in numerical integration. Making use of the Gaussian product theorem (GPT) and Kohn's conjecture, it is readily seen that the calculation of the exact exchange term has an asymptotic $O(N)$ scaling provided suitable thresholding techniques are used. This leaves the Coulomb term as the most-expensive contribution of the Fock (Kohn-Sham) matrix with a large pre-factor and $O(N^2)$ scaling.

The Coulomb contribution to the KS matrix represents a quasi-classical interaction between an electron in a basis function pair (pq) and the entire electron density (ρ). The pre-factor of this term can be drastically reduced (up to two-orders of magnitude) by the so-called "resolution of the identity" (RI) approximation. In this approximation, products of basis functions are expanded in terms of a fixed, atom centered auxiliary basis (AUX). The coefficients for the expansion are determined by minimizing the self-repulsion of the error made in the approximation. This provides a lower bound to the true Coulomb energy and saves computer time because expensive and numerous four-index repulsion integrals over basis function

quadruplets are replaced by much cheaper and less numerous three-index repulsion integrals of basis function pairs and one auxiliary function. The error of the RI approximation is typically significant (up to mEh in larger molecules) but extremely smooth such that energy differences remain very accurate.

In order to reduce the scaling of the Coulomb term to $O(N)$, it is customary to employ multipole methods. Specifically, the fast multipole method (FMM) has gained significant popularity. In this method, real space is divided into boxes. Each box consist then of smaller and smaller sub-boxes up to a pre-defined "depth". The algorithm then proceeds by calculating the multipole moments of the electron density inside each box and then a translation of these multipoles from each sub-level box to the next higher-level box in the hierarchy. The interaction of a given shell pair with the box multipoles then proceeds by the multipole approximation to the integrals that is terminated at a pre-determined angular momentum LMAX provided that a "well-separatedness" (WS) criterion is met. The totality of all interactions handled by the multipole approximation is called "far field" (FF) while the remaining interactions belong to the near-field (NF). Since the NF of a given shell pair typically consists of only next neighbors of which there is an asymptotically constant number for a given shell pair, the calculation of the NF is linear scaling. The FF calculation is then readily shown to be linear scaling as well since it involves a very small number of matrix multiplications to evaluate the multipole interactions.

The FMM method is known to work very well and provide results of high accuracy. However, the boxing algorithm is somewhat problematic since it will arbitrarily cut through chemical bonds or atoms and the distribution of box content might vary drastically over the volume of a molecule. In addition, the content of the boxes will depend on the orientation of the molecule thus potentially leading to slightly rotationally non-invariant results.

In our work, we have developed a variant of the FMM method that avoids some of its pitfalls of the FMM method. In our method, called the "Bubblepole approximation" (BUPO) instead of boxes, a hierarchy of spheres is introduced. These spheres contain shell pairs or auxiliary functions in a way that the boundary of the spheres fully encloses the shell pair or AUX function. The spheres are chosen such that shell pairs with close lying centers are grouped together in one "bubble". This is accomplished by a Kmeans algorithm. This leads to a very even distribution of shell pairs among bubbles and also to a very natural NF / FF division since no leakage of probability amplitudes or electron density out of the bubbles can occur. We demonstrate that this leads to a linear scaling approximation to the Coulomb term that has a small pre-factor and outperforms traditional algorithms for large molecules. Calculations with thousands of atoms and up to 50000 basis functions have been performed on modest hardware with this algorithm.

The BUPO algorithm together with linear scaling approximations to the exact exchange as well as linear scaling numerical integration algorithms for the XC terms leads to fully linear scaling Fock matrix construction algorithms that form the basis for highly efficient SCF calculations on large molecules such as

whole solvated proteins, DNA fragments or solids (in conjunction with embedding techniques).

The algorithms are implemented in the freely available large-scale quantum chemistry program suite ORCA.

References

[1] F. Neese, P. Colinet, B. DeSouza, B. Helmich-Paris, F. Wennmohs, U. Becker, *The "Bublepole" (BUPO) Method for Linear-Scaling Coulomb Matrix Construction with or without Density Fitting*, The Journal of Physical Chemistry A **129**, 10:2618-2637

Toward optimal-scaling (stochastic) density functional theory

Michael Lindsey

Stochastic density functional theory aims to achieve linear computational scaling with respect to the number of grid points or basis functions, independent of the number of electrons. To achieve such optimal scaling, stochastic DFT constructs the electron density using a stochastic estimator that avoids the explicit formation of orbitals. We advance the first mathematical theory of stochastic DFT in the simplified setting of the Hartree approximation. By viewing the method through the lens of mirror descent, we establish a convergence result validating such near-optimal scaling at arbitrary temperature, in both the complete basis set and thermodynamic limits. Implications for more general DFTs are discussed.

References

[1] Ming Chen, Roi Baer, Daniel Neuhauser, Eran Rabani, *Stochastic density functional theory: Real- and energy-space fragmentation for noise reduction*, J. Chem. Phys. **154**, 204108 (2021).

A posteriori error estimates for LCAO basis

Mi-Song Dupuy

(joint work with Geneviève Dusson, Ioanna-Maria Lygatsika)

To compute properties of an electronic system using Kohn-Sham density functional theory, it is customary to first solve a nonlinear eigenvalue problem for $(\psi_i)_{1\leq i\leq N} \in H^1(\mathbb{R}^3)$

$$\left(-\frac{1}{2}\Delta + V[\rho_{[\Psi^0]}]^{\mathrm{KS}}\right)\psi_i^0 = \lambda_i^0\psi_i^0, \quad i=1,\dots,N, \quad \text{with} \quad \rho_{[\Psi^0]} = 2\sum_{i=1}^{N}|\psi_i^0|^2.$$

The potential V^{KS} is the sum of

- an external potential $V_{\mathrm{ext}} = -\sum_{k=1}^{K}\frac{Z_k}{|\cdot - R_k|}$ where $(R_k)_{1\leq k\leq K}$ are the positions of the nuclei and $(Z_k)_{1\leq k\leq K}$ their charges.
- an exchange-correlation potential.

Three types of errors can occur in numerically solving this equation:

- modelling error: the exact exchange-correlation potential is not known, thus its choice induces an error;
- algorithmic error: the equation is nonlinear and is solved iteratively;
- discretisation error: the nonlinear eigenvalue problem is solved using a Galerkin subspace yielding an error.

The main purpose of this work [1] is to investigate the a posteriori error estimates for the discretisation error that are efficient to compute and suited to Gaussian basis sets widely used in quantum chemistry.

We focus the analysis to linear Schrödinger type operators of the form

$$A = -\frac{1}{2}\Delta + \sum_{k=1}^{K} V_k + \sigma,$$

where V_k are radial potentials centered at R_k and σ is a constant such that A is coercive. The Galerkin subspace formed by the Gaussian basis sets are of the form $\{(\chi_{\alpha_i \ell_i m_i}(\cdot - R_1)), \ldots, (\chi_{\alpha_i \ell_i m_i}(\cdot - R_K))\}$ where each $\chi_{\alpha \ell m}$ is the product of a polynomial and a gaussian function. A priori analysis of the approximation by Gaussian basis sets are scarce in the mathematical literature [2], which pushes the need of an efficient adaptive scheme.

For a posteriori error computation for source or eigenvalue problems, dual norms of the form $\langle v, A^{-1} v\rangle$ have to be computed, which is costly. The main idea of our work is to introduce a partition of unity $(p_k)_{1\le k\le K+1}$ where the first K functions have support on balls centered at R_k, to estimate the dual norm by

$$\langle v, A^{-1} v\rangle \le C \sum_{k=1}^{K+1} \langle \sqrt{p_k} v, A_k^{-1} \sqrt{p_k} v\rangle,$$

with $A_k = -\frac{1}{2}\Delta + V_k$ with domain $H_0^2(\Omega_k)$ (except $k = K+1$, $V_{K+1} = \sigma$ and A_{K+1} has domain $H^2(\mathbb{R}^d)$).

The right-hand-side involves the inversion of radial operators which is cheap in practice.

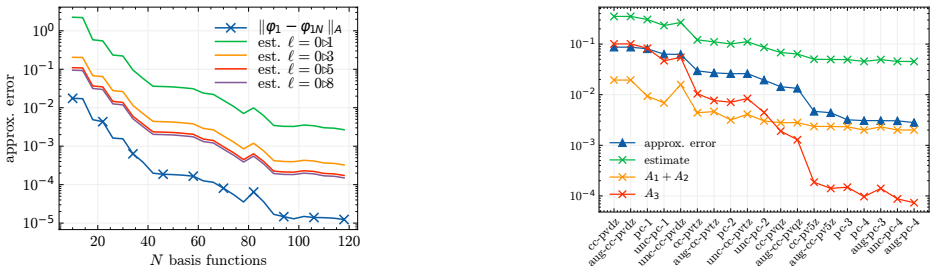

FIGURE 1. Test of the a posteriori bounds for one-dimensional (left) and three-dimensional (right) problems

The error estimator has been tested on one-dimensional and three-dimensional model showing promising results (see Figure 1).

The method can also be used to adaptively tune the basis set. Since the estimator is split between each nucleus (and an extra term), we can identify on which atom it may be better to refine the basis. This has also been tested in one-dimensional and three-dimensional models showing good results.

The next stages would be to design a practical error estimator for other electronic properties, like forces.

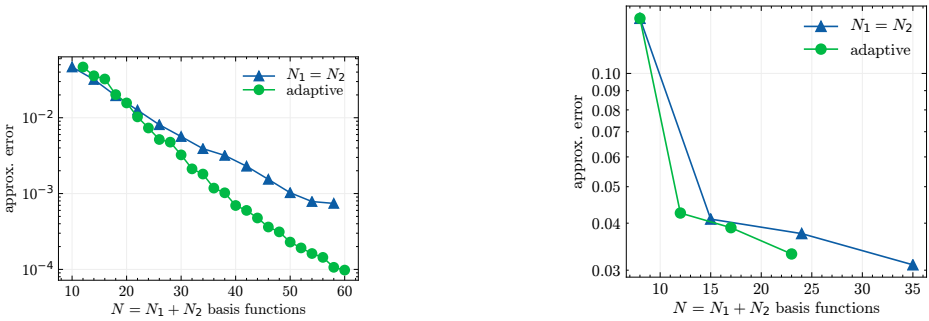

FIGURE 2. Convergence of the adaptive schemes for one-dimensional (left) and three-dimensional (right) problems

REFERENCES

[1] G. Dusson, M.-S. Dupuy, and I.-M. Lygatsika. *A posteriori error estimates for Schrödinger operators discretized with linear combinations of atomic orbitals*, arXiv preprint arXiv:2410.04943 (2024).

[2] M. Bachmayr, H. Chen, and R. Schneider. *Error estimates for Hermite and even-tempered Gaussian approximations in quantum chemistry*, Numerische Mathematik **128** (2014), 1:137–165.

Fully guaranteed and computable error bounds on the energy for periodic Kohn–Sham equations with convex density functionals

GASPARD KEMLIN

(joint work with Andrea Bordignon, Geneviève Dusson, Éric Cancès, Rafael Antonio Lainez Reyes, Benjamin Stamm)

In this talk, we considered a DFT energy functional of the form

$$E(\gamma) = \mathrm{Tr}(h\gamma) + F(\rho_\gamma), \tag{1}$$

where h is the core Hamiltonian and ρ_γ the electronic density. This is the prototypical form of energy in density functional theory, where

$$F(\rho) = \frac{1}{2}\mathcal{D}(\rho,\rho) + E_{\mathrm{xc}}(\rho),$$

with $\mathcal{D}$ the Coulomb interaction-energy while E_{xc} is the exchange-correlation energy. For a molecular or material system with N_{el} electrons without spins, we seek to minimize this energy over the manifold of all density matrices γ such that $\mathrm{Tr}(\gamma) = N_{\mathrm{el}}$, that is to say the manifold of orthonormal projectors of rank N_{el} with finite kinetic energy. Writing the first order condition yields the famous Kohn–Sham equations

$$\begin{cases} H_{\rho_\gamma}\phi_i = \lambda_i\phi_i, \quad i = 1, \dots, N_{\mathrm{el}}, \\ \langle \phi_i, \phi_j \rangle = \delta_{ij}, \quad i, j = 1, \dots, N_{\mathrm{el}}, \\ \gamma = \displaystyle\sum_{i=1}^{N_{\mathrm{el}}} |\phi_i\rangle\langle\phi_i|. \end{cases} \tag{2}$$

These equations take the form of a nonlinear eigenvector problem, where H_{ρ_γ} is the effective Kohn–Sham Hamiltonian. They are typically solved through fixed-point like iterative procedures known as SCF iterations. After discretization in an appropriate finite dimensional subspace $\mathcal{V}_N$ of dimension N (such as planewaves, finite element or localized atomic orbitals bases) the algorithm reads, in its simplest form,

$$\begin{cases} \Big(\Pi_N H_{\rho_{\gamma_{N,m}}} \Pi_N\Big)\, \phi_{i,N,m+1} = \lambda_{i,N,m+1}\phi_{i,N,m+1}, \quad i = 1, \dots, N_{\mathrm{el}}, \\ \langle \phi_{i,N,m+1}, \phi_{j,N,m+1} \rangle = \delta_{ij}, \quad i, j = 1, \dots, N, \\ \gamma_{N,m+1} = \displaystyle\sum_{i=1}^{N_{\mathrm{el}}} |\phi_{i,N,m+1}\rangle\langle\phi_{i,N,m+1}|, \end{cases} \tag{3}$$

where Π_N is the projection onto $\mathcal{V}_N$ and m is the SCF iteration. We assume here that the *Aufbau* principle holds, so that the eigenvalues correspond to the N_{el} smallest ones, and that the spectral gap $\lambda_{N_{\mathrm{el}}+1} - \lambda_{N_{\mathrm{el}}}$ is positive. Applying the strategy developed in [2] for *linear*, bounded below, self-adjoint operators with compact resolvent to the linear operators $H_{\rho_{\gamma_{N,m}}}$, we are able to compute a guaranteed lower bound on the average of the eigenvalues at each iteration of the SCF algorithm. This yields in turn a computable constant $\mu^{\mathrm{lb}}_{N,m+1}$ such that, for any $N > 0$ and $m \in \mathbb{N}$, we have the following guaranteed bound between the energy of the ground-state $\gamma_\star$ and the energy of $\gamma_{N,m}$, the discrete solution at iteration m of the SCF in $\mathcal{V}_N$:

$$\boxed{E(\gamma_{N,m}) - E(\gamma_\star) \leq \mathtt{err}^{\mathrm{disc}}_{N,m} + \mathtt{err}^{\mathrm{SCF}}_{N,m},} \tag{4}$$

where

$$\mathtt{err}^{\mathrm{disc}}_{N,m} \coloneqq \mathrm{Tr}\big((H_{\rho_{\gamma_{N,m}}} - \mu^{\mathrm{lb}}_{N,m+1})\gamma_{N,m+1}\big) \geq 0 \tag{5}$$

represents the contribution of the discretization error to the total error and

$$\mathtt{err}^{\mathrm{SCF}}_{N,m} \coloneqq \mathrm{Tr}(H_{\rho_{\gamma_{N,m}}}\gamma_{N,m}) - \mathrm{Tr}(H_{\rho_{\gamma_{N,m}}}\gamma_{N,m+1}) \geq 0 \tag{6}$$

stands for the algorithmic consistency error during the SCF iterations. Note that such a splitting paves the way for adaptive refinement strategies.

So far, this strategy is basis independent. The constants $\mu^{\mathrm{lb}}_{N,m+1}$ depend on the residuals $H_{\rho_{\gamma_{N,m}}}\phi_{i,N,m+1} - \lambda_{i,N,m+1}\phi_{i,N,m+1}$ in different norms. Their evaluation requires in particular the inversion of the full operator $H_{\rho_{\gamma_{N,m}}}$. This is of course too expensive to be executed at each SCF iteration and we suggest an efficient, but approximate, inversion scheme based on a frequency splitting. We take advantage here of the specificity of periodic systems, where planewaves bases are commonly used, since the Laplace operator is then diagonal and thus immediate to inverse. We refer the interested reader to [1] and references therein for more details.

The talk was concluded by a series of 1D and 3D numerical examples to illustrate the sharpness of the bound for the (convex) rHF model, even with an approximate inversion. We also showed that these bounds are still accurate when the functional F is not convex anymore (such as for LDA and PBE exchange-correlation functionals), see for instance Figure 1 where we track the total error and display the two components of the bound in (4) along the SCF iterations.

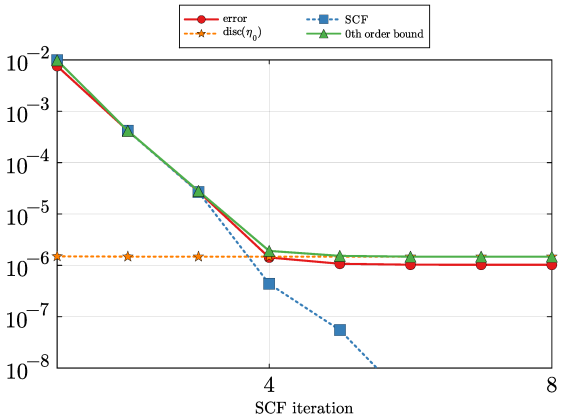

FIGURE 1. Tracking of the discretization and algorithmic errors along SCF iterations for a Silicon crystal with LDA exchange-correlation functional. The green (triangle) curve is the total error bound, written as the sum of the blue (square) and orange (star) curves. The red (circle) is the true error, unknown in practice.

REFERENCES

[1] A. Bordignon, E. Cancès, G. Dusson, G. Kemlin, R.A. Lainez Reyes, B. Stamm, *Fully guaranteed and computable error bounds on the energy for periodic Kohn-Sham equations with convex density functionals*, arXiv preprint arXiv:2409.11769 (2024).

[2] E. Cancès, G. Dusson, Y. Maday, B. Stamm, M. Vohralík, *Guaranteed a posteriori bounds for eigenvalues and eigenvectors: Multiplicities and clusters*, Mathematics of Computation **89** (2020), pp. 2563–2611.

Stochastic Reconfiguration with Warm-Started SVD

Dexuan Zhou
(joint work with Huajie Chen, Cheuk Hin Ho, Xin Liu, Christoph Ortner)

We propose an efficient optimization method for variational Monte Carlo (VMC): the *Warm-Started Stochastic Reconfiguration* (WSSR) method. It enhances the standard stochastic reconfiguration (SR) approach by incorporating warm-started singular value decomposition (SVD), allowing low-rank approximations to be efficiently updated across optimization steps.

Overview

Solving the ground state of the many-electron Schrödinger equation remains challenging. Variational Monte Carlo (VMC) provides a flexible framework for accurate wave function approximations, but optimization remains difficult due to the rough energy landscape and high dimensionality.

Stochastic Reconfiguration (SR) [4], based on imaginary time evolution, preconditions gradients using the Fubini-Study metric. However, computing and inverting the covariance matrix $\mathcal{S} \in \mathbb{R}^{\mathcal{M}\times\mathcal{M}}$, where $\mathcal{M}$ is the number of parameters, is expensive:

$$\mathcal{S}(\boldsymbol{\theta}) := \mathbb{E}_{\boldsymbol{x}\sim P(\cdot;\Psi_{\boldsymbol{\theta}})}\left[\mathcal{O}(\boldsymbol{x};\boldsymbol{\theta})\cdot\mathcal{O}(\boldsymbol{x};\boldsymbol{\theta})^{\top}\right] \in \mathbb{R}^{\mathcal{M}\times\mathcal{M}}, \tag{1}$$

with

$$\mathcal{O}(\boldsymbol{x};\boldsymbol{\theta}) = \left(\partial_{\boldsymbol{\theta}}\log\left|\Psi_{\boldsymbol{\theta}}(\boldsymbol{x})\right| - \mathbb{E}_{\boldsymbol{x}\sim P(\cdot;\Psi_{\boldsymbol{\theta}})}\left[\partial_{\boldsymbol{\theta}}\log\left|\Psi_{\boldsymbol{\theta}}(\boldsymbol{x})\right|\right]\right) \in \mathbb{R}^{\mathcal{M}}. \tag{2}$$

Recent works such as the Minimum-Step Stochastic Reconfiguration (MinSR) method [1] and the Subsampled Projected-Increment Natural Gradient Descent (SPRING) algorithm [2] have been proposed to improve the efficiency and stability of SR-based optimization.

Warm-Started SR Method

Warm-Started Stochastic Reconfiguration method (WSSR) replaces the full inversion of $\mathcal{S}$ with a low-rank approximation using truncated SVD. At each iteration, we update:

- **Low-rank covariance matrix:** Efficiently approximates the matrix $\mathcal{O}(\boldsymbol{x};\boldsymbol{\theta})$ by truncated SVD to construct a low-rank covariance matrix.
- **Gradient:** Computed with respect to the low-rank representation to ensure consistency and reduce computational cost.

Building on the previous iteration, we observe that the dominant singular value decomposition (SVD) can be updated via simple subspace iteration (SSI) or reframed as an optimization problem [3]. By concurrently updating the singular vectors during the solution process, we implement a warm-start strategy that capitalizes on the incremental changes between consecutive iterations to substantially reduce computational costs.

References

[1] A. Chen and M. Heyl, *Empowering deep neural quantum states through efficient optimization*, Nature Physics, 2024, pp. 1–6.

[2] G. Goldshlager, N. Abrahamsen, and L. Lin, *A Kaczmarz-inspired approach to accelerate the optimization of neural network wavefunctions*, Journal of Computational Physics **516**, 113351 (2024).

[3] X. Liu, Z. Wen, and Y. Zhang, *Limited memory block Krylov subspace optimization for computing dominant singular value decompositions*, SIAM Journal on Scientific Computing **35**, pp. A1641–A1668 (2013).

[4] S. Sorella, M. Casula, and D. Rocca, *Weak binding between two aromatic rings: Feeling the van der Waals attraction by quantum Monte Carlo methods*, The Journal of Chemical Physics, **127**, 014105 (2007).

Recent advances in tensor network state methods via mode optimization and AI accelerators: a journey from mathematical aspects towards industrial perspectives

Örs Legeza

In the past three decades, tensor network state (TNS) methods, originating from the seminal work of S. R. White on the density matrix renormalization group (DMRG) method [1], have become vital alternative approaches to treat strongly correlated, i.e., multireference problems in quantum chemistry [2, 3, 4, 5]. Despite great successes in the past thirty years [6], TNS-based methods still witness significant algorithmic and IT-technology-related developments broadening their scope of application to a great extent by reducing computational time drastically.

In this contribution, we present an overview of tensor network state methods and related optimization protocols based on concepts of quantum information theory. We also highlight recent advances that have the potential to broaden their scope of application radically for strongly correlated molecular systems.

We discuss global fermionic mode optimization, i.e., a general approach to finding an optimal matrix product state (MPS) parametrization of a quantum many-body wave function with the minimum number of parameters for a given error margin [7, 8] that also has the potential to compress multireference character of the underlying wave function. The combination of mode optimization and time-dependent phenomena based on the time-dependent variational principle is also addressed, together with Lindbladian evolution in dissipative quantum systems [9].

Various embedding approaches are introduced to capture both static and dynamic correlations, such as the externally corrected DMRG-TCC [10], the self-consistent field DMRG-SCF, or restricted active space DMRG-RAS-X methods [11]. For the latter one, detailed error analysis and a new extrapolation method to recover the full-CI energy within chemical accuracy are also presented.

Finally, we demonstrate that altogether several orders of magnitude in computational time can be saved by performing calculations on an optimized basis and by utilizing modern AI accelerator based hybrid CPU-multiGPU parallelization. A scaling analysis for the SU(2) spin-adapted DMRG on NVIDIA DGXH100 hardware [12] and DMRG-SCF-based orbital optimizations for unprecedented CAS

sizes of up to 82 electrons in 82 orbitals [CAS(82,82)] in molecular systems comprising active spaces sizes of hundreds of electrons in thousands of orbitals [13] closes our journey.

References

[1] S. R. White, *Density matrix formulation for quantum renormalization groups*, Phys. Rev. Lett. **69**, 2863 (1992).

[2] G. K.-L. Chan and S. Sharma, The density matrix renormalization group in quantum chemistry, Annual Review of Physical Chemistry **62**, 465 (2011).

[3] Sz. Szalay, M. Pfeffer, V. Murg, G. Barcza, F. Verstraete, R. Schneider, and O. Legeza, Tensor product methods and entanglement optimization for ab initio quantum chemistry, Int. J. Quantum Chem. **115**, 1342 (2015).

[4] A. Baiardi and M. Reiher, The density matrix renormalization group in chemistry and molecular physics: Recent developments and new challenges, The Journal of Chemical Physics **152**, 040903 (2020).

[5] Y. Cheng, Z. Xie, and H. Ma, Post-density matrix renormalization group methods for describing dynamic electron correlation with large active spaces, The Journal of Physical Chemistry Letters **13**, 904 (2022).

[6] F. Verstraete, T. Nishino, U. Schollwöck, M. C. Banuls, G. K. Chan, and M. E. Stoudenmire, Density matrix renormalization group, 30 years on, Nature Reviews Physics, 1 (2023).

[7] C. Krumnow, L. Veis, O. Legeza, and J. Eisert, Fermionic orbital optimization in tensor network states,Phys. Rev. Lett. **117**, 210402 (2016).

[8] G. Friesecke, M. A. Werner, K. Kapas, A. Menczer, and Ors Legeza, Global fermionic mode optimization via swap gates, arXiv:2406.03449 (2024).

[9] C. P. Moca, M. A. Werner, O Legeza, T. Prosen, M. Kormos, and G. Zarand, Simulating Lindbladian evolution with non-abelian symmetries: Ballistic front propagation in the SU(2) Hubbard model with a localized loss, Phys. Rev. B **105**, 195144 (2022).

[10] L. Veis, A. Antalik, J. Brabec, F. Neese, O. Legeza, and J. Pittner, Coupled cluster method with single and double excitations tailored by matrix product state wave functions, The Journal of Physical Chemistry Letters **7**, 4072 (2016).

[11] G. Friesecke, G. Barcza, and O. Legeza, Predicting the fci energy of large systems to chemical accuracy from restricted active space density matrix renormalization group calculations, Journal of Chemical Theory and Computation **20**, 87 (2023).

[12] A. Menczer, M. van Damme, A. Rask, L. Huntington, J. Hammond, S. S. Xantheas, M. Ganahl, and O. Legeza, Parallel implementation of the Density Matrix Renormalization Group method achieving a quarter petaFLOPS performance on a single DGX-H100 GPU node, Journal of Chemical Theory and Computation **20**, 8397 (2024).

[13] O Legeza, A Menczer, A Ganyecz, M.A. Werner, K. Kapas, J. Hammond, S. S. Xantheas, M. Ganahl, and F. Neese, Orbital optimization of large active spaces via AI-accelerators, arxiv:2503.20700 (2025).

Unitary Coupled-Cluster Theory in a Strong Magnetic Field

Laura Grazioli

(joint work with Stella Stopkowicz, Jürgen Gauss)

The accurate and efficient description of the electron-correlation energy is one of the main issues in theoretical quantum chemistry. For the so-called single-reference problems, the Coupled-Cluster (CC) parameterization of the wave function is able

to recover most of the correlation energy. In particular, the CCSD(T) approximation (which considers single and double excitations exactly, and perturbative triple excitations) is known as the gold standard in quantum chemistry for its accuracy.

However, in specific chemical settings, for example near conical intersections or in the presence of a strong magnetic field, CC theory can give complex energy results, which cannot be given a physical meaning. In this work, we focus on the effect of a strong external magnetic field. In the so-called *mixing regime*, the external magnetic field is of the same order of the atomic unit (around 235 000 T). In this setting, the magnetic field cannot be treated perturbatively: Coulomb and Lorenz forces have to be treated on the same footing. The electronic Hamilton operator in a magnetic field is

$$\hat{H}_{\mathrm{el}} = \hat{H}_{0,\mathrm{el}} + \frac{1}{2}\sum_i \mathbf{B}\cdot\hat{\mathbf{L}}_{i\mathrm{O}} + \sum_i \mathbf{B}\cdot\hat{\mathbf{s}}_i + \frac{1}{8}(B^2 r_{i\mathrm{O}}^2 - (\mathbf{B}\cdot\mathbf{r}_{i\mathrm{O}})^2). \tag{1}$$

where $\hat{H}_{0,\mathrm{el}}$ is the field-free electronic Hamilton operator. The angular momentum operator $\hat{L}$ is a complex operator. This makes calculations in the presence of a magnetic field only feasible with a code with implemented complex algebra. Furthermore, the Hamilton operator depends on the choice of the gauge-origin O. To avoid gauge-origin dependent results, calculations need to be performed with gauge-including atomic orbitals (GIAOs). [1]

CC theory is characterized by an exponential parameterization of the wave function

$$|\Psi_{\mathrm{CC}}\rangle = e^{\hat{T}}\,|\Psi_0\rangle \qquad \hat{T} = \sum_\nu t_\nu \hat{\tau}_\nu = \sum_{ia} t_i^a \{\hat{a}^\dagger \hat{i}\} + \frac{1}{4}\sum_{ijab} t_{ij}^{ab}\{\hat{a}^\dagger \hat{b}^\dagger \hat{j}\hat{i}\} + \dots \tag{2}$$

where $|\Psi_0\rangle$ is the reference Slater determinant, here chosen to be the Hartree-Fock wave function, and the $\hat{T}$ operator (cluster operator) is given by a linear combination of excitation operators. From the time-independent Schrödinger equation

$$\hat{H}e^{\hat{T}}\,|\Psi_0\rangle = E_{\mathrm{CC}}e^{\hat{T}}\,|\Psi_0\rangle \tag{3}$$

the energy is determined via projection on the reference determinant, giving

$$E_{\mathrm{CC}} = \langle\Psi_0|\, e^{-\hat{T}}\hat{H}e^{\hat{T}}\,|\Psi_0\rangle\,. \tag{4}$$

This expression is not Hermitian, thus not guaranteeing real energy values and leading to the unphysical results previously mentioned.

The aim of this work is to explore a unitary parameterization of the wave function, retaining the exponential form typical of standard CC theory. The ansatz for the so-called Unitary Coupled-Cluster (UCC) theory is

$$|\Psi_{\mathrm{UCC}}\rangle = e^{\hat{\sigma}-\hat{\sigma}^\dagger}\,|\Psi_0\rangle \qquad \hat{\sigma} = \sum_\nu \sigma_\nu \hat{\tau}_\nu = \sum_{ia} \sigma_i^a \{\hat{a}^\dagger \hat{i}\} + \frac{1}{4}\sum_{ijab} \sigma_{ij}^{ab}\{\hat{a}^\dagger \hat{b}^\dagger \hat{j}\hat{i}\} + \dots, \tag{5}$$

where the $\hat{\sigma}$ operator is the cluster excitation operator, analogous to the CC one. In the UCC framework, the time-independent Schrödinger equation is formulated

as

$$\hat{H}e^{\hat{\sigma}-\hat{\sigma}^\dagger}\,|\Psi_0\rangle = E_{\mathrm{UCC}}e^{\hat{\sigma}-\hat{\sigma}^\dagger}\,|\Psi_0\rangle\,. \tag{6}$$

The UCC energy and amplitudes are found through projection on the reference and the excited determinants, respectively

$$E_{\mathrm{UCC}} = \langle\Psi_0|\,e^{-(\hat{\sigma}-\hat{\sigma}^\dagger)}\hat{H}e^{\hat{\sigma}-\hat{\sigma}^\dagger}\,|\Psi_0\rangle \tag{7}$$

$$0 = \langle\Psi_{ijk\ldots}^{abc\cdots}|\,e^{-(\hat{\sigma}-\hat{\sigma}^\dagger)}\hat{H}e^{\hat{\sigma}-\hat{\sigma}^\dagger}\,|\Psi_0\rangle \tag{8}$$

The energy expression is Hermitian and yields only real values. The presence of both excitation and de-excitation operators in the exponential makes the expansion of the similarity-transformed Hamiltonian $\bar{H} = e^{-(\hat{\sigma}-\hat{\sigma}^\dagger)}\hat{H}e^{\hat{\sigma}-\hat{\sigma}^\dagger}$ more involved than for CC, as the resulting series of nested commutators does not self-truncate. One of the main issues debated in UCC theory is the choice of the truncation scheme. In this work, we focus on a particular scheme, in which the excitation space is restricted to single and double excitations (analogously to CCSD), while the amplitude equations are truncated at third order in Møller-Plesset perturbation theory. This approach has been denominated UCC3. [2]

The unitary parameterization can be extended to describe the excited states, through the form

$$|\Psi_k\rangle = e^{\hat{\sigma}-\hat{\sigma}^\dagger}\hat{R}_k\,|\Psi_0\rangle \qquad \hat{R}_k = r_0 + \sum_{ia} r_i^a\{\hat{a}^\dagger\hat{i}\} + \frac{1}{4}\sum_{ijab} r_{ij}^{ab}\{\hat{a}^\dagger\hat{b}^\dagger\hat{j}\hat{i}\} + \ldots \tag{9}$$

where a linear excitation operator $\hat{R}_k$ is applied to the reference determinant, before applying the unitary transformation.

The UCC3 scheme is directly comparable to CCSD, as it is characterized by the same excitation space (single and double excitations) and shares the same scaling properties ($\sim N^6$ with system size).

In this study, we have compared energy results obtained with CCSD and UCC3 theories, in order to understand whether the imaginary part in the CCSD energy values can be related to properties of the wave function, or if it is just an artifact arising from the non-Hermiticity of CC theory. [3]

CC theory also leads to unphysical results in the calculation of transition dipole moments. In exact theory, the transition dipole moment from state Ψ_I to state Ψ_J is the complex conjugate of the transition dipole moment from state Ψ_J to state Ψ_I, giving $\langle\Psi_I|\,\hat{\mu}\,|\Psi_J\rangle = \langle\Psi_J|\,\hat{\mu}\,|\Psi_I\rangle^*$. However, due to the non-Hermiticity of CC theory, this symmetry is no longer satisfied. Thus, when calculating the transition probability as

$$|\mu_{IJ}^{\mathrm{CC}}|^2 = \langle\Psi_I|\,\hat{\mu}\,|\Psi_J\rangle\,\langle\Psi_J|\,\hat{\mu}\,|\Psi_I\rangle \tag{10}$$

negative probabilities can be obtained, which clearly have no physical meaning.

We have developed a response-theory approach for the calculation of transition dipole moments in the framework of UCC3 theory. We have formulated a Lagrange functional which satisfies the symmetry $\langle\Psi_I|\,\hat{\mu}\,|\Psi_J\rangle = \langle\Psi_J|\,\hat{\mu}\,|\Psi_I\rangle^*$, due to the Hermiticity of UCC theory.

Through this formulation, we were able to calculate spectra of molecules for which CC theory fails, giving always strictly positive transition probabilities. [4]

The promising results of UCC3 theory, which showed to have an accuracy comparable to CCSD, encourage to investigate also other truncation schemes, for example higher orders in perturbation theory or non-perturbative approaches.

References

[1] F. London, *Théorie quantique des courants interatomiques dans les combinaisons aromatiques*, J. Phys. Radium **8** (1937), 397–409.

[2] J. Liu, A. Asthana, L. Cheng, and D. Mukherjee, *Unitary coupled-cluster based self-consistent polarization propagator theory: A third-order formulation and pilot applications*, J. Chem. Phys. **148** (2018), 244110

[3] L. Grazioli, and S. Stopkowicz, *Unitary coupled-cluster theory for the treatment of molecules in strong magnetic fields*, in preparation (2025).

[4] L. Grazioli, S. Stopkowicz, and J. Gauss, *Coupled-cluster and unitary coupled-cluster transition dipole moments through response theory*, in preparation (2025).

Numerical Algebraic Geometry and Correlated Electrons

Fabian M. Faulstich

(joint work with Bernd Sturmfels and Svala Sverrisdóttir)

Electronic structure theory is deeply intertwined with algebraic and combinatorial structures. While this connection was historically underutilized due to limitations in computational algebra, advances such as PHCpack [1], Bertini [2], HOM4PS [3, 4], NAG4M2 [5], and HomotopyContinuation.jl [6] have enabled the numerical solubility of high-dimensional polynomial systems arising in quantum chemistry. These developments open new avenues for integrating computational algebraic geometry into electronic structure theory, particularly within the framework of coupled cluster (CC) methods [7, 8, 9, 10, 11].

We develop a geometric framework for CC theory by approximating the electronic Schrödinger equation through hierarchies of polynomial systems that reflect different levels of excitation truncation. The exponential ansatz for CC wavefunctions gives rise to algebraic objects we term truncation varieties, which generalize Grassmannians in their Plücker embeddings. We characterize these varieties, compute their degrees, and investigate the structure of the associated polynomial solution spaces.

Using monodromy and parametric homotopy continuation techniques, we compute the full solution sets of the CC equations, with particular focus on CCD and CCSD. Our analysis of the resulting root structures yields new insights into the theoretical upper bounds on the number of solutions and their practical attainability. We examine dissociation pathways for four-electron systems, including $(H_2)_2$ in D_{2h} and $D_{\infty h}$ symmetries, circularly distorted H_4, and lithium hydride, and observe that multiple CC roots can accurately approximate not only ground states but also several low-lying excited states. In particular, we find that in systems like

lithium hydride, single-reference CC solutions provide high-fidelity approximations to both excited-state energies and wavefunctions.

This work highlights the promise of numerical algebraic geometry as a powerful tool for advancing our understanding of coupled cluster theory and, more broadly, electronic structure theory. These ideas will take center stage at the 2027 IPAM long program, *Numerical Algebraic Geometry and Correlated Electrons: Generalized Grassmannians, Response Functions, and Excited States* [12].

References

[1] J. Verschelde, *Algorithm 795: Phcpack: A general-purpose solver for polynomial systems by homotopy continuation*, ACM Transactions on Mathematical Software (TOMS), **25**, no. 2, pp. 251–276 (1999).

[2] D. J. Bates, J. D. Hauenstein, A. J. Sommese, and C. W. Wampler, *Bertini: Software for numerical algebraic geometry* (2006).

[3] T. Chen, T.-L. Lee, and T.-Y. Li, *Hom4ps-3: a parallel numerical solver for systems of polynomial equations based on polyhedral homotopy continuation methods*, Mathematical Software–ICMS 2014: 4th International Congress, Seoul, South Korea, August 5-9, 2014. Proceedings 4. Springer, pp. 183–190 (2014).

[4] T.-L. Lee, T.-Y. Li, and C.-H. Tsai, *Hom4ps-2.0: a software package for solving polynomial systems by the polyhedral homotopy continuation method*, Computing, **83**, pp. 109–133 (2008).

[5] D. J. Bates, P. Breiding, T. Chen, J. D. Hauenstein, A. Leykin, and F. Sottile, *Numerical nonlinear algebra*, ArXiv preprint arXiv:2302.08585 (2023).

[6] P. Breiding and S. Timme, *Homotopycontinuation. jl: A package for homotopy continuation in julia*, Mathematical Software–ICMS 2018: 6th International Conference, South Bend, IN, USA, July 24–27, 2018, Proceedings 6. Springer, pp. 458–465 (2018).

[7] F. M. Faulstich, B. Sturmfels, and S. Sverrisdóttir, *Algebraic varieties in quantum chemistry*, Foundations of Computational Mathematics, pp. 1–32 (2024).

[8] F. M. Faulstich and M. Oster, *Coupled cluster theory: Toward an algebraic geometry formulation*, SIAM Journal on Applied Algebra and Geometry, **8**, no. 1, pp. 138–188 (2024).

[9] F. M. Faulstich and A. Laestadius, *Homotopy continuation methods for coupled-cluster theory in quantum chemistry*, Molecular Physics, p. e2258599 (2023).

[10] V. Borovik, B. Sturmfels, and S. Sverrisdóttir, *Coupled cluster degree of the grassmannian*, Journal of Symbolic Computation (2024).

[11] S. Sverrisdóttir and F. M. Faulstich, *Exploring ground and excited states via single reference coupled-cluster theory and algebraic geometry*, Journal of Chemical Theory and Computation (2024).

[12] https://www.ipam.ucla.edu/programs/long-programs/numerical-algebraic-geometry-and-correlated-electrons-generalized-grassmannians-response-functions-and-excited-states/

A new mathematical formulation of coupled-cluster theory

Simen Kvaal

(joint work with Snorre Bergan, Håkon R. Fredheim, Nadia S. Larsen, Sergiy Neshveyev)

The coupled-cluster method and its variants form the most widely-used wavefunction-based class of methods for solving the Schrödinger equation in chemistry. Its mathematical analysis in the form of a priori and a posteriori error estimation has been approached by several groups, including Rohwedder–Schneider

[1, 2], Laestadius–Kvaal [3], Csirik–Laestadius [4], and Hassan–Maday–Wang [5, 6]. In this talk, I will outline work being carried out in an interdisciplinary project between members of the Hylleraas Centre for Quantum Molecular Sciences, Department of Chemistry, and the Operator Algebra group, Department of Mathematics, UiO. We have done a complete reformulation of coupled-cluster methods starting from the bivariational principle of Arponen [7], which gives a more "geometric" view, i.e., an optimization problem over a smooth Hilbert manifold. We have formulated general strategies for a posteriori and a priori error estimation using a nonlinear inf-sup theorem, which is based on results by Caloz–Rappaz [8]. Several results and proofs are simplified compared to those found in the literature. We are able to place all the analyses presently in the literature in this framework, in particular the seminal works by Rohwedder–Schneider, Laestadius–Kvaal, and Hassan–Maday–Wang.

References

[1] Thorsten Rohwedder. The continuous coupled cluster formulation for the electronic schrödinger equation. *ESAIM: Mathematical Modelling and Numerical Analysis*, **47** (2), 421–447 (2013).
[2] T. Rohwedder and R. Schneider. Error estimates for the coupled cluster method. *ESAIM: Math. Mod. Num. Anal.*, **47**, 1553–1582 (2013).
[3] A. Laestadius and S. Kvaal. Analysis of the extended coupled-cluster method in quantum chemistry. *SIAM J. Numer. Anal.*, **56** (2), 660–683 (2018).
[4] Mihály A. Csirik and Andre Laestadius. Coupled-cluster theory revisited: Part ii: Analysis of the single-reference coupled-cluster equations. *ESAIM: Mathematical Modelling and Numerical Analysis*, **57** (2), 545–583 (2023).
[5] Muhammad Hassan, Yvon Maday, and Yipeng Wang. Analysis of the single reference coupled cluster method for electronic structure calculations: The full-coupled cluster equations. *Numerische Mathematik*, **155** (1), 121–173 (2023).
[6] Muhammad Hassan, Yvon Maday, and Yipeng Wang. Analysis of the single reference coupled cluster method for electronic structure calculations: The discrete coupled cluster equations (2023).
[7] J.S. Arponen. Variational principles and linked-cluster exp s expansions for static and dynamic many-body problems. *Annals of Physics*, **151** (2), 311–382 (1983).
[8] Gabriel Caloz and Jacques Rappaz. Numerical analysis for nonlinear and bifurcation problems. In *Handbook of Numerical Analysis*, volume 5, pages 487–637. Elsevier (1997).

Scientific Machine Learning at the Electronic and Atomistic Scales and Conformal Prediction for Uncertainty in Atomistic Simulation

James Kermode

Scientific machine learning (SciML) combines the positive features of mechanistic and data-driven approaches. In my talk, I described recent work to leverage its advantages to model materials failure processes such as fracture and plasticity which simultaneously require large model systems and high accuracy by constructing efficient surrogates at the electronic structure [1, 2] and interatomic potential scales [3, 4, 5, 6, 7].

The talk was illustrated with ongoing industrially relevant applications, e.g. austenitic stainless steels subject to radiation damage [4] and point/extended defects in BCC metals [5, 6]. Collaboration with numerical analysts has already proved very valuable in this area, for example through the development of efficient preconditioners for geometry optimisation [8] and transition state search [9].

Hierarchical and concurrent approaches to multiscale materials modelling have both been employed with success, for example through machine learning interatomic potentials (MLIPs) which extract an effective description of the electronic behavior usable at the atomistic scale, and quantum mechanics/molecular mechanics (QM/MM) which combine a local QM treatment with a larger scale embedding region to capture elastic relaxation, respectively. Concurrent approaches are transferable to increased chemical complexities, but are still limited in the timescale which can be addressed (tens of picoseconds). In the latter case, collaboration with mathematicians has led to improved algorithms to select the spatial region to be modelled with QM precision [10].

Recently, there has been rapid progress in the development and application of MLIPs for chemomechanical systems that combine the effects of local chemistry and long-range stress fields. In particular, the Gaussian approximation potential (GAP) and Atomic Cluster Expansion (ACE) approaches have been successfully applied to a range of problems include the brittle fracture of silicon that previously could only be correctly modelled using concurrent QM/MM approaches [11]. Since MLIPs themselves remain relatively expensive in comparison to traditional interatomic potentials, a promising route is to combine two (or more) potentials with different accuracy/cost tradeoff choices in different parts of a large system: for example to track a diffusing He impurity in a bulk W crystal [12]. There is scope for the use of similar approaches to produce effective models for electronic structure, e.g. using the ACEhamiltonians approach to learn the mapping from local chemical environment to blocks of the Hamiltonian matrix [1, 2].

I focussed in detail on the importance of robust uncertainty estimates when using MLIPs as surrogate models [3]. Bayesian approaches to uncertainty quantification often fail to correctly account for mis-specification uncertainties that arise from the incompleteness of the representation of local environments and non-locality, instead attributing to aleatoric uncertainty (which is typically in fact very low when training on QM data). Conformal prediction [13] provides a remedy for this by providing a simple approach to rescale error estimates using a score function such as

$$s_i = \frac{\mu_i - y_{\mathrm{cal},i}}{\sigma_i}$$

where μ_i and σ_i are the mean and standard deviation prediction and $y_{\mathrm{cal},i}$ is held-back calibration data. Multiplicative scale factor for uncertainties can then be obtained from a quantile of these scores to provide prediction sets $\mathcal{C} = [\mu_{\mathrm{pred}} - \hat{q}\sigma_{\mathrm{pred}}, \mu_{\mathrm{pred}} + \hat{q}\sigma_{\mathrm{pred}}]$ with any desired level of coverage via $\mathbb{P}(\mathbf{y} \in \mathcal{C}) \geq 1 - \zeta$

$$\hat{q} = \mathrm{quantile}\left(\frac{\lceil (n+1)(1-\zeta) \rceil}{n}, \mathbf{s}\right)$$

where n is the size of the calibration set and $\mathbf{s} = [s_1, s_2, \dots s_n]$ collects the scores s_i. This approach has been applied to ACE models for silicon and titanum using the Bayesian linear regression interpretation of the parameter estimation process, and propagated through to quatities of interest including elastic constants, vacancy formation energies, vacancy migration barriers and solid-solid phase boundaries [3].

References

[1] L. Zhang et al., npj Comput. Mater. **8** 158 (2022)
[2] P. Stishenko et al. J. Chem. Phys. **161**, 012502 (2024)
[3] I. R. Best, T. J. Sullivan, and J. R. Kermode, J. Chem. Phys. **161**, 064112 (2024)
[4] L. Shenoy et al., Phys. Rev. Mater. **8**, 033804 (2024)
[5] P. Grigorev, A. M. Goryaeva, M.-C. Marinica, J. R. Kermode, and T. D. Swinburne, Acta Mater. **247** 118734 (2023)
[6] M. Nutter, J. R. Kermode, and A. P. Bartók [arXiv:2406.08368] (2024)
[7] I. Batatia et al., A Foundation Model for Atomistic Materials Chemistry [arXiv:2401.00096] (2024)
[8] D. Packwood, J. Kermode, L. Mones, N. Bernstein, J. Woolley, N. Gould, C. Ortner, and G. Csányi, J. Chem. Phys. **144**, 164109 (2016)
[9] S. Makri, C. Ortner, and J. R. Kermode, J. Chem. Phys. **150**, 094109 (2019)
[10] Y. Wang, J. R. Kermode, C. Ortner, and L. Zhang, Comput. Methods Appl. Mech. Eng. **428**, 117097 (2024)
[11] W. C. Witt et al., ACEpotentials.jl, J. Chem. Phys. **159**, 164101 (2023)
[12] F. Birks, T. D. Swinburne, and J. R. Kermode, [arXiv:2502.19081] (2025)
[13] A. N. Angelopoulos and S. Bates, [arXiv:2107.07511] (2021)

A symmetry-preserving and transferable representation for learning the Kohn-Sham density matrix

Liwei Zhang

(joint work with Patrizia Mazzeo, Michele Nottoli, Edoardo Cignoni, Lorenzo Cupellini and Benjamin Stamm)

The Kohn-Sham (KS) density matrix is one of the most essential properties in KS density functional theory (DFT), from which many other physical properties of interest can be derived. In this talk, a parameterized representation for learning the mapping from a molecular configuration to its corresponding density matrix using the equivariant Atomic Cluster Expansion (ACE) framework [1, 2, 3] is presented, which preserves the physical symmetries of the mapping, including isometric equivariance and Grassmannianity.

Specifically, given a molecular configuration $\mathbf{R} = \{(Z_I, \boldsymbol{r}_I)\}_{I=1}^{N_{\mathrm{at}}} := \{\sigma_I\}_{I=1}^{N_{\mathrm{at}}}$ consisting of N_{at} atoms and N (valence) electron-pairs, where $Z_I \in \mathbb{N}$ and $\boldsymbol{r}_I \in \mathbb{R}^3$ characterize the atomic number and the position of the I-th atom, and a set of atomic orbitals $\{\phi_{I\alpha}\}_{I,\alpha}$ with which the KS equation is discretized, then the

elements of the (discretized) density matrix are given by

$$\begin{aligned}\left[D_{\mathbf{R}}\right]_{IJ\alpha\beta} &= \int_{\mathbb{R}^3} \phi_{I\alpha}(\boldsymbol{r})^* D(\boldsymbol{r};\mathbf{R})\phi_{J\beta}(\boldsymbol{r})d\boldsymbol{r} \\ &= \int_{\mathbb{R}^3} \phi_{\alpha}(\boldsymbol{r}-\boldsymbol{r}_I)^* D(\boldsymbol{r};\mathbf{R})\phi_{\beta}(\boldsymbol{r}-\boldsymbol{r}_J)d\boldsymbol{r} \\ &= \int_{\mathbb{R}^3} \phi_{\alpha}(\boldsymbol{r}-\boldsymbol{r}_I)^* \tilde{D}(\boldsymbol{r};\mathbf{R}_{IJ})\phi_{\beta}(\boldsymbol{r}-\boldsymbol{r}_J)d\boldsymbol{r},\end{aligned}$$

where $D(\boldsymbol{r};\mathbf{R})$ is the electronic density. In the last line, the whole configuration $\mathbf{R}$ is shifted to be centred at a proper position depending on I and J. As a result, the density matrix $D_{\mathbf{R}}$ has a block structure illustrated in Figure 1.

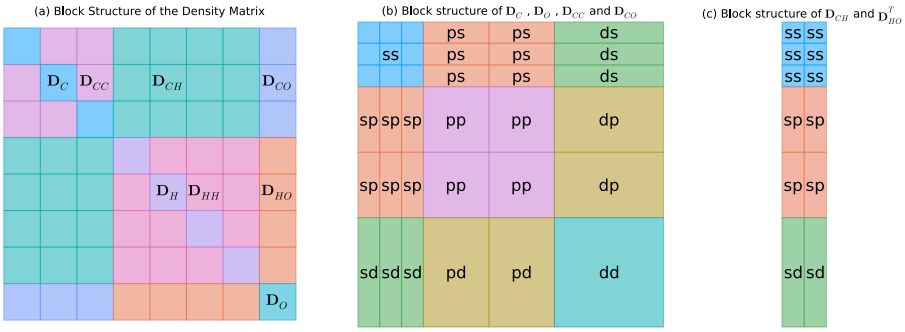

FIGURE 1. Block structure of the density matrix of a C_3H_4O molecule, where the atomic basis 6-31G(d) is used.

The subblocks in Figure 1(b) and (c) are independent of each other and are themselves isometrically equivariant (*i.e.* equivariant under rotations, translations and reflections of the configuration). For each subblock $\mathcal{D}$, there exists a set of ACE bases $\{\mathcal{B}_{\boldsymbol{v}}\}_{\boldsymbol{v}}$ as functions of the local environments $\mathbf{R}_{IJ}$, which has the same equivariance as $\mathcal{D}$ and asymptotically spans the function space to which $\mathcal{D}$ belongs [4]. Hence, $\mathcal{D}$ can be approximated by a linear combination of $\{\mathcal{B}_{\boldsymbol{v}}\}_{\boldsymbol{v}}$:

$$\mathcal{D} \approx \sum_{\boldsymbol{v}} c_{\boldsymbol{v}} \mathcal{B}_{\boldsymbol{v}}.$$

The coefficients $\{c_{\boldsymbol{v}}\}_{\boldsymbol{v}}$ are then obtained by solving a least squares problem that minimizes the difference between the predicted and referenced density matrices. After all the subblocks are predicted, a retraction operator is applied to the predicted density matrix (as a whole), to guarantee that the obtained density matrix is Grassmannian without destroying the equivariance of the predictions.

Trained on several typical molecules, the proposed representation is shown to be systematically improvable with the increase of the model parameters. In particular, it can accurately reproduce the Kohn-Sham density matrix across diverse

systems, with excellent generalization to unseen molecules that are not part of the training set and can even be more complex than those in the training set. Such an approach can either accelerate the DFT calculations or provide approximations to some properties of the molecules directly (*cf.* Figure 2).

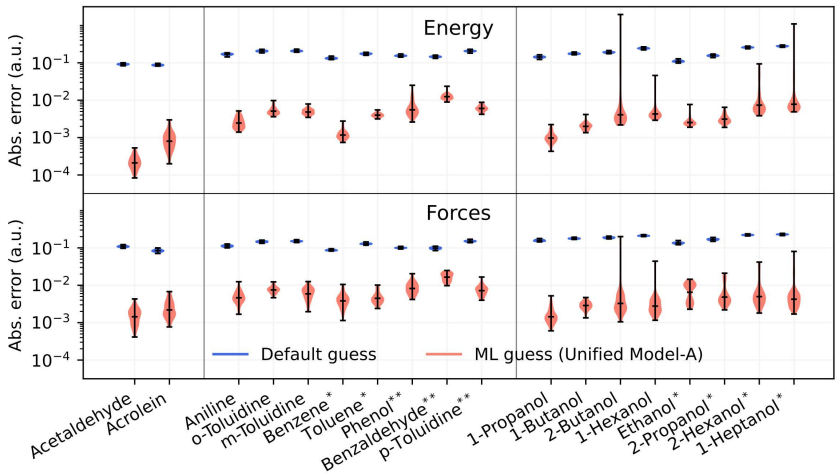

FIGURE 2. Plot of the error for energy and forces obtained by different density matrices (blue: Gaussian default guess, pink: ML density matrices). The molecules with a superscript $*$ and $**$ are not (or barely) included in the training process.

The results also suggest that the performance of the models generated by the proposed representation is mainly limited by the design of the training set rather than the representation itself. It is therefore likely that a better selection of training points, obtained for example by active learning approaches, will give more stable results (*e.g.* help to identify or remove the outliers in Figure 2). Another observation in the experiments indicates that there is an empirical algebraic relation between the commutator violation error ($\|FD - DF\|_F$ where D is the predicted density matrix and F is the Hamiltonian matrix induced by D) and the relative error of energy, as shown in Figure 3.

This finding highlights the potential to utilize such indicators to refine active learning approaches, enabling the learning procedure to prioritize data points that align less well with the model's current understanding and thereby improve both efficiency and accuracy. This is one of our future works.

The scientific works reported in this talk can be found in [5].

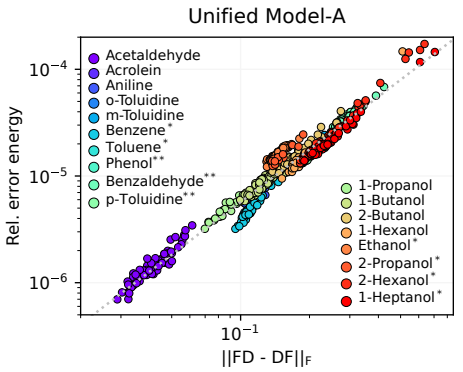

FIGURE 3. Plot of the commutator error versus the relative error in energy using the predicted density matrix.

REFERENCES

[1] R. Drautz, *Atomic cluster expansion for accurate and transferable interatomic potentials*, Phys. Rev. B **99**, 014104 (2019).

[2] R. Drautz, *Atomic cluster expansion of scalar, vectorial, and tensorial properties including magnetism and charge transfer*, Phys. Rev. B **102**, 024104 (2020).

[3] L. Zhang, B. Onat, G. Dusson, A. McSloy, G. Anand, R. J. Maurer, C. Ortner, and J. R. Kermode, *Equivariant analytical mapping of first principles Hamiltonians to accurate and transferable materials models*, npj Comput. Mater. **8** (2022).

[4] G. Dusson, M. Bachmayr, G. Csányi, R. Drautz, S. Etter, C. van der Oord, and C. Ortner, *Atomic Cluster Expansion: Completeness, Efficiency and Stability*, J. Comput. Phys. **454**, 110946 (2022).

[5] L. Zhang, P. Mazzeo, M. Nottoli, E. Cignoni, L. Cupellini, and B. Stamm, *A symmetry-preserving and transferable representation for learning the Kohn-Sham density matrix*, arXiv:2503.08400 (2025).

Designing surrogate models with opportunistic training sets

KATHARINE FISHER

(joint work with Michael F. Herbst, Matthew Li, Timo Schorlepp, Youssef Marzouk)

Data generation remains a bottleneck in training surrogate models to predict molecular properties. Highly accurate CCSD(T) methods scale like N^7 where N is the number of electrons in a system. A plethora of less expensive electronic structure methods are available, but often there is limited insight as to which is optimal for a particular chemical system. This talk focuses on the design of models that can effectively use multiple sources of information to learn to make predictions. First, we discuss a multitask framework for Gaussian process regression which relates multiple training sets through a covariance structure, then we describe tools for designing neural networks to learn from observation gradients.

Multitask Gaussian process regression overcomes data generation cost by leveraging both expensive and cheap data sources [1, 2]. This learning framework naturally accommodates more than two sources of training data without the need to impose inaccurate assumptions on the accuracy hierarchy of the sources. We show the results from models trained on heterogeneous data sets generated via coupled-cluster (CC) and density functional theory with various exchange correlation functionals. In particular, multitask surrogates can predict at CC-level accuracy with a reduction in data generation cost by over an order of magnitude. By constructing kernels functions that are robust to the outliers, we show that incorporating foundation model predictions can further improve the performance of multitask models for a given data generation cost. These results suggest that using foundation models within the multitask framework could be a viable alternative to the obtuse process of finetuning foundation model networks with problem specifc data. Future work will directly compare multitask models to the state of the art in finetuning.

Other future directions involve adaptively constructing trainings sets. Given an existing multitask model, we aim to select molecules to add to the training set as well as to recommend an electronic structure method to compute the new data point which optimally balances accuracy and efficiency. Gaussian process regression provides probabilistic predictions, and the multitask models we describe predict distributions for the difference between each data source and the primary source of interest. These predictive distributions can likely be leveraged for recommendation of electronic structure methods.

In discussions spurred by this talk, seminar participants considered the open question of how the multitask framework may be applied to Hamiltonian learning from data generated with different levels of theory. It is not obvious how to build such a surrogate since different electronic structure methods use different orbital sets.

In the last part of this talk, we describe an approach for efficiently predicting the performance of a neural network when gradients of the observation set are available for training. This work is motivated by the common practice of training machine learning interatomic potentials with both energy and force data. Extensively testing the performance of network models with different activations, dimensions, and regularization would be prohibitively expensive, so we seek to evaluate the error at the optimal network parameter setting without actually finding the optimal network parameters. We borrow methods developed in statistical physics for characterization of phase transitions in spin glasses and apply them to predict phase transitions in neural network training [3, 4]. Following this approach, we can systematically investigate the impact of training set size, network dimensions, regularization, and gradient observation noise on prediction error of random features models. Carrying out this systematic investigation and extending the approach to more elaborate classes of network models is work for the near future.

References

[1] K.E. Fisher, M.F. Herbst, and Y.M. Marzouk, *Multitask methods for predicting molecular properties from heterogeneous data*, J. Chem. Phys. **161** (2024), 014114.
[2] G. Leen, J. Peltonen, S. Kaski, *Focused multi-task learning in a Gaussian process framework*, Machine Learning **89** (2012), 157-182.
[3] F. Gerace, B. Loureiro, F. Krzakala, M. Mezard, and L. Zdeborova, *Generalisation error in learning with random features and the hidden manifold model*, Journal of Statistical Mechanics: Theory and Experiment **12** (2021).
[4] S. Mei and A. Montanari, *The generalization error of random features regression: Precise asymptotics and the double descent curve*, Communications on Pure and Applied Mathematics **75** (2022).

Observability in periodic crystals via optimal transport

Virginie Ehrlacher
(joint work with Thomas Borsoni)

Observability estimates are needed to address controllability questions. The aim of the talk was to state recent results about new observability estimates obtained in periodic crystals with an infinite number of electrons. The approach relies heavily on the optimal transport approach introduced in [1] for systems with a finite number of electrons. The approach uses pseudometrics between quantum and classical densities, which can be generalized to treat periodic systems for an infinite number of electrons by combining them with Bloch theory.

In this extended abstract, I will only give the precise expression of the periodic version of the classical to quantum optimal transport metric used to obtain these observability estimates for periodic crystals. Let us consider $\mathcal{L}$ a periodic lattice of $\mathbb{R}^d$ with $d \in \mathbb{N}^*$. Let Γ be a unit cell of $\mathcal{L}$ and Γ^* be its Brilouin zone. Let us first recall some basic facts about Bloch theory. It then holds that for all $u \in \mathcal{H} = L^2(\mathbb{R}^d, \mathbb{C})$ and all $k \in \Gamma^*$, the function $u_k : \mathbb{R}^d \to \mathbb{C}$ defined by

$$\forall x \in \mathbb{R}^d, \quad u_k(x) = \sum_{\ell \in \mathcal{L}} u(x+\ell) e^{ik\cdot(x+\ell)}$$

belongs to $\mathcal{H}_{\rm per} := L^2_{\rm per}(\Gamma; \mathbb{C})$. It also holds that

$$\forall x \in \mathbb{R}^d, \quad u(x) = \fint_{\Gamma^*} u_k(x)\, dk.$$

For any self-adjoint operator A on $\mathcal{H}$ such that $A\tau_\ell = \tau_\ell A$ for all $\ell \in \mathcal{L}$, there exists a unique family $(A_k)_{k\in\Gamma^*}$ of self-adjoint operators on $\mathcal{H}_{\rm per}$ such that

$$\forall f \in \mathcal{H} \cap D(A), \quad (Af)_k = A_k f_k$$

Then, denoting by $\mathcal{L}(\mathcal{H})$ the set of bounded linear operators on $\mathcal{H}$, if an operator A satisfying $0 \le A^* = A \in \mathcal{L}(\mathcal{H})$ is such that $\tau_\ell A = A\tau_\ell$ for all $\ell \in \mathcal{L}$, one can define its periodic trace as

$$\underline{\rm Tr}\, A := \fint_{\Gamma^*} {\rm Tr}_{\mathcal{H}_{\rm per}} A_k\, dk.$$

Then, for any pair (f, R) of classical/quantum states such that

- $f \in L^1_{\rm loc}(\mathbb{R}^d \times \mathbb{R}^d)$ with $f \geq 0$, $f(\cdot, \xi)$ Γ-periodic for all $\xi \in \mathbb{R}^d$ and $\int_\Gamma \int_{\mathbb{R}^d} f(x,\xi)\, \xi\, dx = 1$,
- $R \in \{0 \leq T^* = T \in \mathcal{L}(\mathcal{H}) :\ \tau_\ell T = T\tau_\ell\ \forall \ell \in \mathcal{L},\ \underline{\rm Tr}\, T = 1\}$,

one can consider the set $\underline{\mathcal{C}}(f, R)$ of classical to quantum couplings between f and R defined as the set of mappings

$$Q : \Gamma \times \mathbb{R}^d \ni (x, \xi) \mapsto Q(x, \xi) \in \mathcal{L}(\mathcal{H})$$

such that for all $(x, \xi) \in \Gamma \times \mathbb{R}^d$, $0 \leq Q(x, \xi)^* = Q(x, \xi) \in \mathcal{L}(\mathcal{H})$, $\tau_\ell Q(x, \xi) = Q(x, \xi)\tau_\ell\ \forall \ell \in \mathcal{L}$, $\underline{\rm Tr}\, Q(x, \xi) = f(x, \xi)$ and $\int_\Gamma \int_{\mathbb{R}^d} Q(x, \xi)\, d\xi\, dx = R$.

For a given $\lambda > 0$ and all $(x, \xi) \in \Gamma \times \mathbb{R}^d$, one can consider the parametric self-adjoint operator $C^\lambda(x, \xi)$ on $\mathcal{H}$ defined as

$$C^\lambda(x, \xi) = \lambda^2 \min_{\ell \in \mathcal{L}} |x - y - \ell|^2 + |\xi + i\hbar\nabla_y|^2.$$

The classical to quantum optimal transport metric between f and R is then defined as

$$\mathfrak{d}_\lambda(f, R) = \inf_{Q \in \underline{\mathcal{C}}(f,R)} \int_\Gamma \int_{\mathbb{R}^d} \underline{\rm Tr} \left(Q(x, \xi)^{1/2} C^\lambda(x, \xi) Q(x, \xi)^{1/2} \right) dx\, d\xi.$$

Extensions of propagation and observability results proved in [1, 2] can thus be proved in this periodic context. This preliminary work paves the way to the treatment of more complex and realistic systems which will be the object of future work.

References

[1] F. Golse and T. Paul, *Quantitative observability for the Schrödinger and Heisenberg equations: An optimal transport approach*, Mathematical Models and Methods in Applied Sciences **32** (2022), 5:941–963.

[2] F. Golse and T. Paul, *Optimal transport pseudometrics for quantum and classical densities*, Journal of Functional Analysis **282** (2022), 9:109417.

DMRG and refinements: Theoretical results and numerical illustrations

Gero Friesecke

The density-matrix renormalization group method, or DMRG for short, is an accurate computational method for tackling the N-electron Schrödinger equation $H\Psi = E\Psi$ for molecules. It was pioneered by White (1999), Chan and Head-Gordon (2002), and Legeza et al (2003), following earlier work by White on spin chains. It is much younger than coupled-cluster theory, but in the light of recent advances it is rapidly becoming a competitive alternative.

1. DMRG

Starting point is the N-electron Schrödiner equation $H\Psi = E\Psi$, which for the ground state amounts to solving the Rayleigh-Ritz variational principle

$$E_0 \;=\; \min_{\Psi\in\mathcal{H}_N} \frac{\langle\Psi, H\Psi\rangle}{\langle\Psi,\Psi\rangle}.$$

Here quantum wavefunctions Ψ belong to the Hilbert space $\mathcal{H}_N = L^2_{anti}((\mathbb{R}^3 \times \mathbb{Z}_2)^N)$, the Hamiltonian is

$$H = -\frac{1}{2}\nabla^2 + \sum_{1\le i<j\le N} \frac{1}{|r_i - r_j|} + \sum_{i=1}^{N} \mathrm{v}(r_i),$$

and $\mathrm{v}(r) = -\sum_{\alpha=1}^{M} Z_\alpha/|r - R_\alpha|$ is the potential exerted by the atomic nuclei. One wants to compute energy levels to chemical accuracy 1 kcal/mole = 0.0016 a.u.

DMRG simplifies the high-dimensional Schrödinger partial differential equation by the following 4 steps, the first two being the standard reduction to Full CI.

1. Orbital space One approximates the single-electron Hilbert space by a finite-dimensional subspace, typically spanned by the occupied and lowest unoccupied Hartree-Fock orbitals, $\mathcal{H}_1 = L^2(\mathbb{R}^3 \times \mathbb{Z}_2) \approx \mathrm{span}\{\varphi_1, ..., \varphi_L\}$.

2. Full CI space One approximates the N-electron space by the ensuing FCI space, i.e., the N-fold antisymmetric tensor product of the above finite-dimensonal space with itself: $\mathcal{H}_N \approx \mathrm{span}\{|\varphi_{i_1} \cdots \varphi_{i_N}\rangle \,:\, 1 \le i_1 < ... < i_N \le L\}$. Mathematically this is a Galerkin approximation with a tensor product basis.

3. Passage from N-body space to Fock space, and to an occupation number representation One re-encodes any Slater determinant built from the orbitals in $\mathcal{H}_1$ with the help of L Q-bits with the i-th Q-bit indicating whether the orbital φ_i is present or absent, as in the following example for $L = 8$:

$$|\varphi_2\,\varphi_3\,\varphi_6\,\varphi_8\,\rangle \rightsquigarrow |0\rangle\otimes|1\rangle\otimes|1\rangle\otimes|0\rangle\otimes|0\rangle\otimes|1\rangle\otimes|0\rangle\otimes|1\rangle.$$

In the new representation any wavefunction has an expansion

$$\Psi \quad = \sum_{\mu_1,\ldots,\mu_L=0}^{1} C_{\mu_1\ldots\mu_L}\; |\mu_1\rangle\otimes\cdots\otimes|\mu_L\rangle.$$

The tensor $(C_{\mu_1\ldots\mu_L})_{\mu_1,\ldots,\mu_L\in\{0,1\}}$ is called the occupation tensor for Ψ.

4. Matrix product state approximation of occupation tensor One now approximates the occupation tensor as follows

$$C_{\mu_1\ldots\mu_L} \;\approx\; \sum_{\alpha_1,\ldots,\alpha_{L-1}=1}^{M} \underbrace{\mathrm{A}_1(\mu_1)}_{1\times M}{}_{\alpha_1}\; \underbrace{\mathrm{A}_2(\mu_2)}_{M\times M}{}_{\alpha_1\alpha_2}\; \underbrace{\mathrm{A}_3(\mu_3)}_{M\times M}{}_{\alpha_2\alpha_3} \cdots \underbrace{\mathrm{A}_{\mathrm{L}}(\mu_L)}_{M\times 1}{}_{\alpha_{L-1}}.$$

Here M is an important rank parameter (called bond dimension). The passage N-body space $\to$ Fock space $\to$ space of node tensors $\theta = (A_1, ..., A_L)$ corresponds

to a dimension reduction

$$\binom{L}{N} \;\to 2^L = \sum_{N=0}^{L} \binom{L}{N} \;\to\; L \cdot M^2 \cdot 2.$$

The node tensors are now used as variational parameters in the Rayleigh-Ritz principle,

$$E_0^{\mathrm{DMRG}} = \min_{\theta} \frac{\langle \Psi_\theta, H\Psi_\theta \rangle}{\langle \Psi_\theta, \Psi_\theta \rangle}$$

where the minimization is subject to the constraint of fixed particle number, mathematically: $\mathcal{N}\Psi = N\Psi$ where $\mathcal{N}$ is the number operator. Within the DMRG algorithm this is done by sucessive minimization over neighbouring pairs of node tensors. Attractively, unlike coupled cluster the method is variational and structure-preserving: the problem for pairs of node tensors is again a Rayleigh-Ritz problem for a selfadjoint Hamiltonian).

2. Two-electron wavefunctions have bond dimension Three

The following result was proved in joint work with Graswald [1].

Theorem: For any 2-electron state $\Psi \in \mathcal{H}_L \wedge \mathcal{H}_L$, there exists an orthonormal basis of $\mathcal{H}_L$ such that Ψ can be written as an MPS with bond dimension 3. Moreover for $L \geq 4$, 3 is optimal and the sequence of bond dimensions $m_1, ..., m_L$ with minimal sum such that the A_i are of size $m_{i-1} \times m_i$ is $m_1, ..., m_{L-1}) = (2, 2, 3, 2, 3, ..., 2, 3, 2, 2)$.

Note that a priori the number of coefficients for a two-electron wavefunction is $O(L^2)$; in the DMRG format it can be brought down to $O(L)$ while retaining the *exact* wavefunction.

An important corollary is that DMRG combined with fermionic mode optimization is exact for 2-particle systems.

3. DMRG with restricted active space

To extend DMRG to larger systems, Barca et al (2022) combined DMRG with the familiar quantum chemistry idea of a restricted active space and called the ensuing method DMRG-RAS. One partitions the orbitals into CAS orbitals $\varphi_1, ..., \varphi_\ell$ and RAS orbitals $\varphi_{\ell+1}, ..., \varphi_L$, and introduces the following reduced many-body Hibert space

$$\tilde{\mathcal{H}} \;=\; \mathcal{H}_{CAS}(\ell) \;\oplus\; \mathcal{H}_{RAS}(L-\ell, k)$$

where the first space is spanned by all Slater det's of CAS orbitals and the second space by all Slater determinants with at least 1 and at most k RAS orbitals. The excitation level k is a parameter of the method. The RAS energy is given by minimization of the Rayleigh quotient over the reduced Hilbert space, and satisfies

$$E_{RAS}(\ell, k) = \min_{\Psi \in \tilde{\mathcal{H}},\ \langle \Psi, \Psi \rangle = 1} \langle \Psi, H\Psi \rangle \quad < \quad E_{CAS}(\ell) = \min_{\Psi \in \mathcal{H}_{CAS}(\ell),\ \langle \Psi, \Psi \rangle = 1} \langle \Psi, H\Psi \rangle.$$

When ℓ is minimal, i.e. $N/2$, one obtains k-fold excited CI. When k is maximal, i.e. N, one recovers full CI. For $N/2 < \ell < N$, DMRG-RAS is an *embedding method*.

This method was analyzed, developed further, and applied to large-scale examples in joint work with Barcza and Legeza [2]. Our findings are the following.

(1) For a prototypical strongly correlated system, the Chromium dimer, DMRG-RAS was found to be more accurate than coupled-cluster. Using a $cc-pVDZ$ orbital space with $L = 136$, a natural orbital basis, and a CAS(12,68), we found

$$E_{RAS}(\ell = 17, k = 2) = -2086.877 < -2086,869 = E_{CCSDTQ}.$$

(2) We investigated how the RAS error behaves at fixed excitation level ($k = 2$) when the size ℓ of the CAS space is increased. We found across all investigated systems (for an example see the plot on the right) that the RAS error satisfies, to high accuracy, a power law scaling with respect to the CAS error:

$$\epsilon_{\mathrm{RAS}} \sim a \left(\epsilon_{\mathrm{CAS}}\right)^{p}.$$

To verify the scaling law, as in in this example, we need to have access to the FCI energy. The true power of the scaling law lies in yielding an accurate extrapolation method, termed DMRG-RAS-X, if the FCI energy is not available: one simply minimizes the mean squared regression error of the RAS versus CAS error in a log-log plot not just over the parameters of the regression line but also over the (unknown) FCI energy. In the examples we investiated, the extrapolation yields an important error reduction allowing one to reach chemical accuracy. See the table below.

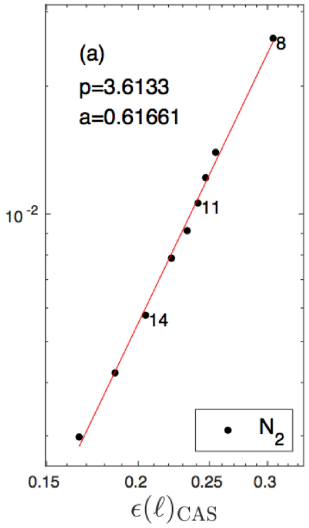

absolute error [a.u.], ground state energy

system	$\varepsilon_{\mathrm{CAS}}$	$\varepsilon_{\mathrm{RAS}}$	$\varepsilon_{\mathrm{RAS-X}}$	L/ℓ_{max}	$\varepsilon_{\mathrm{RAS-X}}/\varepsilon_{\mathrm{RAS}}$	
F_2	0.0941	0.0023	0.0011	1.20	0.48	CAS(18.18)
CH_2	0.0690	0.0009	-0.0004	1.33	0.29	CAS(6,12)
N_2	0.1662	0.0030	0.0007	1.75	0.23	CAS(14,28)
C_2	0.1159	0.0014	0.0001	3.22	0.07	CAS(8.54)

e. g. N_2 : cc−pVDZ basis, L = 28, $\ell_{\mathrm{max}} = 16$, N = 14

We also found a power law scaling in large examples we investiated: the Chromium dimer and the FeMoco enzyme (the latter being used by nature for nitrogen fixation $2N_2 + 3\,H_2 \rightarrow 2\,NH_3$), with 54 resolved electrons on 54 spatial orbitals as proposed by Reiher and a Hilbert space dimension 2.5×10^{31}.

An theoretical challenge is to understand the non-universal exponents p observed in the scaling law. As a first step we designed a simplified model. Starting point are states $\Psi_1, \Psi_2, \Psi_3, ...$ where Ψ_j only contains $2(j-1)$-fold excited determinants with respect to $\mathcal{H}_{CAS}(\ell_0)$. The Hamiltonian in the subspace of these states then has bandwidth 3, on account of the Hamiltonian H being a two-body operator. Assuming equi-spaced levels and a fixed interaction strength with next level leads to a simple matrix model (shown here for 4 states),

$$H = \begin{pmatrix} h & \mathrm{v} & 0 & 0 \\ \mathrm{v} & h+a & \mathrm{v} & 0 \\ 0 & \mathrm{v} & h+2a & \mathrm{v} \\ 0 & 0 & \mathrm{v} & h+3a \end{pmatrix}.$$

For this model, which we termed *ladder model*, we proved rigorously that the scaling law holds asymptotically as the coupling strength v is decreased, with the following non-universal exponents: $p = 2$ for 1d CAS and 1d RAS, $p = 3$ for 1d CAS and 2d RAS, and $p = 3/2$ for 2d CAS and 1d RAS.

As regards the full problem, in [2] we also gave a rigorous error estimate on the RAS error based on a partitioning of the Hamiltonian into a CAS Hamiltonian H_0 and a part which contains the RAS Hamiltonian and the CAS-RAS coupling. Our error estimate is of the form $|E_{RAS} - E_{FCI}| \leq f(H' \tilde{\Psi}_0)$ for some explicit f with $f(0) = 0$. Here $\tilde{\Psi}_0$ is the dressed CAS ground state (i.e. the normalized projection of the FCI ground state onto the CAS). In particular, the error goes to zero when H' becomes small on the dressed CAS GS, which is true in practice for a moderate-sized CAS. By contrast, standard error estimates for Rayleigh-Schrödinger perturbation theory and its variants only go to zero if H' becomes small *on the whole CAS*, which is never true in practice. Applied to the ladder model, the error estimate captures the correct scaling law of RAS versus CAS error.

Summary. DMRG and its refinements are a viable alternative to coupled cluster theory for highly accurate electronic structure computations. Large-scale computations and some rigorous theory are emerging.

References

[1] G. Friesecke, B. Graswald, *Two-electron wavefunctions have bond dimension Three*, J. Math. Phys. **63**, 091901 (2022).

[2] G. Friesecke, G. Barcza, Ö. Legeza, *Predicting the FCI energy of large systems to chemical accuracy from restricted active space density matrix renormalization group calculations*, J Chem Theory Comput. **20**(1), 87–102 (2024).

Relativistic electronic-structure methods based on effective quantum electrodynamics

Julien Toulouse

(joint work with Timothée Audinet, Umberto Morellini, Antoine Levitt)

It is important to take into account the effects of special relativity in the quantum description of electronic systems with heavy elements. Relativistic electronic-structure computational methods based on the no-pair Dirac-Coulomb or Dirac-Coulomb-Breit Hamiltonian have thus been developed and are now routinely applied to molecular systems (see, e.g., Refs. [1, 2, 3]. The next challenge for relativistic quantum chemistry is to go beyond the no-pair approximation, i.e., including the quantum-electrodynamics (QED) effect of virtual electron-positron pairs. This is desirable not only for an increased accuracy but also in order to put relativistic quantum chemistry on deeper theoretical grounds.

An attractive approach to performing ab initio relativistic calculations beyond the no-pair approximation is to use an effective QED Hamiltonian with the Coulomb or Coulomb–Breit two-particle interaction (see, e.g., Refs. [2, 4, 5, 6, 7]). This effective QED theory properly includes the effects of vacuum polarization through the creation of electron-positron pairs but does not explicitly include the photon degrees of freedom. It is, thus, a more tractable alternative to full QED for electronic-structure calculations.

In this presentation, I have reviewed this effective QED theory, I have discussed the possibility to formulate a relativistic density-functional theory based on it [7], and I have shown results on a one-dimensional hydrogen-like model system for the calculation of the vacuum-polarization density [8, 9].

References

[1] T. Saue and L. Visscher, *Four-component electronic structure methods for molecules*, in Theoretical Chemistry and Physics of Heavy and Superheavy Elements, edited by S. Wilson and U. Kaldor (Kluwer, Dordrecht, 2003), 211–267.

[2] K. G. Dyall and K. Faegri, Jr., *Introduction to Relativistic Quantum Chemistry* (Oxford University Press, 2007).

[3] M. Reiher and A. Wolf, *Relativistic Quantum Chemistry: The Fundamental Theory of Molecular Science* (Wiley VCH, Weinheim, 2009).

[4] P. Chaix and D. Iracane, *From quantum electrodynamics to mean-field theory. I. The Bogoliubov-Dirac-Fock formalism*, Journal of Physics B **22**, 3791 (1989).

[5] C. Hainzl, M. Lewin, E. Séré, and J. P. Solovej, *Minimization method for relativistic electrons in a mean-field approximation of quantum electrodynamics*, Physical Review A **76**, 052104 (2007).

[6] W. Liu and I. Lindgren, *Going beyond no-pair relativistic quantum chemistry*, Journal of Chemical Physics **139**, 014108 (2013).

[7] J. Toulouse, *Relativistic density-functional theory based on effective quantum electrodynamics*, SciPost Chemistry **1**, 002 (2021).

[8] T. Audinet, J. Toulouse, *Effective quantum electrodynamics: One-dimensional model of the relativistic hydrogen-like atom*, Journal of Chemical Physics **158**, 244108 (2023).

[9] T. Audinet, U. Morellini, A. Levitt, J. Toulouse, *Vacuum polarization in a one-dimensional effective quantum-electrodynamics model*, Journal of Physics A **58**, 125304 (2025).

Coupling perturbation theory and reduced basis methods

Louis Garrigue
(joint work with Benjamin Stamm)

A standard issue in eigenvalue problems is to reduce the number of degrees of freedom of the variational Hilbert space $\mathcal{H}$. For instance it is legitimate to do so for the many-body Schrödinger operator

$$H(\lambda) := \sum_{n=1}^{N} -\Delta_j + v(x_j) + \lambda \sum_{1\leq i<j\leq N} w(x_i - x_j), \tag{1}$$

where one can compute every quantity at $\lambda = 0$ but not at $\lambda \neq 0$. Reduced basis method approximations aim at approximating $\mathcal{H}$ by a well-chosen low-dimensional subset $\mathcal{P}\mathcal{H}$, created via an orthogonal projector $\mathcal{P}$. In quantum physics, this procedure is also called the variational approximation. Reduced basis for eigenvalue problems have been investigated in [2, 3] for instance, but mostly in an a posteriori point of view.

Perturbation theory is also one of the most traditional concepts in quantum mechanics. It consists in considering an operator $H(\lambda) = \sum_{n=0}^{+\infty} \lambda^n H^n$ dependent on a parameter $\lambda \in \mathbb{R}$, considering $(E(\lambda), \phi(\lambda))$ an eigenpair of $H(\lambda)$, computing the series $\phi(\lambda) = \sum_{n=0}^{+\infty} \lambda^n \phi^n$ and truncating it to obtain an approximation of $\phi(\lambda)$.

It is now natural to try to merge the two methods, that is the reduced basis method (RBM) and perturbation theory (PT) to simultaneously use their benefits, and we call RBM+PT the resulting method. To this purpose, we build the reduced space by using the perturbative series ϕ^n up to order ℓ, that is we assume that

$$\mathrm{Span}(\phi^0, \ldots, \phi^\ell) \subset \mathcal{P}\mathcal{H}.$$

This idea was already previously stated in several works [4, 5, 1]. We present an illustration of the situation on Figure 1, where we denote by $(\mathcal{E}(\lambda), \psi(\lambda))$ the eigenpair of the reduced operator $(\mathcal{P}H(\lambda)\mathcal{P})_{|\mathcal{P}\mathcal{H}\to\mathcal{P}\mathcal{H}}$.

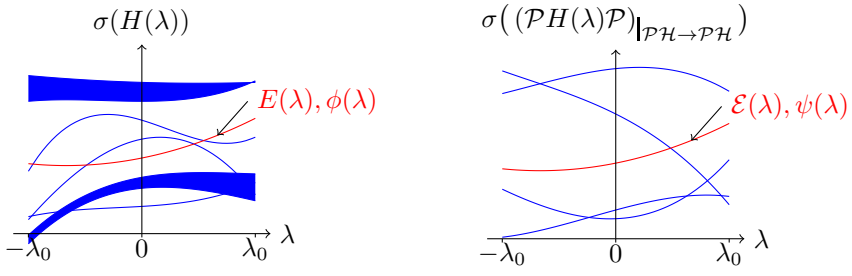

Figure 1. Left : spectrum of the exact operator. Right : spectrum of the effective one.

To quantify the error between the exact and approximate eigenvectors, we need the following evaluation

$$\phi(\lambda) - \psi(\lambda) = (1 + R(\lambda)H(\lambda))\,\mathcal{P}^{\perp}\phi(\lambda) + O\left(\|\phi(\lambda) - \psi(\lambda)\|^2\right),$$

where $R(\lambda)$ is the pseudo-inverse of $(\mathcal{P}H(\lambda)\mathcal{P})_{|\mathcal{P}\mathcal{H}\to\mathcal{P}\mathcal{H}}$ at level $\mathcal{E}(\lambda)$. Then one can prove that

$$\|\phi(\lambda) - \psi(\lambda)\| \leq |\lambda|^{\ell+1} \left\|(1 + R(0)H(0))\,\mathcal{P}^{\perp}\phi^{\ell+1}\right\| + O\left(|\lambda|^{\ell+2}\right).$$

One can then compare the asymptotic acceleration of RBM+PT with respect to PT, which is given by the quantity

$$\xi_\ell := \lim_{\lambda\to 0} \frac{\|\phi(\lambda) - \varphi(\lambda)\|}{\|\phi(\lambda) - \psi(\lambda)\|} = \frac{\left\|\phi^{\ell+1}\right\|}{\|(1 + R(0)H(0))\mathcal{P}^{\perp}\phi^{\ell+1}\|} \simeq \frac{\left\|\phi^{\ell+1}\right\|}{\|\mathcal{P}^{\perp}\phi^{\ell+1}\|}.$$

We numerically observe that this quantity grows exponentially in ℓ. One can also compare RBM+PT with a more traditional way of using RBM, consisting in adding excited states of $H(0)$, which we call RBM+ES. With a simple Hamiltonian $H(\lambda) = H^0 + \lambda H^1$, where $H^0 = -\Delta + v_0$ and $H^1 = v_1$, v_0 and v_1 being binding potentials, we saw in simulations that using RBM+PT with vectors $\phi^1, \ldots, \phi^3$ is equivalent, in precision to obtain $\phi(\lambda)$, as using RBM+ES with 18 excited states, indicating that RBM+PT is a more efficient way of building a reduced space.

References

[1] D. Frame, R. He, I. Ipsen, D. Lee, D. Lee, and E. Rrapaj, *Eigenvector continuation with subspace learning*, Phys. Rev. Lett. **121** (2018), p. 032501.

[2] Y. Maday, A. T. Patera, and J. Peraire, *A general formulation for a posteriori bounds for output functionals of partial differential equations; application to the eigenvalue problem*, C. R. Acad. Sci. Paris Sér. I Math, **328** (1999), pp. 823–828.

[3] L. Machiels, Y. Maday, I. B. Oliveira, A. T. Patera, and D. V. Rovas, *Output bounds for reduced-basis approximations of symmetric positive definite eigenvalue problems*, C. R. Acad. Sci. Paris Sér. I Math, **331** (2000), pp. 153–158.

[4] J. N. Silverman and J. C. van Leuven, *Perturbational-variational approach to the calculation of variational wave functions. i. theory*, Phys. Rev, **162** (1967), p. 1175.

[5] A. K. Noor and H. E. Lowder, *Approximate techniques of structural reanalysis*, Comput. Struct, **4** (1974), pp. 801–812.

Reporter: Gaspard Kemlin

Participants

Prof. Dr. Kieron Burke
University of California, Irvine
2145 Natural Sciences II
Irvine, CA 92697-2025
UNITED STATES

Prof. Dr. Eric Cancès
CERMICS
École des Ponts and INRIA
Cité Descartes
Champs-sur-Marne
6 et 8 Avenue Blaise Pascal
77455 Marne-la-Vallée Cedex 2
FRANCE

Dr. Thiago Carvalho Corso
Fachbereich Mathematik
Universität Stuttgart
Pfaffenwaldring 57
70569 Stuttgart
GERMANY

Prof. Dr. Paul Cazeaux
Department of Mathematics
Virginia Tech
Blacksburg VA 24061-0123
UNITED STATES

Prof. Dr. Huajie Chen
School of Mathematical Sciences
Beijing Normal University
19 Xinjiekou Wai Street
100875 Beijing
CHINA

Dr. Xioaying Dai
Institute of Computational Mathematics
and
Scientific Engineering Computing
Academy of Mathematics and Systems
Science Chinese Academy of Sciences
No.55, Zhong-Guan-Cun East Road,
Haidian
100 190 Beijing
CHINA

Dr. Mi-Song Dupuy
Sorbonne Université
Laboratoire Jacques-Louis LIONS
4 Place Jussieu
P.O. Box 187
75252 Paris
FRANCE

Dr. Geneviève Dusson
Faculté des Sciences et Techniques
Laboratoire Mathématiques de Besancon
Université de Franche-Comté
16, route de Gray
25030 Besançon Cedex
FRANCE

Prof. Dr. Virginie Ehrlacher
CERMICS - ENPC
Bât. Coriolis B 312
Cité Descartes, Champs-sur-Marne
6 et 8 Avenue Blaise Pascal
77455 Marne-la-Vallée Cedex 2
FRANCE

Dr. Fabian M. Faulstich
Department of Mathematics
Rensselaer Polytechnic Institute
1121 Sage Ave
Troy, NY 12180
UNITED STATES

Katharine Fisher
Department of Aeronautics and Astronautics
Massachusetts Institute of Technology
77 Massachusetts Avenue
Cambridge, MA 02139-4307
UNITED STATES

Prof. Dr. Gero Friesecke
Department of Mathematics
School of Computation, Information and Technology
Technische Universität München
Boltzmannstraße 3
85748 Garching bei München
GERMANY

Dr. Louis Garrigue
Département de Mathématiques
Université de Cergy-Pontoise
Site Saint-Martin, BP 222
2, avenue Adolphe Chauvin
95302 Cergy-Pontoise Cedex
FRANCE

Dr. Laura Grazioli
École des Ponts
6 avenue Blaise Pascal
77455 Marne-la-Vallée
FRANCE

Dr. Muhammad Hassan
EPFL
MA-C1-573
Station 8
1015 Lausanne
SWITZERLAND

Prof. Dr. Patrick Henning
Fakultät für Mathematik
Ruhr-Universität Bochum
Universitätsstr. 150
44801 Bochum
GERMANY

Prof. Dr. Michael F. Herbst
Mathematics for Materials Modelling (MatMat)
École Polytechnique Fédérale de Lausanne
Station 8
1015 Lausanne
SWITZERLAND

Dr. Gaspard Kemlin
LAMFA, UMR CNRS 7352
UFR des Sciences
Université de Picardie Jules Verne
33 rue Saint Leu
80039 Amiens Cedex
FRANCE

Prof. Dr. James Kermode
School of Engineering
University of Warwick
Coventry CV4 7AL
UNITED KINGDOM

Dr. Alfred Kirsch
CERMICS - ENPC
Cite Descartes, Champs-sur-Marne
6 et 8 avenue Blaise Pascal
77455 Marne-la-Vallée Cedex 2
FRANCE

Dr. Simen Kvaal
Hylleraas Centre for Quantum Molecular Sciences
University of Oslo
Blindern
P.O. Box 1033
0315 Oslo
NORWAY

Prof. Dr. Andre Laestadius
Oslo Metropolitan University
Pilestredet 35
P.O. Box 4
0130 Oslo
NORWAY

Dr. Rafael Lainez Reyes
Mathematisches Institut A
Universität Stuttgart
Pfaffenwaldring 57
70569 Stuttgart
GERMANY

Prof. Dr. Caroline Lasser
Zentrum Mathematik
Technische Universität München
Boltzmannstraße 3
85748 Garching bei München
GERMANY

Prof. Dr. Örs Legeza
Wigner Research Centre for Physics, Budapest
P.O. Box 49
1525 Budapest 114
HUNGARY

Prof. Dr. Antoine Levitt
Université de Paris-Sud
Centre d'Orsay
91400 Orsay Cedex
FRANCE

Prof. Dr. Mathieu Lewin
CEREMADE
Université Paris-Dauphine
Place de Lattre de Tassigny
75016 Paris
FRANCE

Prof. Dr. Lin Lin
Department of Mathematics
University of California, Berkeley
1083 Evans Hall
Berkeley CA 94270
UNITED STATES

Prof. Dr. Michael Lindsey
Department of Mathematics
University of California, Berkeley
970 Evans Hall
Berkeley CA 94720-3840
UNITED STATES

Prof. Dr. Christian Lubich
Mathematisches Institut
Universität Tübingen
Auf der Morgenstelle 10
72076 Tübingen
GERMANY

Prof. Dr. Yvon Maday
Université Pierre et Marie Curie
Laboratoire Jacques-Louis Lions
Boite courrier 187
4 place Jussieu
75252 Paris Cedex 05
FRANCE

Prof. Dr. Daniel Massat
Department of Mathematics
Louisiana State University
Baton Rouge LA 70803-4918
UNITED STATES

Prof. Dr. Frank Neese
Max Planck Institut für Kohlenforschung
Kaiser-Wilhelm-Platz 1
45470 Mülheim an der Ruhr
GERMANY

Dr. Michele Nottoli
Fachbereich Mathematik
Universität Stuttgart
Pfaffenwaldring 57
70569 Stuttgart
GERMANY

Prof. Dr. Thomas Bondo Pedersen
Hylleraas Centre for Quantum Molecular Sciences, Department of Chemistry, University of Oslo
P.O. Box 1033
0315 Oslo
NORWAY

Dr. Markus Penz
Max Planck Institute for the Structure and Dynamics of Matter (Hamburg) and OsloMet University
6020 Innsbruck
AUSTRIA

Prof. Dr. Daniel Peterseim
Institut für Mathematik &
Centre for Advanced Analytics and Predictive Sciences
Universität Augsburg
Universitätsstraße 12a
86159 Augsburg
GERMANY

Bruno Ploumhans
Section de Mathématiques
Station 8
École Polytechnique Fédérale de Lausanne
1015 Lausanne
SWITZERLAND

Niklas Schmitz
EPFL
MA-C1-573
Station 8
1015 Lausanne
SWITZERLAND

Prof. Dr. Reinhold Schneider
Fakultät II – Institut für Mathematik
Technische Universität Berlin
Sekr. MA 5 – 3
Straße des 17. Juni 136
10623 Berlin
GERMANY

Prof. Dr. Benjamin Stamm
Fachbereich Mathematik
Universität Stuttgart
Pfaffenwaldring 57
70569 Stuttgart
GERMANY

Dr. Timothy Stroschein
ETHZ
Department Mathematik
HG J 55
Rämistr. 101
8092 Zürich
SWITZERLAND

Dr. Julien Toulouse
Sorbonne Université
Laboratoire de Chimie Théorique
4 Place Jussieu
P.O. Box 137
75005 Paris
FRANCE

Prof. Dr. Robert van Leeuwen
Department of Physics
University of Jyväskylä
Survontie 9
40520 Jyväskylä
FINLAND

Zhuoyao Zeng
Fachbereich Mathematik
Universität Stuttgart
Pfaffenwaldring 57
70569 Stuttgart
GERMANY

Dr. Liwei Zhang
Institut für Mathematik
RWTH Aachen
Templergraben 55
52062 Aachen
GERMANY

Dexuan Zhou
School of Mathematical Sciences
Beijing Normal University
Beijing 100875
CHINA